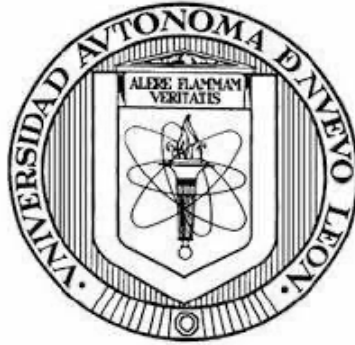


UNIVERSIDAD AUTÓNOMA DE NUEVO LEÓN
FACULTAD DE CIENCIAS BIOLÓGICAS



STUDY OF THE EFFECT OF IMMUNEPOTENT CRP IN COMBINATION WITH
CHEMOTHERAPIES ON CANCER CELLS AND IMMUNE SYSTEM CELLS

BY

ANA LUISA RIVERA LAZARÍN

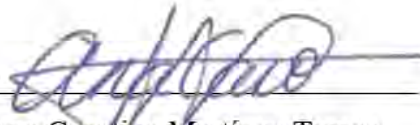
IN PARTIAL FULFILLMENT OF THE REQUIREMENTS FOR THE DEGREE OF

DOCTOR OF SCIENCES
WITH ORIENTATION IN IMMUNOBIOLOGY

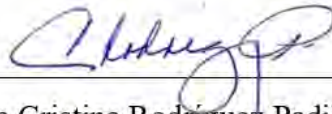
2024

STUDY OF THE EFFECT OF IMMUNEPOTENT CRP IN COMBINATION WITH
CHEMOTHERAPIES ON CANCER CELLS AND IMMUNE SYSTEM CELLS

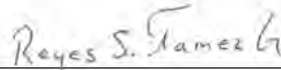
THESIS COMMITTEE



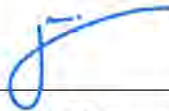
Dra. Ana Carolina Martínez Torres
Presidente



Dra. María Cristina Rodríguez Padilla
Secretario



Dr. Reyes S. Tamez Guerra
Vocal



Dr. José Manuel Vázquez Guillén
Vocal



Dr. Pablo Zapata Benavides
Vocal



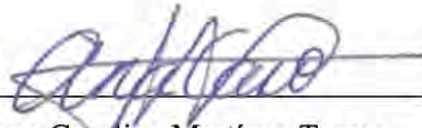
PhD. Katiuska Arévalo Niño
Subdirector de Posgrado



SUBDIRECCION
DE POSGRADO

STUDY OF THE EFFECT OF IMMUNEPOTENT CRP IN COMBINATION WITH
CHEMOTHERAPIES ON CANCER CELLS AND IMMUNE SYSTEM CELLS

THESIS DIRECTION



Dra. Ana Carolina Martínez Torres

Director



Dr. Philippe Karoyan

External Advisor

**DERECHOS RESERVADOS© PROHIBIDA SU REPRODUCCIÓN TOTAL O
PARCIAL**

Todo el material contenido en esta Tesis está protegido, el uso de imágenes, fragmentos de videos, y demás material contenido que sea objeto de protección de los derechos de autor, será exclusivamente para fines educativos e informativos y deberá citar la fuente donde se obtuvo mencionando al autor o autores.

SPECIAL ACKNOWLEDGEMENTS



The present work would not have been possible without the economic support and the infrastructure provided by the Laboratory of Immunology and Virology at the FCB UANL, the DRUGLab (Drug Research University Group Lab) from the Laboratory of Biomolécules UMR 7203 at Sorbonne Université, the Mexican Council of Science of Technology (CONACYT), and ECOS- NORD-ANUIES-CONACYT.

ACKNOWLEDGEMENTS

I thank CONAHCYT for the scholarship provided.

I want to extend Dra. Ana Carolina Martínez my sincerest thanks for all your support, guidance, and constant encouragement throughout my thesis. Thank you for the countless hours you invested in me and my work.

My deepest gratitude to Pr. Philippe Karoyan, your mentorship, expertise, and dedication were invaluable in shaping my professional formation. Thank you for trusting in me and my work. Je vous prie de recevoir ma profonde gratitude pour m'avoir accueilli dans votre laboratoire et pour votre soutien inestimable.

Also, I would like to thank my thesis committee members, Dra. Cristina Rodríguez Padilla, Dr. Reyes Támez Guerra, Dr. José Manuel Vázquez Guillén, and Dr. Pablo Zapata Benavidez for your guidance, and invaluable feedback which has greatly enriched my work.

To my labmates from L14, Helen, María, Rodolfo, Andrea, Daniel, Roberto, Cassandra, Fer, Fati, and Alejandro (from TEC de Monterrey but a temporal member in the L14). To Rafael, Mizael, and Kenny who shared long hours of hard work with me, thank you for teaching me, for your advice, and technical help.

Special acknowledgments to the members of the DRUG Lab, Valisoa, Julien, Jean Philippe, Dra. Sarah, Dr. Christophe, Luis, Olivia, Natasha, Xavier, and Steren, merci pour votre accueil, d'avoir partagé avec moi votre temps et votre expertise, de m'avoir inspiré par votre esprit scientifique, et de m'avoir montré une immense gentillesse. Je tiens également à remercier le personnel d'Oncodesign de m'avoir accueilli, ainsi que pour le soutien technique et la gentillesse que chacun m'a offert.

To my classmates and friends Juan Manuel, Pedro, and Paola, for sharing your knowledge, questions, support, and advice with me.

A mis amigos de Francia, por convertirse en familia, por abrirme las puertas de sus casas y de sus vidas apenas conociéndome, por toda la solidaridad y el sentido humano que me han mostrado, por apoyarme a la distancia y estar presente en todos los procesos que he atravesado, a Rodrigo (desde Barcelona), y a Enrique (desde Munich). Mi infinito y más sincero agradecimiento a ustedes.

A mis amigos en México, Karlita, Paloma, Salvador, Jesús, Pedro, Rubén y Kass, que han permanecido a pesar del tiempo, la distancia, las ausencias y sin importar las circunstancias.

A mi familia,

Mami, siempre pienso en ti y te llevo conmigo a dondequiera que vaya.

A mi papá, Carlos Rivera, este título te lo debo a ti. Gracias por todos tus sabios consejos, por escucharme y por ser el mayor ejemplo de fortaleza, temple, sabiduría y resiliencia. Gracias por guiarme y por amarme. Esto definitivamente hubiera sido imposible sin tu incondicional apoyo en cada paso. Infinitas gracias.

A mis hermanas, Alhelí y Perla Rivera, son mi mayor apoyo, mis cómplices y mejores amigas. Gracias por siempre estar ahí, por escucharme, motivarme, aconsejarme, por acompañarme, por ser la mano que está siempre para ayudarme, por ser la razón de no sentirme sola nunca. Gracias por salvarme.

Gracias familia por ser mi motor y motivación. Los amo.

To Carlos Rivera Rodríguez, with my deepest and sincere respect for you,

Ma. Patricia Lazarín Cierra

Perla Patricia Rivera Lazarín

And Fátima Alhelí Rivera Lazarín

*“El cáncer es ubicuo en la población humana; la única manera cierta de evitarlo
consiste en no nacer, ya que vivir supone un riesgo.”*

Robbins y Cotran. 2015. Patología estructural y funcional. Barcelona; Editorial Elsevier.

INDEX

| | |
|--|-----------|
| ABSTRACT | 1 |
| RESUMEN..... | 2 |
| 1. INTRODUCTION | 3 |
| 2. BACKGROUND | 5 |
| 2.1 CELL DEATH: THE RESULT OF LIFE | 5 |
| 2.1.1 <i>Regulated Cell Death (RCD)</i> | 5 |
| 2.2 CANCER: THE THOUSAND DISEASES | 8 |
| 2.2.1 <i>Breast cancer</i> | 9 |
| 2.2.2 <i>Hematologic malignancies</i> | 10 |
| 2.2.2.1 <i>Acute T-cell lymphoblastic leukemia (T-ALL)</i> | 11 |
| 2.2.3 <i>Cancer treatment</i> | 12 |
| 2.2.4 <i>Cyclophosphamide (CTX)</i> | 14 |
| 2.3 COMBINATIONAL THERAPY: THE FIVE UNITS IN ONE UNIT | 18 |
| 2.3.1 <i>Immunepotent CRP (ICRP)</i> | 19 |
| 3. JUSTIFICATION | 20 |
| 4. HYPOTHESIS | 21 |
| 5. OBJECTIVES | 21 |
| GENERAL OBJECTIVE: | 21 |
| SPECIFIC OBJECTIVES: | 21 |
| 6. RESULTS | 22 |
| CHAPTER 1. STUDY OF THE CYTOTOXIC EFFECT INDUCED BY IMMUNEPOTENT CRP IN COMBINATION WITH CHEMOTHERAPIES IN CANCER CELLS | 22 |
| 1.1 THE BOVINE DIALYZABLE LEUKOCYTE EXTRACT, IMMUNEPOTENT CRP, SYNERGICALLY ENHANCES CYCLOPHOSPHAMIDE-INDUCED BREAST CANCER CELL DEATH, THROUGH A CASPASE-INDEPENDENT MECHANISM..... | 23 |
| 1.2 SYNERGISTIC ENHANCEMENT OF CHEMOTHERAPY-INDUCED CELL DEATH AND ANTITUMOR EFFICACY AGAINST TUMORAL T-CELL LYMPHOBLASTS BY IMMUNEPOTENT CRP, A BOVINE DIALYZABLE LEUKOCYTE EXTRACT | 39 |

| | |
|--|-----------|
| CHAPTER 2. STUDY OF THE CYTOTOXIC EFFECT INDUCED BY IMMUNEPOTENT CRP IN COMBINATION WITH CHEMOTHERAPIES IN IMMUNE SYSTEM CELLS | 61 |
| 2.1 CYCLOPHOSPHAMIDE AND EPIRUBICIN INDUCE HIGH APOPTOSIS IN MICROGLIA CELLS WHILE EPIRUBICIN PROVOKES DNA DAMAGE AND MICROGLIAL ACTIVATION AT SUB-LETHAL CONCENTRATIONS | 62 |
| 2.2 IMMUNEPOTENT CRP PROTECTS MICROGLIA CELLS FROM EPIRUBICIN-INDUCED DAMAGE | 79 |
| 2.2.1 INTRODUCTION | 79 |
| 2.2.2 METHODS..... | 80 |
| 2.2.3 RESULTS | 82 |
| 2.2.4 DISCUSSION..... | 85 |
| 2.2.5 REFERENCES | 86 |
| 7. CONCLUSIONS | 90 |
| 8. PERSPECTIVES | 91 |
| 9. REFERENCES | 92 |
| 10. BIOGRAPHICAL ABSTRACT | 98 |

ABSTRACT

Chemotherapies are widely used in cancer treatment despite cell death resistance and numerous side effects. Current approaches suggest utilizing combinatorial therapies to enhance the effectiveness of individual agents, potentially reducing cell death resistance and minimizing side effects. This thesis aimed to explore the combined effects of Immunepotent CRP (ICRP) with several chemotherapies in breast cancer and T-cell malignancies, as well as its impact on immune system cells. Our research demonstrates that combining ICRP with cyclophosphamide (CTX) results in enhanced cell death characterized by morphological changes, dissipation of mitochondrial membrane potential, elevated reactive oxygen species (ROS)-production, and caspases activation. In addition, in breast cancer cells, the cell death induced by ICRP and CTX is caspase-independent. Conversely, in malignant T-cell lymphoblasts, the cytotoxicity of the ICRP and CTX combination is dependent on caspases, ROS, and calcium, involving dissipation of mitochondrial membrane potential and elevated ROS production. Additionally, ICRP combined with CTX overcomes bone marrow-induced resistance to CTX-caused cell death and enhances the antitumor activity of CTX *in vivo*, resulting in reduced tumor volume, lower expression of Ki-67, and a decrease in the granulocyte/lymphocyte ratio. Furthermore, ICRP protects bone marrow, spleen, and microglia cells from cell death induced by epirubicin (EPI), doxorubicin (DOX), and CTX. ICRP also reduces ROS and nitric oxide (NO) production in microglia cells, inducing autophagy as a protective mechanism against EPI-induced cytotoxicity in microglia cells. These results indicate that combining ICRP with chemotherapies may be a potent approach to enhance cancer treatment success.

RESUMEN

Las quimioterapias son ampliamente utilizadas en el tratamiento del cáncer a pesar de generar resistencia a la muerte celular y numerosos efectos secundarios. Los enfoques actuales sugieren el uso de terapias combinatorias para mejorar la efectividad de los agentes individuales, potencialmente reduciendo la resistencia a la muerte celular y minimizando los efectos secundarios. Esta tesis tuvo como objetivo explorar los efectos de la combinación de Immunepotent CRP (ICRP) con diversas quimioterapias en cáncer de mama y malignidades de células T, así como su impacto en las células del sistema inmunológico. Nuestro estudio muestra que la combinación de ICRP con ciclofosfamida (CTX) produce potenciación de la muerte celular, evidenciada con cambios morfológicos, dismunición del potencial de membrana mitocondrial, incremento en la generación de especies reactivas de oxígeno (ROS) y activación de caspasas. Además, en las células de tumor mamario, la muerte celular provocada por ICRP y CTX no está relacionada a la actividad de caspasas. Por el contrario, en los linfoblastos malignos de células T, la citotoxicidad inducida por ICRP junto con CTX requiere la activación de caspasas, de ROS y calcio, con la implicación de una disminución del potencial de la membrana de la mitocondria y un incremento en la generación de ROS. Además, la combinación de ICRP con CTX sobrepasa la resistencia inducida por la médula ósea a la muerte celular mediada por CTX y mejora el efecto antitumoral de CTX *in vivo*, resultando en una reducción del volumen tumoral, menor expresión de Ki-67 y una disminución en la relación granulocito/linfocito. Asimismo, ICRP protege las células de la médula ósea, el bazo y la microglía de la muerte celular inducida por epirrubicina (EPI), doxorubicina (DOX) y CTX. El ICRP también reduce la producción de ROS y óxido nítrico (NO) en células de microglía, induciendo autofagia como un mecanismo de protección contra la citotoxicidad inducida por EPI en las células de microglía.

Estos hallazgos sugieren que la combinación de ICRP con quimioterapias podría ser una estrategia efectiva para mejorar el tratamiento contra el cáncer.

1. INTRODUCTION

Chemotherapies have been used widely for cancer treatment including breast cancer and hematological cancers, despite cell death resistance and multiple adverse effects. This treatment aims to induce regulated cell death (RCD), which refers to a specific type of cellular demise that can be influenced by pharmacological or genetic means (Galluzzi et al. 2018).

Current trends propose the use of combinatorial therapies. This treatment approach combines two or more treatments that enhance the effectiveness of the individual agent, based on inducing death synergistically or additively. This approach aims to mitigate resistance mechanisms and minimize adverse effects while enhancing therapeutic efficacy (Mokhtari et al. 2017). Current studies have revealed that chemotherapies could also be used with immunotherapies, so the integration of these potentially complementary methods represents an effective anticancer strategy (Luo et al. 2019).

In this sense, IMMUNEPOTENT CRP (ICRP) is an immunotherapeutic agent demonstrated to induce a cytotoxic effect in various cell lines including breast cancer lines: MCF7, BT-474, and MDA-MB-453, as well as hematologic cancer cells: CEM, Molt-4 and L5178Y-R, and without affecting the viability of mononuclear cells from the peripheral blood (Franco Molina et al. 2006).

Notwithstanding the molecular disparities among the cancer lines studied, certain aspects of ICRP-induced mechanism of cell demise remain consistent across various types of cancer. In all cancer cell lines, ICRP has been shown to elevate the production of reactive oxygen species (ROS), leading to the dissipation of the membrane potential of the mitochondria, damage in the DNA that induces cell cycle detention, evoking eventual DNA degradation (Lorenzo-Anota et al., 2020; Martinez-Torres et al., 2018, 2019; Reyes-Ruiz et al., 2021). Interestingly, solid tumor cells exposed to ICRP undergo a non-caspase-mediated, ROS-driven cell demise, whereas in leukemic cells it triggers caspase activation, leading to ROS overload and caspase-driven cell demise.

Clinical phase studies with ICRP have shown that it can enhance the well-being of individuals diagnosed with lung and breast cancer who were undergoing conventional chemotherapeutic regimens, observing an increase in total leukocytes and subpopulations

of lymphocytes (Franco Molina et al. 2008; Lara et al. 2010). Furthermore, ICRP has demonstrated myeloprotective effects in murine models treated with 5-fluorouracil (Coronado Cerda et al. 2016).

Other studies demonstrated that treatment using the combination of ICRP with oxaliplatin (OXP) increased the cytotoxic effect against the murine melanoma cell line, B16F10, induced by both agents independently (Rodríguez Salazar et al. 2017). In another recent study, it was determined that ICRP in combination with the Doxorubicin/Cyclophosphamide polychemotherapy can modulate the tumor microenvironment while reducing tumor volume and prolonging survival in a mouse model of TNBC (Santana Krimskaya et al. 2020). These results offer evidence of the beneficial effects of ICRP in combination with chemotherapy, by increasing its cytotoxic effect on cancer cells.

Therefore, this thesis aimed to elucidate the cytotoxic effect, the type of combined effect, the molecular mechanism, and the antitumor effect induced by ICRP in combination with chemotherapies. This research seeks to provide a deeper understanding of its potential application in combination therapies against different types of cancers.

2. BACKGROUND

2.1 CELL DEATH: THE RESULT OF LIFE

“Life and death are one thread, the same line viewed from different sides.” Lao Tzu.

Over the past few years, our understanding of cell death has evolved significantly from viewing it merely as an inevitable and passive end of life (Fuchs & Steller, 2015). Advances in cell biology have uncovered insights into how cells respond to disruptions in their normal homeostasis. A common theme is that disturbances in cellular balance prompt responses ranging from stress management and repair to cellular senescence or regulated cell death (RCD) when restoring normal function proves impossible. This latter process maintains organismal homeostasis by deactivating or eliminating severely damaged, irreversibly infected, dysfunctional, or potentially cancerous cells (Galluzzi 2018a).

2.1.1 Regulated Cell Death (RCD)

Regulated cell death (RCD) refers to a specific type of cellular demise relying on specialized cell machinery as a target, such as caspases, calpains, and reactive oxygen species (ROS), among others, and it can be influenced by pharmacological or genetic means (Galluzzi 2018a). The inhibitory and promoting-RCD signals coexist and balance one another; at some stage, one predominates over the other.

On one hand, RCD can take place without any external environmental perturbations, functioning within physiological processes for tissue turnover. These physiological forms of regulated cell death (RCD) are termed programmed cell death (PCD). Alternatively, RCD can arise from severe disruptions in the intracellular or extracellular environment that exceed cellular coping mechanisms.

The Nomenclature Committee on Cell Death (NCCD) in 2018 proposed a classification of RCD mechanisms focusing on fundamental molecular aspects of the process (Galluzzi 2018b). Such RCD modalities could be classified based on the nuclear phenotypes, protease activation, alterations of intracellular organelles, or other phenotypical

characteristics of the dying cell (Galluzzi et al. 2012). As caspases play such a role in apoptosis and are the proteases that provide the classic apoptotic phenotype, RCD is classified biochemically as caspase-dependent or caspase-independent RCD. For this thesis, we will follow this binomial classification.

2.1.1.1 Caspase-dependent cell death

Cell demise is classified as **caspase-dependent** if it can be prevented by caspase inhibitors with broad spectrum such as N-benzyloxycarbonyl-Val-Ala-Asp-fluoromethylketone (Z-VAD-fmk), or quinoline-Val-Asp-Difluorophenoxymethylketone (Q-VD-Oph), among others (Kroemer et al. 2009, Vandenabeele 2006).

2.1.1.2 Caspase-independent cell death

On the other hand, a cell death pathway independent of caspase activation can occur even when caspases are effectively inhibited., even though it exhibits some morphological effects of caspase activation, such as partial chromatin condensation (Kroemer et al. 2009). Table 1 summarizes the different cell death pathways based on the fundamental molecular aspects of the process described to date, classified by their caspase dependence.

| Table 1. Principal regulated cell death-pathways | | |
|--|---------------------|--|
| | Cell death pathways | Definition |
| Caspase-dependent | Extrinsic apoptosis | A form of RCD initiated by perturbations of the extracellular microenvironment detected by plasma membrane receptors, propagated by caspase 8 (CASP8) and precipitated by executioner caspases, mainly CASP3. |
| | Intrinsic apoptosis | Type of RCD initiated by perturbations of the extracellular or intracellular microenvironment, demarcated by mitochondrial outer membrane permeabilization (MOMP), and precipitated by executioner caspases, mainly CASP3. |
| | Atypical | <u>Anoikis</u> : Variant of intrinsic apoptosis initiated by the loss of integrin-dependent anchorage. It lacks external matrix-signals. <u>Pyroptosis</u> : A type of RCD that critically depends on the formation of plasma membrane pores by members of the <u>gasdermin</u> protein family, often (but not always) because of inflammatory caspase activation. It exhibits apoptotic and or necrosis morphological features. |
| Caspase-independent | Autophagy | A form of RCD that mechanically depends on the autophagic machinery (or components thereof) and involves massive vacuolization of the cytoplasm by double-membraned autophagic vacuoles. |
| | Regulated necrosis | <u>Necroptosis</u> : A modality of RCD triggered by perturbations of extracellular or intracellular homeostasis that critically depends on MLKL, RIPK3, and on the kinase activity of RIPK1 (in some settings). <u>Parthanatos</u> : A modality of RCD initiated by PARP1 hyperactivation and precipitated by the consequent bioenergetic catastrophe coupled to AIF-dependent and MIF-dependent DNA degradation. |
| | | <u>Mitochondrial permeability transition (MPT)-driven necrosis</u> : Specific form of RCD triggered by perturbations of the intracellular microenvironment and relying on CYPD. <u>Ferroptosis</u> : A form of RCD initiated by oxidative perturbations of the intracellular microenvironment that is under constitutive control by GPX4 and can be inhibited by iron chelators and lipophilic antioxidants. It is caused by a failure in the system that does not allow the chelation of intracellular iron through increased ROS through the inhibition of glutathione (GSH) and loss of GPX4 function, lipid peroxidation, Ca ²⁺ influx and cell death. |
| | Atypical | <u>NETotic cell death</u> : A ROS-dependent modality of RCD restricted to cells of hematopoietic derivation and associated with NET extrusion. <u>Entotic cell death</u> : A type of RCD that originates from actomyosin-dependent cell-in-cell internalization (<u>entosis</u>) and is executed by lysosomes. |

Adapted from Galluzzi et al. 2018.

2.2 CANCER: THE THOUSAND DISEASES.

“Down to their innate molecular core, cancer cells are hyperactive, survival-endowed, scrappy, fecund, inventive copies of ourselves”. Siddhartha Mukherjee

According to the World Health Organization (WHO), cancer is the process of uncontrolled growth and spread of cells and represents one of the main pathologies worldwide (WHO, 2020). Multiple mechanisms contribute to tumor growth and progression.

Hanahan and Weinberg outlined in 2011 the “hallmarks of cancer”, providing a greater understanding of the complexity of neoplastic diseases, and knowledge of them can lead to multiple applications of these concepts, such as the development of new ways to treat cancer. These hallmarks that all cancer diseases share include continuous signaling for cell proliferation, avoidance of growth inhibitors, evasion of immune system destruction, acquisition of limitless replication potential, promotion of tumor-related inflammation, activation of invasion and metastasis, angiogenesis, genomic instability, evasion of cell death, and dysregulation of cellular energy metabolism (Hanahan & Weinberg, 2011). Recently included are polymorphic microbiomes and senescent cells, epigenetic reprogramming without mutations, and the unlocking of phenotypic adaptability (Hanahan 2022).

As reported by the National Cancer Institute (NCI), from 2016 to 2020, the most prevalent types of cancer causing the highest mortality in adolescents and young adults (AYAs, 15-39 years old) included cancer in the breast, brain, and others from the nervous system (ONS), colon and rectum, leukemia, among others, which are shown in figure 1 (NCI, 2023).

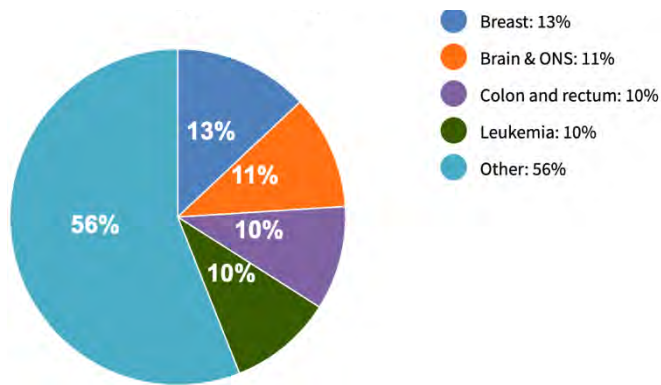


Figure 1. Ranking of the most common types of cancer that cause mortality among adolescents and young adults. Distribution based on mortality rates in ages 15-39 from 2016-2020. Retrieved from NCI, 2023.

2.2.1 Breast cancer

"We shall look back on this time and find it barbaric that once a woman diagnosed with breast cancer had to choose between disfiguring surgery and death". Susan Love, 1990

Breast cancer arises from the interaction of multiple factors, making it a complex and heterogeneous disease (García Foncillas et al. 2001), it is the most common cancer and the leading cause of cancer-related deaths in most nations (157 out of 185) (WHO, 2024). In breast cancer, the stage at diagnosis determines the stage of the disease, crucial for treatment guidelines and prognosis, which are further influenced by the occurrence of estrogen receptors (ER) and progesterone receptors (PR), and/or expression levels of human epidermal growth factor receptor 2 (HER2, a growth-promoting protein) (ACS, 2019). In 2000, Perou and collaborators managed to characterize this highly heterogeneous disease into four main molecular subtypes, which were called "intrinsic" subtypes (Perou et al., 2000).

2.2.1.1 Breast Cancer molecular subtypes

Luminal A (ER+ PR+ HER2-): This is the highly widespread molecular subtype of breast cancer and typically exhibits slower proliferation and less aggressiveness compared to other subtypes. Luminal A tumors generally have the most favorable prognosis, largely because they typically respond well to hormonal therapy, boasting a survival rate of 92%.

Luminal B (ER+ PR +/- HER2+): Additionally to hormone-receptor-positive (HR+), it was initially characterized as always HER2-positive (HER2+), Luminal B subtype has more recently been defined by high positivity for the Ki67 protein (indicative of actively dividing cells) and/or HER2 expression. These cancers are typically more aggressive than Luminal A and are associated with a poorer prognosis. It has a percentage of about 89%.

HER2-enriched (ER- PR- HER2+): Historically, this subtype had the poorest prognosis; however, the widespread adoption of targeted therapies for HER2-positive cancers has significantly improved outcomes for these patients. The survival rate for HER2-enriched breast cancer is approximately 83%.

Basal-like (ER- PR- HER2-): Also known as triple-negative breast cancer (TNBC), this subtype is characterized by the absence of estrogen and progesterone receptors and lacks HER2 expression. Around 75% of TNBC cases fall into the basal-like category based on gene expression profiles. TNBC generally has the least favorable prognosis among breast cancer subtypes, partly due to slower advances in treatment options compared to other molecular subtypes. It has a survival rate of approximately 77%. (ACS, 2019).

2.2.2 Hematologic malignancies

Hematologic cancers arise from abnormalities in the blood-forming function, affecting both myeloid and lymphoid lineages. These cancers are divided into various prevalent subtypes such as leukemia, multiple myeloma (MM), non-Hodgkin lymphoma (NHL), and Hodgkin lymphoma (HL) (Zhang et al., 2023). These subtypes can be further classified based on the affected progenitor cell type such as T-cell cancers or B-cell cancers, generally. B-cell cancers are generally more prevalent than T-cell malignancies. However, T-cell cancers typically have a significantly poorer prognosis than B-cell's. T-cell lymphoblastic leukemia (T-ALL) or T-cell lymphoblastic lymphoma (T-LBL) originates from the early stages of normal precursor T-cells and exhibits a unique immunophenotype, often expressing stem cell and/or myeloid markers (Alaggio et al., 2022).

2.2.2.1 Acute T-cell lymphoblastic leukemia (T-ALL)

Acute T-cell lymphoblastic leukemia (T-ALL) is an especially aggressive blood cancer and the most predominant form of childhood cancer, standing as a major cause of death worldwide (WHO, 2020). Among the subtypes of acute lymphoblastic leukemia (ALL), T-ALL is defined by the unregulated proliferation of immature thymocytes and is notoriously associated with the poorest prognosis (Vadillo et al., 2018). The main T-ALL issue is recurrence, in fact, 20% of pediatric and 50% of adult patients die owing to recurrence or residual disease (Cordo et al. 2022, Raetz and Teachey 2016).

Chromosomal abnormalities are a hallmark of ALL, primarily involving translocations such as t(12;21)(ETV6-RUNX1), t(1;19)(TCF3-PBX1), t(9;22)(BCR-ABL1), among others. Approximately 71% of cases exhibit changes in tyrosine kinase or RAS pathway signaling, while mutations in p53 are prevalent in 91% of cases (Terwilliger & Abdul-Hay, 2017).

2.2.2.2 T-cell lymphoblastic lymphoma (T-LBL)

T-cell lymphoblastic lymphoma (T-LBL) is diagnosed when tumor is localized primarily to tissue lesions with minimal or no inclusion of bone marrow or the blood. Genes associated with angiogenesis, chemotactic response, and nodal metastasis are significantly expressed in T-LBL. Additionally, genes encoding cell-cell adhesion proteins like BCL2, S1P1, and ICAM1, exhibit differential expression compared to T-ALL, which may hinder tumor cell intravasation into the bloodstream, thereby explaining the close association of T-LBL with stromal cells near lymphoid tissues (Bontoux et al., 2022). The most common genetic abnormalities in T-LBL involve the 14q11-13 region, where the TCR- α and TCR- δ genes are located. Also rearrangements affecting regions encoding TCR- β (7q34) and TCR- γ (7p14.1) are observed. Other chromosomal changes such as pseudodiploidy, various deletions, hyperdiploidy, and translocations frequently affect the 9q34 region. Deletion of FLASH (also termed as CASP8AP2) and dysregulated signaling of Notch receptor contribute to the T-LBL pathogenesis (Lepretre et al., 2017).

Molecular cytogenetic studies comparing T-LBL and T-ALL suggest that these T-cell cancers could potentially represent different manifestations of a unified condition. Yet, there exists a scarcity of immunophenotypic and genetic expression data for T-LBL

patients in contrast to those with T-ALL. Hence, comprehensive genetic screening of samples from both T-ALL and T-LBL patients is crucial to thoroughly investigate this hypothesis (Kroeze et al., 2020).

2.2.3 Cancer treatment

The treatment decision is made considering The biological traits of the cancer, the patient's age, health status, and the potential advantages and disadvantages linked to each alternative. Currently, conventional treatments may encompass one or more modalities, such as surgery (for breast cancer), radiotherapy, or chemotherapy (WHO, 2024).

The main goal of **surgery** is to excise the cancerous tissue and ascertain its phase. Therapeutic surgery involves mastectomy (complete or conservative surgical removal of the breast). **Radiotherapy** is usually used after surgery to destroy the remaining cancer cells in breast cancer and to a lesser extent as a treatment for leukemia (ACS, 2022).

In addition, for leukemia, medical practices such as **leukapheresis** are used, which is a technique that consists of selectively extracting leukocytes from circulating blood through centrifugation, with the remanent of the blood content being returned to the patient to reduce the leukocytosis that may occur. As well as **bone marrow transplantation**, which consists in transplanting stem cells from a donor with healthy bone marrow to replace damaged or destroyed bone marrow (Ortega Sánchez et al. 2007).

On the other hand, for breast cancer, other treatments are used, such as **hormone therapy**, to inhibit the growth of breast cancer cells with positive hormone receptors (HR); as well as **targeted therapy** with trastuzumab, a monoclonal antibody specifically designed to target the HER2 protein directly, available for the treatment of the HER2+ subtype (ACS, 2022). Recently, **immunotherapies** have emerged as a treatment option due to their ability to initiate an anti-tumor immune response (Wu & Waxman, 2018). This can involve either stimulating the patient's immune system or administering components of the immune system.

Despite significant advancements in the treatment of breast cancer and hematologic cancers, chemotherapy remains a cornerstone of cancer treatment. **Chemotherapy** involves the administration of chemical compounds or medications aimed at combating cancer. These medications vary widely in their chemical composition, treatment

schedules, methods of administration, effectiveness against specific types of cancer, and potential side effects (ACS, 2022).

Chemotherapies can be categorized based on their mechanism of action, chemical structure, and their interactions with other drugs into:

2.2.3.1 Alkylating agents

Alkylating treatments function by damaging cells' DNA, thereby hindering their replication. These agents are effective across all stages of cell division and are employed in addressing diverse cancers, including cancer in the lung and breast, as well as ovarian cancer, leukemia, lymphoma, Hodgkin's disease, multiple myeloma, and sarcoma. Due to their DNA-damaging effects, alkylating agents also affect the bone marrow that generates new blood cells. Examples of common alkylating agents include carboplatin, cisplatin, cyclophosphamide, ifosfamide, and oxaliplatin, among others (ACS, 2022).

2.2.3.2 Antimetabolites

Antimetabolites disrupt the synthesis of nucleic acids by integrating into their molecular structure certain nucleic bases thanks to an antagonism mechanism that finds its explanation in the structural analogy with the bases involved (Coeffic et al 2002). When these agents act, DNA replication is hindered, preventing cell division. They are frequently employed in treating leukemias, breast, ovarian, and gastrointestinal cancers, among others. Antimetabolites like 5-fluorouracil (5FU), 6-mercaptopurine (6-MP), and Capecitabine (Xeloda), Gemcitabine (Gemzar), Methotrexate (Mtx), Thioguanine, among others are examples.

2.2.3.3 Antitumor antibiotics

These medications function by altering the DNA within cancer cells to inhibit their ability to proliferate and replicate.

2.2.3.3.1 Anthracyclines: Anthracyclines are antibiotics with antitumor properties that disrupt enzymes crucial for DNA replication during the cell cycle. They bind to DNA, preventing its replication and thus halting cell division. Anthracyclines are extensively used in treating various cancers. Examples include Daunorubicin, Doxorubicin, and Epirubicin. A significant concern with these drugs is their potential to cause irreversible heart damage if given in high doses. Therefore, strict lifetime dose limits, also known as cumulative doses, are imposed when using these medications.

Other antitumor antibiotics that are not anthracyclines include Bleomycin, and Mitomycin-C, among others (Tacar O. et al., 2013; Khasraw M. et al., 2012).

2.2.3.4 Topoisomerase Inhibitors

Also known as plant alkaloids, disrupt enzymes called topoisomerases, crucial for separating the strands of DNA during replication. These medications target certain leukemias and are effective against lung, ovarian, gastrointestinal, colorectal, and pancreatic cancers. They are categorized based on the type of enzyme they target:

2.2.3.4.1 Topoisomerase I inhibitors (also termed as camptothecins) Irinotecan and Topotecan are examples.

2.4.4.2 Topoisomerase II inhibitors (also termed as epipodophyllotoxins) Etoposide (ETO), Mitoxantrone (also functions as antitumor antibiotic), and Teniposide are some examples (Bazun K. et al., 2020; Wood L. et al., 2006).

Treatment of breast cancer and hematologic cancers mainly includes chemotherapies such as cyclophosphamide (CTX), anthracyclines (such as doxorubicin, DOX or epirubicin, EPI), etoposide (ETO), methotrexate (MTX), among others (Bayón et al. 2020).

2.2.4 Cyclophosphamide (CTX)

It is an alkylating agent indicated for the treatment of various neoplasms such as malignant lymphoma, multiple myeloma, leukemias, sarcomas, neuroblastoma, ovarian and breast carcinoma, among others. It is also employed in the treatment of Hodgkin's lymphoma and serves as an immunosuppressant in lupus erythematosus, severe rheumatoid arthritis, rheumatoid vasculitis and is part of the conditioning regimen for bone marrow transplant (VADEMECUM 2022).

Cyclophosphamide disrupts normal DNA function through alkylation and by preventing cell division by forming cross-links between DNA strands, which unbalances cell growth and results in cell death. The drug is rapidly distributed after intravenous administration throughout the body, including the brain and cerebrospinal fluid (CSF). This drug passes through the placenta and is detectable in breast milk. The plasma half-life of cyclophosphamide fluctuates between 4-8 hours and the primary drug and its metabolites are expelled through urine in proportions of <20% and 85-90%, respectively (PLM 2018).

After its absorption through the digestive tract, it undergoes a metabolic activation dependent on the hepatic cytochrome P450 system (mainly CYP 2B6 and 3A4 (Ahlmann and Hempel 2016)) (which generates a hydroxylation reaction in the oxazosphorin ring) forming 4-hydroxycyclophosphamide, a metabolite that is in equilibrium with its tautomer aldophosphamide. In tumor cells, aldophosphamide is spontaneously cleaved to generate acrolein and phosphoramidate mustard. The latter would be the cause of the cytotoxic effects by eliminating chloride, resulting in the formation of a cation cyclic aziridinium. This reactive cation is rapidly targeted by various nucleophiles, such as guanine residues, leading to the alkylation of its nitrogen 7. This mechanism liberates the alkylating agent, enabling its interaction with the second side of the 2-chloroethyl chain to form another covalent bond with other nucleophile and subsequently alkylating the 7 nitrogen of the guanine residues of the DNA (Emadi et al. 2009). In DNA, guanine pairs with cytosine residues, its complementary nitrogenous base. However, when alkylated, the guanine residue becomes more acidic and the enolic form predominates. During DNA synthesis, modified guanine can mispair thymidine residues leading to the replacement of the thymine-adenine base pair with guanine-cytosine, resulting in the cross-linking of two strands of nucleic acids and giving rise to mutagenic effects. Furthermore, alkylation makes the imidazole ring more labile, causing it to open or the guanine to be cleaved, causing serious damage to the DNA strand. These damages are recorded, leading to the beginning of the apoptotic process (Lieberman et al. 2008).

While CYP cytotoxicity is attributed to DNA cross-linking, much remains unknown about how cell death is initiated and carried out through this process (Goldstein et al. 2008). However, biochemical characteristics observed in CYP-induced cell demise in MCF-7 indicate apoptosis with phosphatidylserine exposure and late-phase plasma membrane permeabilization. This mechanism can induce dose-dependent cell cycle detention in G0/G1, S, or G2/M phases. At low doses (1-5 mM), cells accumulate in the G0/G1 phase compared to controls, allowing time for DNA damage repair. At higher concentrations, the severity of damage surpasses the repair capacity, leading to cell death. Additionally, there is a rise in caspase 8 and 9 activity that varies with concentration, and this effect is countered by Z-VAD-FMK (a general caspase inhibitor). The use of this inhibitor prevents CYP-induced cell demise, highlighting the dependence of cell demise on caspases. On the

other hand, treatment with CYP led to an increase in the active p53 protein that was related to the upregulation of other proteins such as p21 and Fas, contrary to what was observed in the modulation of the Bax/Bcl-2 ratio, where no changes in expression were found. Nevertheless, more research is necessary to elucidate the roles of both internal and external pathways in CYP-induced apoptosis (Singh et al. 2009).

For solid tumors treatment, cyclophosphamide is administered intravenously, conventional doses typically range from 400-1000 mg/m² either alone or in combination with 5-fluorouracil, etoposide, methotrexate, or doxorubicin. Metronomic therapy protocols for treating solid tumors and multiple myeloma involve daily administration of cyclophosphamide at doses ranging from 25-100 mg of cyclophosphamide, sometimes in combination with cytostatics or other drugs. Thus far, metronomic therapy regimens have been limited to clinical studies aimed at optimizing treatment and are not yet established as standard therapy (Ahlmann and Hempel 2016).

Treatment with cyclophosphamide can more or less frequently promote adverse effects such as myelosuppression on bone marrow and spleen, leukopenia and thrombocytopenia, cardiotoxicity, hepatotoxicity, hemorrhagic cystitis, and nephrotoxicity (all these effects are dependent on high doses), nausea, alopecia, and vomiting may also occur (Ahlmann and Hempel 2016; PLM 2018).

2.2.4.1 Cell death resistances

The most relevant factor governing how cells respond to cyclophosphamide is their intrinsic susceptibility to apoptosis after DNA damage (Emadi et al. 2009). However, deregulations in the cell death machinery can result in resistance to cell death, which is associated with carcinogenesis. Evading cell death is part of the previously mentioned cancer hallmarks. Cells primarily evade death by impairing key cellular function of the tumor suppressor protein p53. Additionally, tumors can achieve similar effects by upregulating antiapoptotic proteins like Bcl-2 and Bcl-xL, enhancing survival signals such as insulin-like growth factors (IGF1/2), downregulating the expression of apoptosis-promoting proteins such as Bax, Bim, and PUMA, or blocking the extrinsic pathway of apoptosis triggered by death ligands. The structure of the RCD machinery and the strategies employed by cancer cells to escape its functions reflect the diverse adaptations

within cancer cell populations as they progress towards malignancy. (Hanahan and Weinberg 2011).

Moreover, bone marrow (BM) is a specialized area supporting T-ALL development. The interaction between T-ALL cells and the microenvironment promotes cancer cell survival and shields them from chemotherapy. Two distinct bone marrow niches exist: osteoblastic and vascular. The osteoblastic one supports hematopoietic stem cells (HSCs) quiescence, whereas the vascular one promotes cell growth, cell differentiation, and mobilization (Pastorczyk et al. 2021, Chiarini et al. 2016).

Mature and immature cells of myeloid origin have a role in immune evasion in ALL. The immature myeloid populations participating in immunoregulation are the myeloid-derived suppressor cells (MDSCs). The mature myeloid populations encompass granulocytes, monocytes, macrophages, and dendritic cells (DCs). Every cells enriches the vascular niche producing HSCs-supporting chemokines and cytokines, including stromal-derived factors. Macrophages get immunosuppressive characteristics and transform into tumor-associated macrophages (TAMs) or leukemia-associated macrophages (LAMs). The majority of LAMs exhibit an M2-like phenotype, which has been demonstrated to promote survival signals in T-ALL.

Numerous studies *in vitro* have indicated that ALL cells are not efficiently eliminated by NK cells. It has been observed that leukemia progression alters the education and maturation of NK cells. ALL cells evade NK cell-mediated lysis primarily by reducing the expression of ligands for the NK cells-activating receptors (Pastorczyk et al. 2021). However, as the tumor advances, signals from tumor cells and their surrounding microenvironment disrupt the dendritic cells differentiation, maturation, and function converting them into immunosuppressive types that promote tumor growth (Valencia et al. 2019).

This evidence makes the hallmark of resistance to cell death one of the main targets of cancer therapies. In this sense, multiple or combinational therapy has been introduced in an attempt to overcome the resistance that tumor cells present to conventional treatments.

2.3 COMBINATIONAL THERAPY: THE FIVE UNITS IN ONE UNIT

“I also began contacting scientists about the heterogeneity of cancers from a therapeutic standpoint. In other words, if the solution to cancer heterogeneity is reaching a broad spectrum of molecular targets, the existing chemistry and approved therapeutics are too toxic to accomplish that. Therefore, we should be looking at softer chemicals that can easily be combined to reach a broader spectrum of high-priority molecular targets”.

Leroy Lowe

In the search to increase the therapeutic effect of chemotherapy with lower doses, multiple studies of combinatorial therapies have been published under this term.

Although combination therapy can pose toxicity risks when using chemotherapeutic agents, the toxicity is significantly mitigated due to their distinct mechanisms of action. Ultimately, these agents work synergistically or additively, allowing for lower therapeutic doses required of each drug (Mokhtari et al., 2017). These interactions are categorized as:

- **Additive:** Combined effect equals the cumulative of individual responses ($1 + 1 = 2$).
- **Synergy:** The joint response exceeds the total of the sole effects ($1 + 1 = 7$).
- **Potentiation:** type of synergy in which one substance that has no effect enhances the toxic effects of another in a specific area of the body ($0 + 1 = 5$).
- **Antagonism:** The overall response is smaller than the cumulative effect of each part ($1 + 1 = 0$) (CIDTA).

Chou and Talalay (1983) introduced the combination index (CI) as a quantifiable measure of synergism or antagonism of 2 or more drugs through a general equation. A CI of 1 signifies an **additive** effect, a value below 1 signifies **synergy**, and a value above 1 signifies **antagonism** (Chou & Talay 1983).

Based on the induction of pharmacological synergism, the combined treatment reduces toxicity to healthy cells while enhancing the cytotoxic impact on cancerous cells. This happens when one drug in the regimen counteracts the other drug's effects in non-cancer cells, effectively shielding them from damage (Mokhtari et al. 2017).

In this sense, various studies have explored the effects of conventional chemotherapies in combination with immunotherapies (Wu and Waxman 2018).

2.3.1 Immunepotent CRP (ICRP)

The leukocyte dialysate, Immunepotent CRP (ICRP), is a bovine spleen extract (bDLE) (Martínez Torres et al. 2018). *In vitro*, it has been described for its cytotoxic effect in various cancer types including cancer of the breast (MCF-7, BT-4T4, and MDA-MB-453) (Franco Molina et al. 2006; Reyes-Ruiz et al. 2021), as well as in leukemic cells (K562, MOLT-3, and MOLT-4), without affecting the viability of mononuclear cells from the peripheral blood (PBMC) (Sierra-Rivera et al. 2016; Lorenzo-Anota et al. 2020), verifying the ICRP-selectivity towards tumor cells.

Concerning chemotherapy, clinical phase studies with the ICRP improved the well-being of patients with lung and breast cancer receiving standard chemotherapy treatments, with an observed rise in overall leukocytes and subsets of T lymphocytes (Franco-Molina et al. 2008; Lara et al. 2010).

Furthermore, ICRP has demonstrated myeloprotective effects in murine models treated with 5-fluorouracil (5-FU), maintaining a normal serum leukocyte, granulocyte, and erythrocyte count (Coronado Cerda et al. 2016). Subsequent studies demonstrated that treatment with ICRP + oxaliplatin (OXP) induced an increase in cell death compared to monotherapy (Rodríguez-Salazar et al. 2017). More recently, the effect of ICRP in combination with Doxorubicin/Cyclophosphamide and its impact on the tumor microenvironment was evaluated, identifying a reduction in tumor volume, improved survival, and modulation of CD8⁺ cells both locally within tumors and systemically, alongside inhibition of PD-L1, Gal-3, and IL-10 (Santana-Krimskaya et al. 2020).

Altogether, these results propose that ICRP can increase the cell death and antitumor effect of chemotherapy even though the protection is provided by the bone marrow microenvironment.

3. JUSTIFICATION

Chemotherapy remains the backbone of cancer treatment despite multiple adverse effects on immune system cells, and in spite, cancer cells can develop resistance to cell death. Combination therapy has been suggested as an alternative to address these issues. Under this concept, the combination of chemotherapies with immunotherapies has been carried out to reduce cell death resistance by triggering several mechanisms of cell death simultaneously, by overcoming the bone marrow microenvironment protection, and reducing adverse effects.

In this sense, Immunepotent CRP is an immunotherapy with a selective cytotoxic capacity that could be a promising agent to give the chance to reduce the doses required to counteract the tumoral process and prevent adverse effects. However, there is a lack of information concerning the cytotoxic effect and the type of combined effect induced by ICRP in combination with chemotherapy against breast cancer and hematologic cancers. This thesis pretended to elucidate the cellular death mechanism triggered by combining ICRP with CTX to pave the way on the effect induced by this combination to determine if it could be used to overcome cell death resistance and to determine if ICRP could have a protective effect against the chemotherapy-induced damage .

4. HYPOTHESIS

IMMUNEPOTENT CRP enhances the therapeutic efficacy of chemotherapy against breast cancer and hematological malignancies, without increasing its cytotoxicity in immune system cells.

5. OBJECTIVES

GENERAL OBJECTIVE:

Assessing the effect of combining IMMUNEPOTENT CRP with chemotherapy on tumor and non-tumor cells

SPECIFIC OBJECTIVES:

1. To analyze the cytotoxic and antitumor effects induced by the combination of chemotherapy with ICRP in breast cancer cells and hematological malignancies.
2. To analyze the cytotoxicity induced by the combination of chemotherapy with ICRP on immune system cells

6. RESULTS

CHAPTER 1. STUDY OF THE CYTOTOXIC EFFECT INDUCED BY IMMUNEPOTENT CRP IN COMBINATION WITH CHEMOTHERAPIES IN CANCER CELLS

1.1 The bovine dialyzable leukocyte extract, Immunepotent CRP, synergically enhances cyclophosphamide-induced breast cancer cell death, through a caspase-independent mechanism.

Original article:

**THE BOVINE DIALYZABLE LEUKOCYTE EXTRACT,
IMMUNEPOTENT CRP, SYNERGICALLY ENHANCES
CYCLOPHOSPHAMIDE-INDUCED BREAST CANCER CELL DEATH,
THROUGH A CASPASE-INDEPENDENT MECHANISM**

Ana Luisa Rivera-Lazarin^{a,+}, Ana Carolina Martínez-Torres^{a,*},
Rafael de la Hoz-Camacho^a, Olga Liliana Guzmán-Aguillón^a,
Moisés Armides Franco-Molina^a, Cristina Rodríguez-Padilla^{a,b}

^a Universidad Autónoma de Nuevo León, Facultad de Ciencias Biológicas, Laboratorio de
Inmunología y Virología, Monterrey 66455, México

^b LONGEVEDEN S.A. de C.V.

⁺ Co-first authors

^{*} **Corresponding author:** Ana Carolina Martínez-Torres, Universidad Autónoma de
Nuevo León, Facultad de Ciencias Biológicas, Laboratorio de Inmunología y Virología,
Monterrey 66455, México. E-mail: ana.martinezto@uanl.edu.mx

<https://dx.doi.org/10.17179/excli2022-5389>

This is an Open Access article distributed under the terms of the Creative Commons Attribution License
(<http://creativecommons.org/licenses/by/4.0/>).

ABSTRACT

Breast cancer (BC) is one of the leading causes of cancer death worldwide. Cyclophosphamide (CTX) remains a mainstay in cancer therapy despite harmful adverse effects and cell death-resistances. To face this, combinational therapy of chemotherapies and immunotherapies has been proposed. IMMUNEPOTENT CRP (ICRP) is an immunotherapy that has cytotoxic effects in several cancer cells without affecting peripheral blood mononuclear cells (PBMC) and CD3⁺ cells. The aim of this study was to evaluate cytotoxicity, the type of cytotoxic effect, and several features involved in cell death induced by the combination of CTX with ICRP (ICRP+CTX) in breast cancer cells as well as their effect on healthy cells. For this purpose, human and murine breast cancer cells, MCF-7, MDA-MB-231 and 4T1, or PBMC were treated for 24 hours with ICRP, CTX or ICRP+CTX in different combination ratios for the assessment of cell death. Flow cytometry and microscopy were used to determine biochemical and morphological characteristics of cell death. Assays showed that ICRP in combination with CTX induce potentiated cell death manifested with morphological changes, loss of mitochondrial membrane potential, reactive oxygen species (ROS) production, and caspase activation. In addition, it was determined that ICRP+CTX-cell death is caspase-independent in all the breast cancer cells assessed. On the other hand, ICRP did not affect CTX-cytotoxicity in PBMC. For all the above, we can propose that the combination of ICRP with CTX an effective combination therapy, promoting their use even in tumoral cells with defects on proteins implicated in the apoptotic pathway.

Keywords: Cyclophosphamide, synergistic effect, breast cancer, cell death, chemotherapy, apoptosis

INTRODUCTION

Breast cancer (BC) is one of the leading causes of women death among cancers worldwide. Chemotherapy remains a mainstay in

BC treatment and mostly in triple negative-breast cancer (TNBC) (ACS, 2019), the most lethal BC subtype. Cyclophosphamide (CTX) is an alkylating agent that interferes with DNA replication and is one of the most

widely used chemotherapies for BC (Emadi et al., 2009). CTX is considered a first-line treatment against BC, despite its immunosuppressive effects (Rasmussen and Arvin, 1982) when used in high-doses, and even if BC cells can develop cell death-resistance to CTX (Ji et al., 2019).

One of the principal issues leading to high mortality in TNBC is chemoresistance, which is in great part caused by BC-cell death evasion. The principal cell death pathway induced by chemotherapies, including CTX, is apoptosis, a regulated cell death mechanism characterized by caspase-dependence. Since cancer cells evade cell death at multiple stages during tumorigenesis and metastasis, cells develop numerous ways to inhibit apoptosis, therefore, impairing the sensitivity of tumor cells to conventional chemotherapies (Hanahan and Weinberg, 2011; Nedeljković and Damjanović, 2019; Tait and Green, 2008). To face this issue, drug combination therapy has been proposed as an interesting approach to overcome negative secondary effects associated with chemotherapy, and chemo-resistance (Apetoh et al., 2015).

Depending on the measurement of the drug combination effect, drug combinations could be defined as synergistic, additive, or antagonistic by several models that quantify the level of drug response. One of the most commonly used is the Chou-Talay combination index analysis, which allows the scoring of synergistic drug effects and avoiding ambiguities in the identification of effective combination treatments (Pemovska et al., 2018; Chou and Talay, 1983). Several studies testing drug combinations that include chemotherapies and immunotherapies have been carried out (Apetoh et al., 2015) with several advantages such as improved efficacy over tumoral cells, while decreasing unwarranted toxicity over immune cells, decreased dosage at an equal or increased level of effectiveness, and counter chemo-resistance (Correia et al., 2018).

Recently, it has been described that an effective combinatorial regimen could be reached based on the targeting of different

mechanisms of cell death (Correia et al., 2018). In that sense, the bovine dialyzable leukocyte extract (bDLE), IMMUNEPOTENT CRP (ICRP), is an immunotherapy with cytotoxic potential in several cancer cell lines (Franco-Molina et al., 2006) including breast cancer cells, without affecting non-cancerous cells (Martinez-Torres et al., 2020; Lorenzo-Anota et al., 2020). Furthermore, the combination of ICRP plus chemotherapy modifies the tumor microenvironment, potentiating and prolonging the antitumor effect (Santana-Krimskaya et al., 2020). Additionally, ICRP alone or in combination with oxaliplatin (OXP) induced immunogenic cell death against murine melanoma (Rodríguez-Salazar et al., 2017). ICRP is an immunogenic cell death inductor in breast cancer cells (Reyes-Ruiz et al., 2021), and it has shown to improve the clinical parameters of breast cancer patients receiving standard chemotherapy schedules (Lara et al., 2010). For all the above, this study aimed to investigate the effect and the mechanism of cell death of CTX in combination with ICRP in a panel of breast cancer cells including the most common subtype of BC, the luminal A, and the most aggressive BC-subtype, TNBC, likewise its effect in non-cancer cells.

METHODS

Reagents

IMMUNEPOTENT CRP[®] (ICRP), a bovine dialyzable leukocyte extract, was produced by Laboratorio de Inmunología y Virología from Facultad de Ciencias Biológicas as previously described (Franco-Molina et al., 2006). The product obtained from 1×10^8 leukocytes is defined as one unit of ICRP. ICRP and Cyclophosphamide (Cryofaxol from Cryopharma; Tlajomulco de Zuñiga, Jalisco, México) were dissolved in complete DMEM-F12 or RPMI (GIBCO by Life Technologies, Grand Island, NY), as suitable. N-acetyl-L-cysteine (NAC) was dissolved in water. QVD.opH (QVD) was dissolved in dimethyl sulfoxide (DMSO). CTX, NAC and QVD (Sigma-Aldrich, St. Louis, MO) were

wrapped in foil and stored following the manufacturer's instructions.

Cell culture

Human breast adenocarcinoma MCF-7 (ATCC® HTB-22™), MDA-MB-231 (ATCC® HTB-26™), and murine breast adenocarcinoma 4T1 (ATCC® CRL-2539™) cells were obtained from the American Type Culture Collection (ATCC) and maintained at 37 °C in a humidified incubator containing 5 % CO₂. MCF-7 and MDA-MB-231 cells were cultured in DMEM-F12 and 4T1 cells in RPMI-1640, both supplemented with 10 % fetal bovine serum (FBS) and 1 % penicillin-streptomycin (GIBCO) referred as complete DMEM or complete RPMI, respectively, and were routinely grown in 25-cm³ cell culture flasks (CORNING Enterprises, Corning, NY).

Peripheral blood mononuclear cells

(PBMC) isolation and death

Written informed consent was obtained from healthy donors from which a blood sample was obtained. PBMC isolation was made by density gradient centrifugation using Ficoll-Paque™ PLUS (GE Healthcare, Chicago, IL). The formation of cell layers was visualized, from which the population corresponding to PBMC was taken, maintained at 1x10⁵ cells per well in complete RPMI at 37 °C in 5 % CO₂ atmosphere and treated using cytotoxic concentrations used in tumoral cells for 24 h, after which cell death was measured as explained in the following section.

Cell death induction, pharmacological inhibition and analysis

For death induction, 5x10⁴ cells were treated with ICRP (0.5-1.45 U/mL) or CTX (5-40 mM) to obtain the cytotoxic concentrations (CC) that were used to perform combination analysis. For the rest of the experiments, cells were exposed to ICRP, CTX and their combination (ICRP+CTX) in different combination-ratios for 24 h in 24-well dishes (Life Sciences). On the other hand, cells were co-treated with or without 30 min of 10 μM

QVD or 5 mM NAC-pre-treatment for cell death inhibition assays. After treatment, cells were detached and washed twice with PBS and resuspended in 100 μL of binding buffer (10 mM HEPES/NaOH pH 7.4, 140 mM NaCl, 2.5 mM CaCl₂) containing Annexin-V-APC (1 μg/mL, BD Pharmingen, San Jose, CA) and 0.5 μg/mL propidium iodide (PI, MilliporeSigma, Eugene, OR) staining to measure cell death with BD Accury6 flow cytometer (Becton Dickinson, Franklin Lakes, NJ) and analyzed using FlowJo Software (LCC, Ashland, OR).

Morphological changes

Cell death associated-morphological changes were observed after 5x10⁴ cells were treated 24 h with ICRP, CTX, or their combination (ICRP+CTX) in the indicated concentrations, using an inverted microscope (Nikon Eclipse TS100) and bright-field-micrographs were taken with a Lummera INFINITY 1-2 CMOS 2.0 MP camera (20X). For this purpose, the focal position with the largest number of cells was selected in order to allow a better comparison of morphological changes.

For chromatin condensation, cells (8x10⁴) were treated with ICRP, CTX, or their combination (ICRP+CTX) in the indicated concentrations for 24 h. Then, cells were washed with PBS and fixed using 4 % paraformaldehyde, after which cells were washed and 0.1 % triton was used for plasma membrane permeabilization. Hoechst staining (5 μg/mL) (SIGMA-ALDRICH) was added, then washed with PBS, and observed using a fluorescence microscope (OLYMPUS IX70) with objective 40X. Analysis was performed with Image-J software.

ROS production analysis

ROS production-quantification was determined by staining cells with 2.5 μM HE (Hydroethidine) (Invitrogen, St. Louis, MO). Cells (5x10⁴) were treated and incubated in 24-well dishes (CORNING) with ICRP, CTX and their combination (ICRP+CTX) for 24 h. Cells were then harvested. The stain was in-

cubated at 37 °C for 30 min, assessed by flow cytometry and analyzed as described above.

Mitochondrial membrane potential analysis

To determine loss of mitochondrial membrane potential, 5×10^4 cells in 24-well dishes (CORNING) were treated as mentioned before. Cells were then collected, stained using 20 nM tetramethyl rhodamine ethyl ester stain (TMRE, Sigma-Aldrich), incubated at 37 °C for 30 min, washed with PBS, and measured loss of TMRE-staining by flow cytometry as described above.

Caspase activity assay

Cells (5×10^4) in 24-well dishes (CORNING) were treated with ICRP, CTX and their combinations (ICRP+CTX) for 24 h. Cells were then harvested and stained following manufacturer's instructions. Caspase activity was determined through Generic Caspase Activity staining kit (TF2-VAD-FMK, Abcam, Cambridge, UK) using flow cytometry as described above.

Statistical analysis

Results are presented as graphs that represent the mean \pm SD of triplicate determinations from at least three independent experiments. Data were analyzed by GraphPad Prism (San Diego, CA), using paired Student's t-tests for *in vitro* studies, and unpaired Student's t-tests for cytotoxicity in PBMC studies, considering statistical significance as $p < 0.05$.

RESULTS

ICRP and CTX induce cell death as single agents through caspase-independent and caspase-dependent mechanisms, respectively, in breast cancer cells

MCF-7, MDA-MB-231 and 4T1 cell viability was determined after treatment with ICRP (dark gray) or CTX (gray). Results showed that ICRP and CTX diminish breast cancer cell viability as treatment concentration increases (Figure 1A). This cytotoxicity was correlated with cell death assays by AnnV/PI staining (Supplementary Figure 1).

ICRP and CTX induced cell death in a concentration-dependent manner in the three cell lines tested (Fig. 1B). It was required 0.7, 0.5 and 0.09 U/mL of ICRP and 25 mM CTX for MCF-7 and 15 mM CTX for MDA-MB-231 and 4T1 cells to induce cell death in 20 % of cell population (CC_{20}). On the other hand, cell death of 50 % of the cells (CC_{50}) was reached at 1, 0.75 and 0.12 U/mL of ICRP in MCF-7, MDA-MB-231 and 4T1 cells, respectively, whereas CTX CC_{50} was 30 mM for MCF-7, and 25 mM for MDA-MB-231 and 4T1 cells.

Furthermore, ICRP and CTX induced loss of mitochondrial membrane potential in 45-60 % in the three BC-cell lines tested after treatment with CC_{50} of each treatment for 24 h, as shown in Figure 1C. Both, the CC_{50} of ICRP and the CC_{50} CTX, induced ROS production in around 45-55 % MCF-7, MDA-MB-231 and 4T1 cells (Figure 1D). Moreover, it was observed that while the CC_{50} of ICRP induced 28-42 % of cells with caspase activation, the CC_{50} CTX induced higher values, ranging from 48-77 % of caspase activation in the three-breast cancer cells lines assessed (Figure 1E).

Despite ICRP and CTX induce similar characteristics in their cell death mechanism, no significant effect in cell death was observed with pre-treatment using the pan-caspase inhibitor, QVD, after treatment with ICRP. In contrast, QVD inhibited CTX-cell death significantly (Figure 1F and Supplementary Figure 2). On the other hand, the antioxidant NAC, significantly diminished ICRP-cell death in the cell lines tested, whereas only 4T1-death showed inhibition after CTX treatment using NAC (Figure 1G and Supplementary Figure 3).

Furthermore, we analyzed cell death induced by ICRP and CTX at the higher concentrations used in breast cancer on PBMC. Figure 1H shows that ICRP only induces a low cytotoxicity in PBMC from healthy donors at CC_{50} of MCF-7 cells (1.0 U/mL), contrary to CTX which since CC_{20} of MCF-7 cells (25 mM), induces high cytotoxicity against PBMC (Figure 1I and Supplementary Figure 4).

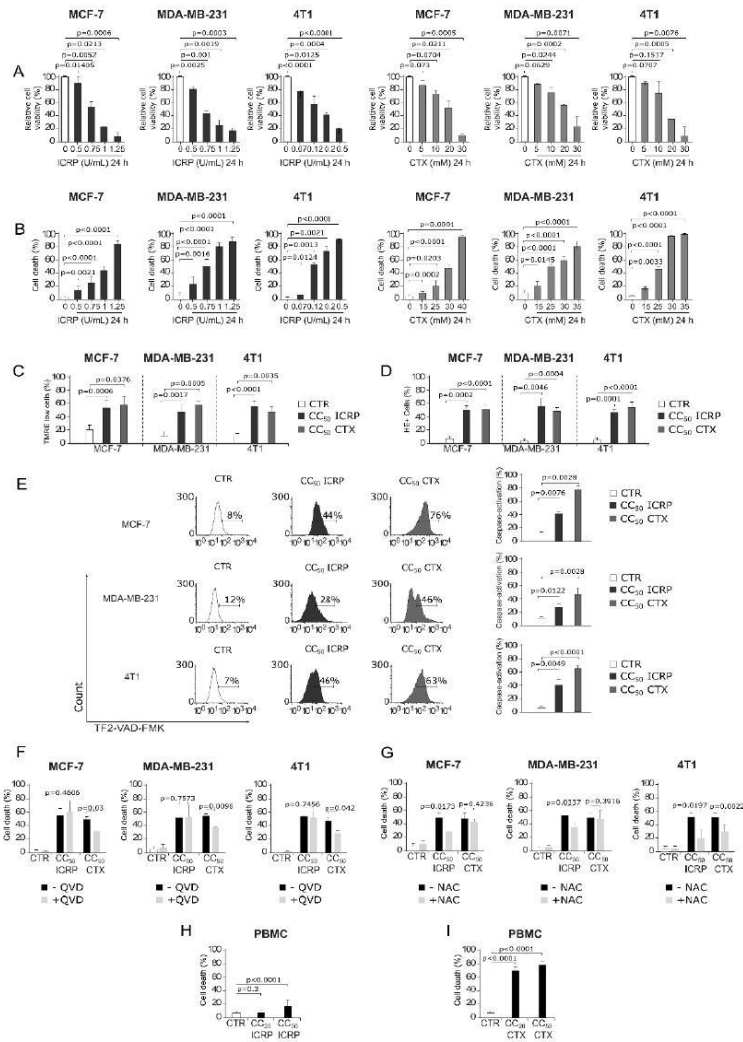


Figure 1: ICRP and CTX mechanisms of cell death in breast cancer cells and its effect in PBMC. MCF-7, MDA-MB-231 and 4T1 cells were treated for 24 h and biochemical features of cell death were evaluated and expressed as percentage. **A)** Relative cell viability was determined using MTT assay considering control cell's absorbance as 100 %. Flow cytometry was used to measure. **B)** Cell death analyzed by AnnV/PI staining. For the next evaluations, 1, 0.75 and 0.12 U/mL of ICRP were used as CC₅₀ in MCF-7, MDA-MB-231 and 4T1 cells of CTX CC₅₀-treatment. **C)** Loss of mitochondrial membrane potential determined using TMRE staining. **D)** ROS production analyzed by HE staining. **E)** Caspase activation measured by TF2-VAD-FMK. **(F, G)** Cell death obtained by AnnV/PI of cells pre-treated in presence or absence of **F)** QVD or **G)** NAC. **(H, I)** Cell death obtained by AnnV/PI of PBMC treated with **H)** ICRP or **I)** CTX. Graphs represent means \pm SD of triplicates from at least three independent experiments.

All these differences in the mechanism of cell death induced by ICRP and CTX allowed us to hypothesize that a potentiated effect on cell death could be achieved by the combination of both treatments, caspase-dependent and -independent mechanisms.

ICRP in combination with CTX synergistically potentiates the cytotoxicity of individual treatments against breast cancer cells but not PBMC

Aiming for substantially diminishing the concentration of chemotherapy, different combination ratios were designed. First, we used a sublethal concentration (non-cytotoxic) of ICRP (SLC), in combination with CC_{50} CTX corresponding to each BC cell line. Furthermore, to investigate if CTX has an effect in the ICRP cell death, we tested a combination of CC_{50} ICRP with SLC CTX. Moreover, to examine the effect of equipotent concentrations of both treatments, we tested the combination of CC_{50} of ICRP and CTX. Results showed non-significant cell death induced by SLC of ICRP or CTX compared to non-treated MCF-7 (Figure 2A), MDA-MB-231 (Figure 2B) and 4T1 cells (Figure 2C). As left panel shows in Figure 2, CC_{50} ICRP induces an increase in double-positive (Annexin V and PI) cell population in the three BC-cell lines, while CC_{50} CTX induces an increase mainly in Annexin V-positive dot plot and in double-positive cell population. When combining treatments in different combination ratios, analysis showed an increase predominantly in double-positive cell populations of MCF-7, MDA-MB-231 and 4T1. This combination ratios also induced morphological changes, demonstrating cell death-morphology like CTX's in MCF-7 treated cells. Moreover, right panel shows a significant increase in cell death of MCF-7 by SLC ICRP+ CC_{50} CTX, CC_{50} ICRP+SLC CTX and CC_{50} ICRP+ CC_{50} CTX compared to single agents, reaching 91.9 %, 70.1 %, and 94.2 % of cell death (Figure 2A). In addition, morphological assessment showed cell conflu-

ence reduction and alterations in cell morphology involving rounding-up of the cell and retraction of the stellate projections of MDA-MB-231-treated cells. Analysis showed that SLC ICRP+ CC_{50} CTX, and CC_{50} ICRP+ CC_{50} CTX reached 86.9 % and 91.2 % of cell death, respectively, whereas CC_{50} ICRP+SLC CTX showed non-significant cell death compared to ICRP alone (52.6 %, Figure 2B). Likewise, 4T1 showed rounding-up of the cell, similar to the treatment with CTX alone, and cell death analysis showed a significant cell death increase to 93.2 %, 70.7 %, and 97 % cell death, when treated with SLC ICRP+ CC_{50} CTX, CC_{50} ICRP+SLC CTX, and CC_{50} ICRP+ CC_{50} CTX, respectively (Figure 2C). Additionally, we chose the highest cytotoxic concentration used in BC cells (MCF-7 ones) to assess the cytotoxic effect of ICRP+CTX in human peripheral blood mononuclear cells (PBMC). As Figure 2D shows, ICRP is not toxic in PBMC, as only a low cytotoxicity was observed at CC_{50} ICRP of MCF-7 (1.0 U/mL, 17.7 %). In addition, non-significant cell death was observed when PBMC were treated with SLC CTX. In contrast, CC_{50} CTX of MCF-7 (30 mM) induced high cell death in PBMC (78.7 %). Moreover, any of the combination ratios tested increased cell death, compared to its corresponding monotherapy, nor, compared to CTX alone in PBMC.

Additionally, the drug interaction effect of ICRP and CTX was assessed by combination index (CI) determination. Figure 3A shows the Fa-CI graphs with the CI values that revealed synergistic effect (CI<1) being specific for the cancer cell line tested with shared synergistic effect at the combination of SLC ICRP+ CC_{50} CTX and CC_{50} ICRP+ CC_{50} CTX in the three cell lines assessed. Furthermore, to estimate the extent to which the dose of CTX can be reduced in combination to achieve a cytotoxic effect comparable to monotherapy, drug reduction index (DRI) was calculated. All the cell lines tested showed DRI values above 1. Figure 3B summarizes the values of CI and DRI.

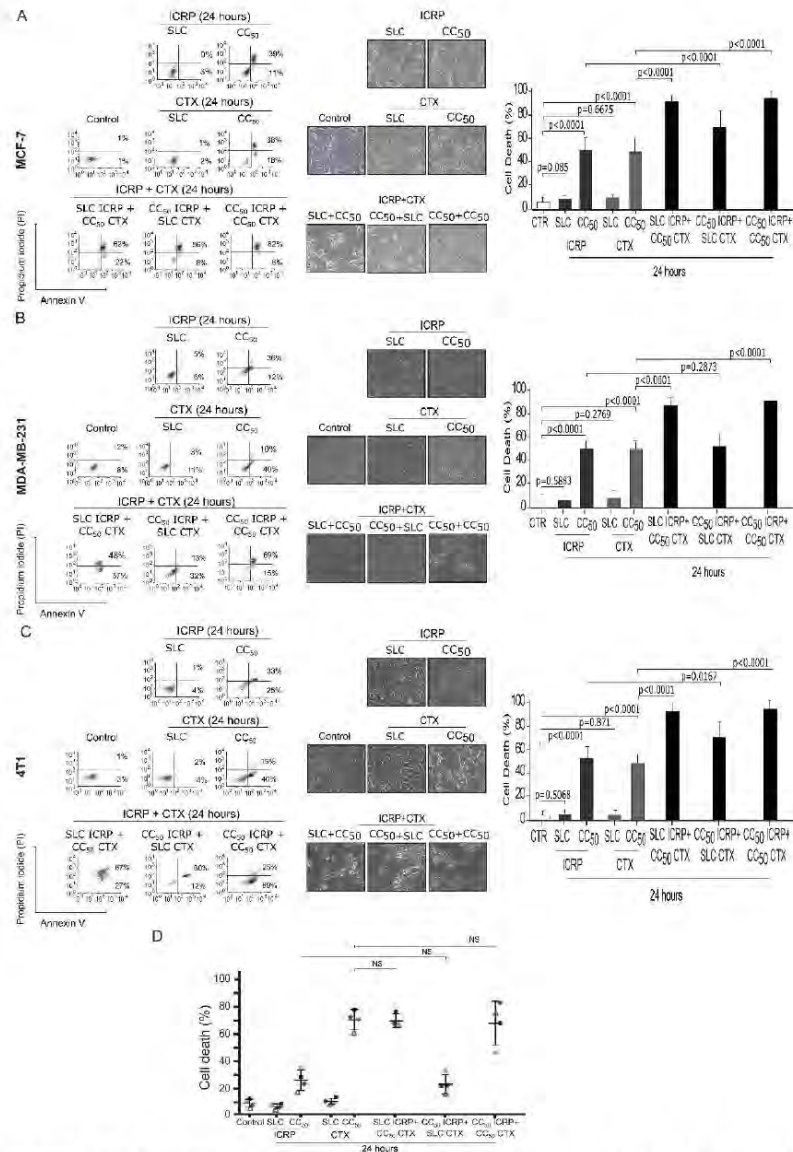


Figure 2: ICRP+CTX cytotoxicity in breast cancer cells and PBMC. MCF-7, MDA-MB-231, 4T1 cells and PBMC were treated for 24 h with ICRP, CTX and their combination at different ratios and analyzed by flow cytometry. AnnV/PI staining was used to analyze cell death of **A)** MCF-7, **B)** MDA-MB-231 and **C)** 4T1 cells. Representative dot plots are shown on the left, representative images of morphological changes were taken in bright field using an inverted microscope (20X), and graphs are on the right. **D)** Cell death of PBMC from healthy donors (n=4). Mean value of at least three independent experiments performed in triplicate \pm SD were graphed.

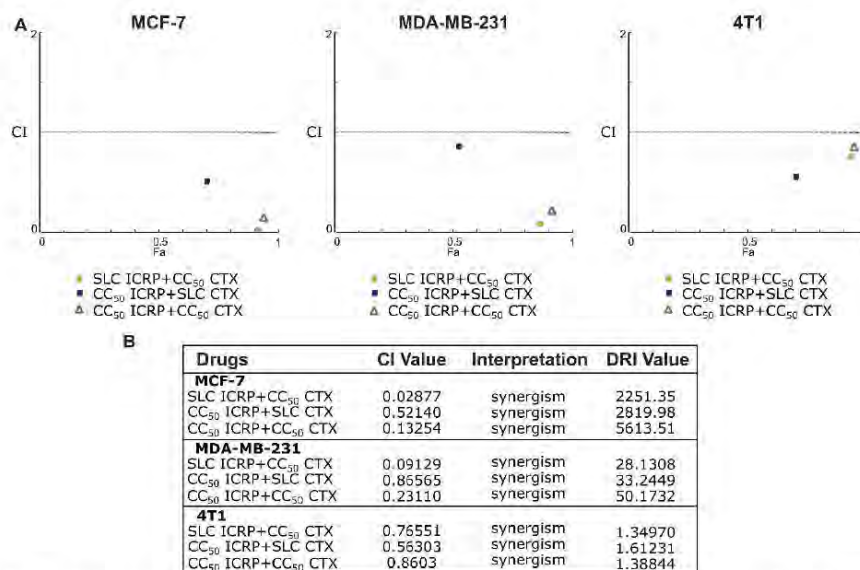


Figure 3: IC RP+CTX induces different cytotoxic effects in breast cancer cells. MCF-7, MDA-MB-231 and 4T1 were treated with the combination of IC RP+CTX in different ratios for 24 h and cell death was analyzed using the software Compusyn. **A)** Fa-CI graphs from cell death. **B)** table with the effect of combined IC RP and CTX treatment. CI<1 indicates synergism, additive effect is CI=1, and CI>1 represents antagonism.

For the shared synergistic effect in the three cell lines, SLC IC RP+CC₅₀ CTX and CC₅₀ IC RP+CC₅₀ CTX were chosen to determine the main biochemical characteristics of IC RP+CTX cell death, evaluating features evoked by the monotherapies.

IC RP in combination with CTX induce morphologic and mitochondrial alterations during cell death in breast cancer cells

A significant augmentation in loss of mitochondrial membrane potential (87 % and 84.33 %) and ROS production (64.4 % and 86.9 %) was induced after treatment with SLC IC RP+CC₅₀ CTX and CC₅₀ IC RP+CC₅₀ CTX in MCF-7 compared to single treatments. MCF-7-treated cells also showed nuclear condensation compared to control cells (p=0.0056 and p=0.0087, respectively) (Figure 4A). In MDA-MB-231, SLC IC RP+CC₅₀

CTX and CC₅₀ IC RP+CC₅₀ CTX caused a significant increase in mitochondrial alterations demonstrated by 83.5 % and 98.98 %, respectively, of loss of mitochondrial membrane potential and 75.94 % and 83.4 %, respectively, of ROS production. Morphological assessment showed nuclear condensation induced by both ratios compared to control cells (p=0.0463 and p=0.0322, respectively) (Figure 4B). The 4T1-treated cells revealed 95.23 % of cells with loss of mitochondrial membrane potential and 90.46 % of cells with increased ROS production after treatment with SLC IC RP+CC₅₀ CTX. Additionally, a significant increase of loss of mitochondrial membrane potential (95.28 %) and ROS production (88.41 %) was observed after CC₅₀ IC RP+CC₅₀ CTX-treatment, compared to single treatments. Moreover, both combination ratios showed significant nuclear condensation compared to control cells (p=0.026 and p=0.0154) (Figure 4C).

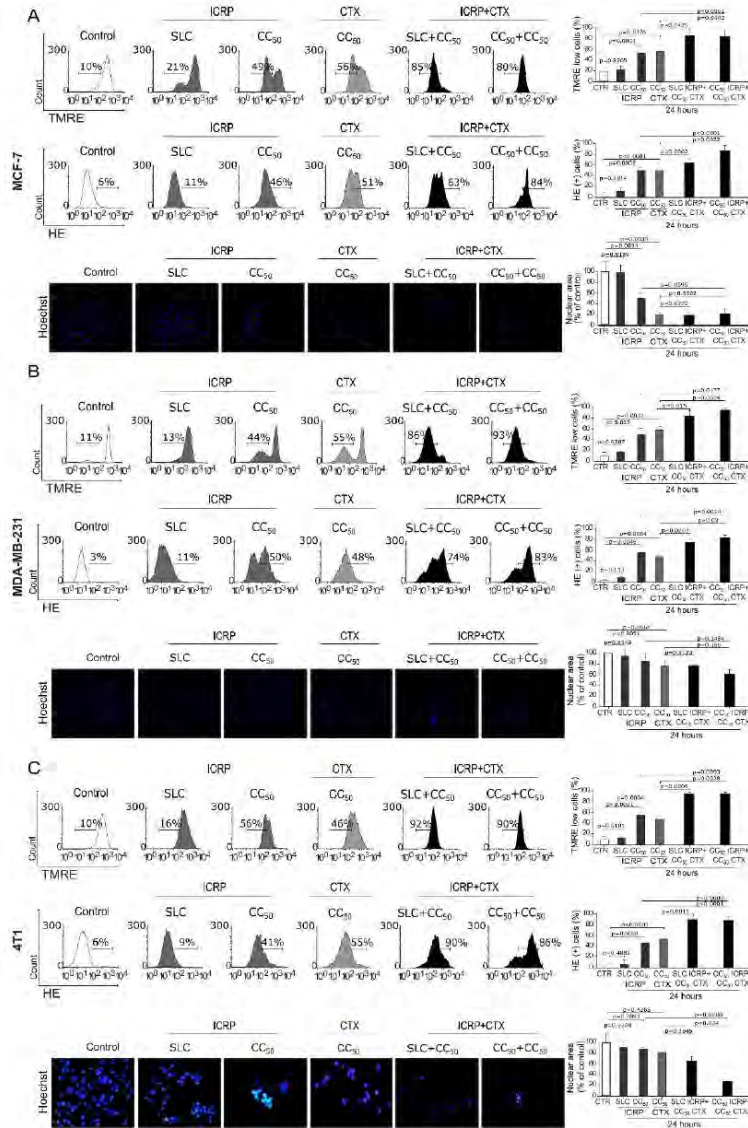


Figure 4: ICRP+CTX cell death causes morphologic and mitochondrial alterations in breast cancer cells. Cells were treated with the combination of ICRP+CTX in two different ratios for 24 h and analyzed by microscopy or flow cytometry. Representative histograms and graphs for loss of mitochondrial membrane potential and ROS production determined using TMRE and HE staining, respectively. Representative images of chromatin condensation analyzed using Hoechst staining by fluorescence microscopy in **A) MCF-7, B) MDA-MB-231 and C) 4T1** cells. The mean value of at least three independent experiments performed in triplicate \pm SD were graphed.

ICRP in combination with CTX turns cell death in a caspase-independent mechanism in breast cancer cells

After evaluation of different features involved in ICRP+CTX cytotoxicity, we investigated if caspase activation takes place during cell death induced by these combinations. As Figure 5 shows, SLC ICRP did not induce significant caspase activation, only at CC₅₀ ICRP induced 28-42 %, however, CTX induced higher caspase activation ranging from 48-77 %. When we tested the combination of SLC ICRP+CC₅₀ CTX, analysis showed no significant increase of caspase activation (78.89 % and 53.86 %) in MCF-7 and MDA-MB-231, respectively (Figure 5A), whereas 4T1 reached 81.3 % caspase activation, significantly higher compared to CTX-treated cells. Furthermore, although MCF-7 reached 89.75 % of caspase activation, a significant

increase of caspase activation was observed in MDA-MB-231 and 4T1 cells treated with CC₅₀ ICRP+CC₅₀ CTX (69.37 % and 83.22 %, respectively) in comparison with CTX monotherapy (Figure 5A). Thus, ICRP+CTX induced caspase activation at equal or increased levels than CTX as monotherapy.

As caspases were activated in combinations of ICRP plus CTX, we wondered if this type of cell death was caspase-dependent as CTX-treatment alone. Thus, we pharmacologically inhibited caspase activation using the pan-caspase inhibitor QVD. This inhibition resulted in non-significant differences in SLC ICRP+CC₅₀ CTX and CC₅₀ ICRP+CC₅₀ CTX-mediated cell death in MCF-7, MDA-MB-231 and 4T1 (Figure 5B).

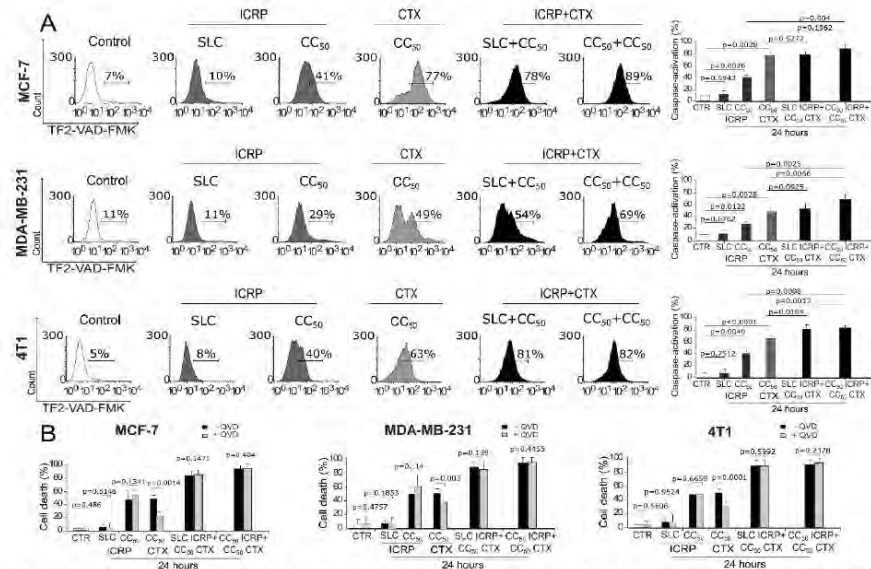


Figure 5: ICRP+CTX treatment induces cell death through a caspase-independent mechanism in breast cancer cells. Cells were treated with the combination of ICRP+CTX in two different ratios for 24 h and analyzed by flow cytometry in MCF-7, MDA-MB-231 and 4T1. **A)** Representative histograms and graphs obtained from caspase activation analysis determined by TF2-VAD-FMK staining. **B)** Cell death analyzed pre-treating MCF-7, MDA-MB-231 and 4T1, in presence or absence of caspase inhibitor (QVD, shown in light gray) using AnnV/PI staining. Graphs represent the mean value of at least three independent experiments performed in triplicate ± SD.

DISCUSSION

Cyclophosphamide is a mainstay chemotherapy for breast cancer; its mechanism of cell death has been explored in several studies, which has been associated with ROS production and caspase-dependent cell death (Emadi and Brodsky et al., 2009; de la Hoz-Camacho et al., 2022). On the other hand, Immunopotent CRP is a promising immunotherapy which modulates immune cells and induces non-apoptotic regulated cell death (caspase-independent) triggered by ROS production and involving mitochondrial and nuclear alterations in cells from cervical, lung and breast cancer cells, suggesting a conserved mechanism of cell death in solid tumors (Lorenzo-Anota et al., 2022; Martínez-Torres et al., 2018 and 2019; Reyes-Ruiz et al., 2021); however, the cytotoxic effect of ICRP in combination with chemotherapies, including CTX, against breast cancer cells was reported here for the first time.

To test the potential of ICRP to synergize CTX-cell death in breast cancer cells, we selected three BC cell lines with several molecular differences, thus, different response to treatment. MCF-7 is a model of luminal A subtype, whereas MDA-MB-231 and 4T1 cells are TNBC subtype. Our results showed that MDA-MB-231 and 4T1 cells are more sensitive to CTX than MCF-7 cells by its CC_{50} (25 mM for MDA-MB-231 and 4T1, and 30 mM for MCF-7). The response to chemotherapy was previously compared between luminal A and TNBC, indicating that even though luminal A is less sensitive to chemotherapy than TNBC, this last subtype has high probability of developing chemotherapy resistance (Harbeck et al., 2019; Parker et al., 2009).

Throughout this work, we demonstrated that ICRP synergically potentiates the cell death induced by CTX in breast cancer cells, while sparing PBMC from healthy donors. Combinations of CC_{50} CTX with other treatments such as sclareol (Scl) and resveratrol (RES) used at SLC in breast cancer cells, reached 60-70 % inhibition of cell viability

(Afshari et al., 2020; Singh et al., 2009). Remarkably, these results are different to the ones presented in this study, owing to when ICRP was used at SLC in combination with CC_{50} CTX, our results showed 86-93 % cell death in all the cell lines tested here, demonstrating the potential of ICRP in potentiating CTX-cell death, since low doses. The use of very low doses of the monotherapies in combination is an interesting approach since one of the drugs is inactive individually, but active in combination, reaching favorable outcomes, such as enhanced efficacy with decreased dosage, as we demonstrated by CI and DRI values.

On the other hand, previously it has been reported combinations of treatments at high doses (CC_{50}) such as thymoquinone (TQ) and RES, with low doses of CTX (SLC) tested in breast cancer cells. CTX at low dose significantly augmented the inhibition in cell viability induced by TQ, reaching values of 82-100 % inhibition of viability, while CTX in combination with RES resulted in modest cytotoxic activity (22 %) (Khan et al., 2019; Singh et al., 2009). In this study, CTX had variable cytotoxic effects depending on the cell line tested, ranging from 52-70 % cell death. All these results together suggest that the capacity of CTX to augment cell death, depends on the cytotoxic compound which is combined with. Nevertheless, SLC CTX maintained or increased the cell death induced by CC_{50} ICRP, depending on the cell line tested, this result reflected in the statistical analysis as synergistic or additive effect. These results could be explained by the fact that quantification of CI is based in an equation considering the biological effect of each drug according to its dose-effect curve and the fraction affected by the combination of the treatments (Chou, 2006).

The cytotoxicity induced by combinations using equipotent concentrations (CC_{50}) of CTX with Scl, RES and Naringenin (Nar), ranged 75-93 % (Afshari et al., 2020; Singh et al., 2009; Noori et al., 2020). Comparably, our results showed that CC_{50} ICRP+ CC_{50} CTX induced 91-97 % cell death, supporting

the potential of ICRP to amplify the effect of CTX.

Noteworthy, none of the studies described above are based on rigorous drug combination methods since its responses were only evaluated by statistical analysis but have not been experimentally scored as we did here. It has been suggested that drug-combination analysis using a rigorous method must be done in order to avoid errors in assessing synergism (Jia et al., 2009). Our results highlight the relevance of specifically defining the level of drug synergy by quantification methods and point out that ICRP is more efficacious in combinational therapy against breast cancer cells when used at similar or lower doses than CTX.

Additionally, to test the effect of the combination therapy on immune system cells, with human peripheral blood mononuclear cells, we demonstrated that ICRP does not augment the cytotoxicity induced by CTX, which is desirable for a combination of treatments in which one of those, is known to have high cytotoxic effects in immune system cells, such as the induced by CTX and epirubicin (EPI), another chemotherapy for the treatment of breast cancer, reported by de la Hoz-Camacho et al. (2022). Using HEK 293 (human embryonic kidney cells) and MDCK cells (Medin-Darby canine kidney), Singh et al., showed modest cytotoxicity induced by the combination of CTX with RES ranging from 5-15 % inhibition of cell viability. However, these values were higher than the induced by CTX as monotherapy in these cells (7 %) (Singh et al., 2009).

Moreover, specific mechanism of cell death has only been fully elucidated for a few of the explored drug combinations. Knowledge of the molecular mechanisms induced by combination therapy can provide clues that favor the discovery and optimization of new successful drug combinations based on a rational design (Jia et al., 2009; Pemovska et al, 2018). Previous studies have reported drug combinations with synergistic effects, most of them involving drugs with the same pathway of action, whose mechanism of

cell death is preserved by the combination of those agents (Tanaka et al., 2005; Pennati et al., 2005; Humeniuk et al., 2007).

Experimental evidence has demonstrated shared characteristics of the mechanism of cell death such as caspase activation induced by the combination of CTX with sclareol in breast cancer cells, likewise the caspase activation and caspase-mediated enhanced cell death induced by the combination of CTX with resveratrol (Afshari et al., 2020; Singh et al., 2009). Yet, we found no reports where the pathway induced by the combination of an agent that induces caspase-independent and a second agent that induces caspase-dependent cell death, switches in the mechanism of cell death activated. Most of the studies of combinations involving CTX, have demonstrated caspase-mediated enhanced cell death, for instance, the combination of resveratrol (RES) with CTX induces caspase-dependent cytotoxic activity on MCF-7 cells (Singh et al., 2009; Pang et al., 2011). Other drug-combinations induce a caspase-independent cell death mechanism in breast cancer cells, such as Mn porphyrin in combination with ascorbate which mediates caspase-independent breast cancer cell death (Evans et al., 2014). Here we found that inhibition of caspases resulted in non-significant changes in cell death induced by ICRP+CTX, suggesting that ICRP+CTX-regulated cell death is different from apoptosis. Remarkably, this finding in the caspase-independent cell death induced by ICRP+CTX occurs even when ICRP is in the lowest dose (SLC ICRP) of the combination ratio, leading us to future studies to elucidate the exact molecular mechanisms involved in this transition. Furthermore, this brings us to hypothesize that the mechanism of cell death induced by the combination of ICRP with CTX may represent an advantage in resistant-tumoral cells with defects on proteins implicated in the apoptotic pathway (Suparji et al., 2016). However, there are still many questions and additional perspectives regarding the effector of the ICRP+CTX-mediated cell death.

In conclusion, the combination of Immunepotent CRP with cyclophosphamide triggers synergistic cell death, involving loss of mitochondrial membrane potential, an increase in ROS production, caspase activation, morphological changes, and caspase-independent cell death in breast cancer cells, while ICRP did not affect CTX-cytotoxicity in PBMC, allowing to reduce the CTX doses. Overall, our results show that the combination of ICRP and CTX may be used to overcome treatment resistance (Figure 6).

Acknowledgments

ALRL, RHC and OLGA thank CONACYT for the scholarship provided.

Conflict of interest

The authors have no conflict of interest to declare.

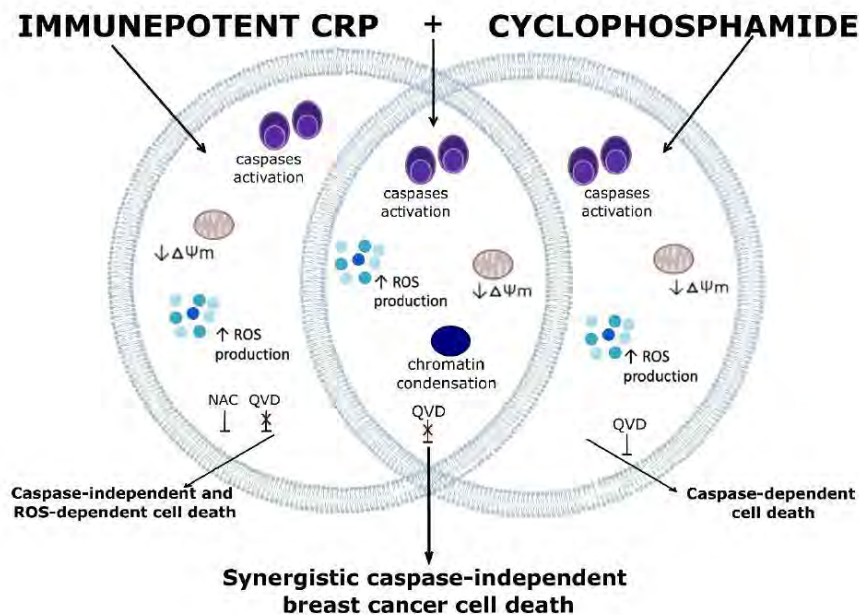


Figure 6: ICRP+CTX cell death depiction in breast cancer cells. ICRP induces caspase-independent and ROS-dependent breast cancer cell death, whereas CTX induces caspase-dependent breast cancer cell death. Here we showed that ICRP in combination with CTX induces synergistic cell death manifested with morphological changes and it involves mitochondrial alterations such as the loss of mitochondrial membrane potential and reactive oxygen species (ROS) production, and even though caspase activation occurs, ICRP+CTX cell death is caspase-independent in all the breast cancer cells assessed.

REFERENCES

- ACS, American Cancer Society. Breast cancer. Facts & Figures 2019-2020. Atlanta, GA: ACS, 2019.
- Afshari H, Nourbakhsh M, Salehi N, Mahboubi-Rabani M, Zarghi A, Noori S. STAT3-mediated apoptotic-enhancing function of sclareol against breast cancer cells and cell sensitization to cyclophosphamide. *Iran J Pharm Res.* 2020;19(1):398-412. doi: 10.22037/ijpr.2020.112587.13843.
- Apetoh L, Ladoire S, Coukos G, Ghiringhelli F. Combining immunotherapy and anticancer agents: the right path to achieve cancer cure? *Ann Oncol.* 2015;26:1813-23. doi: 10.1093/annonc/mdv209.
- Chou TC. Theoretical basis, experimental design, and computerized simulation of synergism and antagonism in drug combination studies. *Pharmacol Rev.* 2006;58:621-81. doi: 10.1124/pr.58.3.10. Erratum in: *Pharmacol Rev.* 2007;59(1):124.
- Chou T-C, Talay P. Analysis of combined drug effects: a new look at a very old problem. *TIPS.* 1983;4:450-54.
- Correia A, Silva D, Correia A, Vilanova M, Gärtner F, Vale N. Study of new therapeutic strategies to combat breast cancer using drug combinations. *Biomolecules.* 2018;8(4):175. doi: 10.3390/biom8040175.
- de la Hoz-Camacho R, Rivera-Lazarin AL, Vázquez-Guillen JM, Caballero-Hernández D, Mendoza-Gamboa E, Martínez-Torres AC, et al. Cyclophosphamide and epirubicin induce high apoptosis in microglia cells while epirubicin provokes DNA damage and microglial activation at sub-lethal concentrations. *EXCLI J.* 2022;21:197-212. doi: 10.17179/excli2021-4160.
- Emadi A, Jones RJ, Brodsky RA. Cyclophosphamide and cancer: golden anniversary. *Nat Rev Clin Oncol.* 2009;6:638-47. doi: 10.1038/nrclinonc.2009.146.
- Evans MK, Tovmasyan A, Batinic-Haberle I, Devi GR. Mn porphyrin in combination with ascorbate acts as a pro-oxidant and mediates caspase-independent cancer cell death. *Free Radic Biol Med.* 2014;68:302-14. doi: 10.1016/j.freeradbiomed.2013.11.031.
- Franco-Molina MA, Mendoza-Gamboa E, Miranda-Hernández D, Zapata-Benavides P, Castillo-León L, Isaza-Brando C, et al. In vitro effects of bovine dialyzable leukocyte extract (bDLE) in cancer cells. *Cytotherapy.* 2006;8:408-14. doi: 10.1080/14653240600847266.
- Hanahan D, Weinberg RA. Hallmarks of cancer: the next generation. *Cell.* 2011;144:646-74. doi: 10.1016/j.cell.2011.02.013.
- Harbeck N, Penault-Llorca F, Cortes J, Gnant M, Houssami N, Poortmans P, et al. Breast cancer. *Nat Rev Dis Primers.* 2019;5(1):66. doi: 10.1038/s41572-019-0111-2.
- Humeniuk R, Menon LG, Mishra PJ, Saydam G, Longo-Sorbello GS, Elisseyeff Y, et al. Aplidin synergizes with cytosine arabinoside: functional relevance of mitochondria in Aplidin-induced cytotoxicity. *Leukemia.* 2007;21:2399-405. doi: 10.1038/sj.leu.2404911.
- Ji X, Lu Y, Tian H, Meng X, Wei M, Cho WC. Chemoresistance mechanisms of breast cancer and their countermeasures. *Biomed Pharmacother.* 2019;114:108800. doi: 10.1016/j.biopha.2019.108800.
- Jia J, Zhu F, Ma X, Cao Z, Cao ZW, Li Y, et al. Mechanisms of drug combinations: interaction and network perspectives. *Nat Rev Drug Discov.* 2009;8:111-28. doi: 10.1038/nrd2683. Erratum in: *Nat Rev Drug Discov.* 2009;8(6):516.
- Khan A, Aldebasi YH, Alsuhaibani SA, Khan MA. Thymoquinone augments cyclophosphamide-mediated inhibition of cell proliferation in breast cancer cells. *Asian Pac J Cancer Prev.* 2019;20:1153-60. doi: 10.31557/APJCP.2019.20.4.1153.
- Lara HH, Turrent LI, Garza-Treviño EN, Tamez-Guerra R, Rodríguez-Padilla C. Clinical and immunological assessment in breast cancer patients receiving anticancer therapy and bovine dialyzable leukocyte extract as an adjuvant. *Exp Ther Med.* 2010;1:425-31. doi: 10.3892/etm.00000066.
- Lorenzo-Anota HY, Martínez-Torres AC, Scott-Algara D, Tamez-Guerra RS, Rodríguez-Padilla C. Bovine dialyzable leukocyte extract IMMUNEPOTENT-CRP induces selective ROS-dependent apoptosis in T-acute lymphoblastic leukemia cell lines. *J Oncol.* 2020;2020:1598503. doi: 10.1155/2020/1598503.
- Lorenzo-Anota HY, Martínez-Loria AB, Tamez-Guerra RS, Scott-Algara D, Martínez-Torres AC, Rodríguez-Padilla C. Changes in the natural killer cell repertoire and function induced by the cancer immune adjuvant candidate IMMUNEPOTENT-CRP. *Cell Immunol.* 2022; 374:104511. doi: 10.1016/j.celimm.2022.104511.
- Martínez-Torres AC, Reyes-Ruiz A, Benítez-Londoño M, Franco-Molina MA, Rodríguez-Padilla C. IMMUNEPOTENT CRP induces cell cycle arrest and caspase-independent regulated cell death in HeLa cells through reactive oxygen species production. *BMC Cancer.* 2018;18(1):13. doi: 10.1186/s12885-017-3954-5.

- Martinez-Torres AC, Gomez-Morales L, Martinez-Loria AB, Uscanga-Palomeque AC, Vazquez-Guillen JM, Rodriguez-Padilla C. Cytotoxic activity of IMMUNEPOTENT CRP against non-small cell lung cancer cell lines. *PeerJ*. 2019;7:e7759. doi: 10.7717/peerj.7759.
- Martinez-Torres AC, Reyes-Ruiz A, Calvillo-Rodriguez KM, Alvarez-Valadez KM, Uscanga-Palomeque AC, Tamez-Guerra RS, et al. IMMUNEPOTENT CRP induces DAMPS release and ROS-dependent autophagosome formation in HeLa and MCF-7 cells. *BMC Cancer*. 2020;20(1):647. doi: 10.1186/s12885-020-07124-5.
- Nedeljković M, Damjanović A. Mechanisms of chemotherapy resistance in triple-negative breast cancer-how we can rise to the challenge. *Cells*. 2019;8(9):957. doi: 10.3390/cells8090957.
- Noori S, Rezaei Tavirani M, Deravi N, Mahboobi Rabani MI, Zarghi A. naringenin enhances the anti-cancer effect of cyclophosphamide against MDA-MB-231 breast cancer cells via targeting the STAT3 signaling pathway. *Iran J Pharm Res*. 2020;19(3):122-33. doi: 10.22037/ijpr.2020.113103.14112.
- Pang H, Cai L, Yang Y, Chen X, Sui G, Zhao C. Knockdown of osteopontin chemosensitizes MDA-MB-231 cells to cyclophosphamide by enhancing apoptosis through activating p38 MAPK pathway. *Cancer Biother Radiopharm*. 2011;26:165-73. doi: 10.1089/cbr.2010.0838.
- Parker JS, Mullins M, Cheang MC, Leung S, Voduc D, Vickery T, et al. Supervised risk predictor of breast cancer based on intrinsic subtypes. *J Clin Oncol*. 2009;27:1160-7. doi: 10.1200/JCO.2008.18.1370.
- Pemovska T, Bigenzahn JW, Superti-Furga G. Recent advances in combinatorial drug screening and synergy scoring. *Curr Opin Pharmacol*. 2018;42:102-10. doi: 10.1016/j.coph.2018.07.008.
- Pennati M, Campbell AJ, Curto M, Binda M, Cheng Y, Wang LZ, et al. Potentiation of paclitaxel-induced apoptosis by the novel cyclin-dependent kinase inhibitor NU6140: a possible role for survivin down-regulation. *Mol Cancer Ther*. 2005;4:1328-37. doi: 10.1158/1535-7163.MCT-05-0022.
- Rasmussen L, Arvin A. Chemotherapy-induced immunosuppression. *Environ Health Perspect*. 1982;43:21-5. doi: 10.1289/ehp.824321.
- Reyes-Ruiz A, Calvillo-Rodriguez KM, Martínez-Torres AC, Rodríguez-Padilla C. The bovine dialysable leukocyte extract IMMUNEPOTENT CRP induces immunogenic cell death in breast cancer cells leading to long-term antitumour memory. *Br J Cancer*. 2021;124:1398-410. doi: 10.1038/s41416-020-01256-y.
- Rodríguez-Salazar MDC, Franco-Molina MA, Mendoza-Gamboa E, Martínez-Torres AC, Zapata-Benavides P, López-González JS, et al. The novel immunomodulator IMMUNEPOTENT CRP combined with chemotherapy agent increased the rate of immunogenic cell death and prevented melanoma growth. *Oncol Lett*. 2017;14:844-852. doi: 10.3892/ol.2017.6202.
- Santana-Krimskaya SE, Franco-Molina MA, Zárate-Triviño DG, Prado-García H, Zapata-Benavides P, Torres-del-Muro F, et al. IMMUNEPOTENT CRP plus doxorubicin/cyclophosphamide chemotherapy remodel the tumor microenvironment in an air pouch triple-negative breast cancer murine model. *Biomed Pharmacother*. 2020;126:110062. doi: 10.1016/j.biopha.2020.110062.
- Singh N, Nigam M, Ranjan V, Sharma R, Balapure AK, Rath SK. Caspase mediated enhanced apoptotic action of cyclophosphamide- and resveratrol-treated MCF-7 cells. *J Pharmacol Sci*. 2009;109:473-85. doi: 10.1254/jphs.08173fp.
- Suparji NS, Chan G, Sapili H, Arshad NM, In LL, Awang K, et al. Geranylated 4-phenylcoumarins exhibit anticancer effects against human prostate cancer cells through caspase-independent mechanism. *PLoS One*. 2016;11(3):e0151472. doi: 10.1371/journal.pone.0151472.
- Tait S, Green D. Caspase-independent cell death: leaving the set without the final cut. *Oncogene*. 2008;27:6452-61. doi: 10.1038/onc.2008.311.
- Tanaka R, Ariyama H, Qin B, Shibata Y, Takii Y, Kusaba H, et al. Synergistic interaction between oxaliplatin and SN-38 in human gastric cancer cell lines in vitro. *Oncol Rep*. 2005;14:683-8. doi: 10.3892/or.14.3.683.

1.2 Synergistic Enhancement of Chemotherapy-Induced Cell Death and Antitumor Efficacy Against Tumoral T-Cell Lymphoblasts by IMMUNEPOTENT CRP, a Bovine Dialyzable Leukocyte Extract



Article

Synergistic Enhancement of Chemotherapy-Induced Cell Death and Antitumor Efficacy against Tumoral T-Cell Lymphoblasts by IMMUNEPOTENT CRP

Ana Luisa Rivera-Lazarín ¹, Kenny Misael Calvillo-Rodríguez ^{1,†}, Mizaël Izaguirre-Rodríguez ^{1,†}, José Manuel Vázquez-Guillén ¹, Ana Carolina Martínez-Torres ^{1,*} and Cristina Rodríguez-Padilla ^{1,2,‡}

¹ Laboratorio de Inmunología y Virología, Facultad de Ciencias Biológicas, Universidad Autónoma de Nuevo León, San Nicolás de los Garza 66455, Mexico

² LONGEVEDEN S.A. De C.V., Guadalupe 67199, Mexico

* Correspondence: ana.martinezto@uanl.edu.mx; Tel.: +52-8121-4115; Fax: +52-81-8352-4212

[†] These authors contributed equally to this work.

[‡] Equal co-seniorship.



Citation: Rivera-Lazarín, A.L.; Calvillo-Rodríguez, K.M.; Izaguirre-Rodríguez, M.; Vázquez-Guillén, J.M.; Martínez-Torres, A.C.; Rodríguez-Padilla, C. Synergistic Enhancement of Chemotherapy-Induced Cell Death and Antitumor Efficacy against Tumoral T-Cell Lymphoblasts by IMMUNEPOTENT CRP. *Int. J. Mol. Sci.* **2024**, *25*, 7938. <https://doi.org/10.3390/ijms25147938>

Academic Editors: Peter J. K. Kuppen and Luca Lo Nigro

Received: 11 May 2024

Revised: 16 July 2024

Accepted: 18 July 2024

Published: 20 July 2024



Copyright: © 2024 by the authors. Licensee MDPI, Basel, Switzerland. This article is an open access article distributed under the terms and conditions of the Creative Commons Attribution (CC BY) license (<https://creativecommons.org/licenses/by/4.0/>).

Abstract: T-cell malignancies, including T-cell acute lymphoblastic leukemia (T-ALL) and T-cell lymphoblastic lymphoma (T-LBL), present significant challenges to treatment due to their aggressive nature and chemoresistance. Chemotherapies remain a mainstay for their management, but the aggressiveness of these cancers and their associated toxicities pose limitations. Immunepotent CRP (ICRP), a bovine dialyzable leukocyte extract, has shown promise in inducing cytotoxicity against various cancer types, including hematological cancers. In this study, we investigated the combined effect of ICRP with a panel of chemotherapies on cell line models of T-ALL and T-LBL (CEM and L5178Y-R cells, respectively) and its impact on immune system cells (peripheral blood mononuclear cells, splenic and bone marrow cells). Our findings demonstrate that combining ICRP with chemotherapies enhances cytotoxicity against tumoral T-cell lymphoblasts. ICRP + Cyclophosphamide (CTX) cytotoxicity is induced through a caspase-, reactive oxygen species (ROS)-, and calcium-dependent mechanism involving the loss of mitochondrial membrane potential, an increase in ROS production, and caspase activation. Low doses of ICRP in combination with CTX spare non-tumoral immune cells, overcome the bone marrow-induced resistance to CTX cell death, and improves the CTX antitumor effect in vivo in syngeneic Balb/c mice challenged with L5178Y-R. This led to a reduction in tumor volume and a decrease in Ki-67 proliferation marker expression and the granulocyte/lymphocyte ratio. These results set the basis for further research into the clinical application of ICRP in combination with chemotherapeutic regimens for improving outcomes in T-cell malignancies.

Keywords: ICRP; chemotherapy; synergism; apoptosis; bone marrow

1. Introduction

T-cell malignancies comprise a group of neoplasms that arise from the expansion of dysfunctional T-cells at different stages of development. T-cell acute lymphoblastic leukemia (T-ALL) is the most common T-cell cancer in children. In contrast, T-cell lymphoblastic lymphoma (T-LBL) accounts for 20% of the non-Hodgkin lymphoma cases in children. Studies have lent strength to the theory that T-LBL and T-ALL may evolve from a common malignant precursor cell [1,2]; moreover, both diseases are aggressive forms of hematological cancers since T-cell's overall prognosis is poorer than B-cell malignancies [3,4]. Chemotherapies, such as cyclophosphamide (CTX), etoposide (ETO), and anthracyclines such as doxorubicin (DOX) and epirubicin (EPI) remain a potential strategy for T-ALL/T-LBL [5–9]. Several chemotherapies act primarily through the induction of apoptosis beyond distinct targets for these agents in susceptible cancer cells [10]. Also, in

high doses, they cause severe secondary effects, such as bone marrow suppression, spleen toxicity [5–9], cognitive impairment, and microglial death [7].

Managing treatment during disease recurrence remains challenging due to chemoresistance, which arises from various mechanisms, including the inherent sensitivity of cancer cells to evade cell death [5,11,12]. Therefore, efforts to overcome resistance have pointed out the use of multi-targeted agents through the assessment of drug combinations, guided by an understanding of the molecular mechanisms underlying cell death. In this regard, recent studies highlighted the advances and the growing relevance of simultaneously blocking multiple pathogenic pathways in B-cell malignancies and lymphoma [13,14]. The multiple targets can belong to the same or different pathways of cell death that converge at a pathway site, resulting in an enhanced effect. Combination therapy works in a synergistic, additive, or antagonistic manner depending on the amount of the drug combination effect, which can be quantified by several models [15]. A substantial amount of evidence uses the combination index (CI) analysis proposed by Chou-Talay, which mitigates uncertainties in identifying effective combination treatments by enabling the scoring of synergistic drug effects [16,17]. Multiple reports provide evidence of combining chemotherapies and immunotherapies [18], which enables a reduction in the toxic effects on healthy cells and enhances efficacy against cancer cells at lower dosages, potentially overcoming chemo-resistance [19].

Immunopotent CRP (ICRP), a bovine dialyzable leukocyte extract, is an immunotherapy reported to exhibit immunomodulatory properties and cytotoxicity against several cancer cell lines [20,21]. The combinational therapy of ICRP with DOX and CTX modified the tumor microenvironment in a murine breast cancer model [22]. Furthermore, the combination of ICRP and oxaliplatin (OXP), induced immunogenic cell death (ICD) in murine melanoma [23]. ICRP was also reported to improve the clinical parameters of breast cancer patients receiving standard chemotherapy [24]. Therefore, ICRP shows potential when combined with various chemotherapies, including CTX, a major chemotherapy used for hematologic malignancies. Thus, in the present study, we investigated the combinatorial effects of a panel of chemotherapies and ICRP treatment on two T-cell malignancies, T-ALL and T-LBL c, chosen for their aggressive nature, poor prognosis, response to therapy, and chemoresistance, focusing on the mechanism of the CTX-ICRP combination and its *in vivo* effects.

2. Results

2.1. ICRP, CTX, DOX, EPI, and ETO Induce Tumoral T-Cell Lymphoblasts Cell Death

CEM and L5178Y-R death was analyzed after ICRP (dark gray) or chemotherapy (light gray) treatment. Results showed that all treatments augment tumoral T-cell lymphoblast cell death as treatment concentration increases (Figure 1A–E). Data show cell death of 20% of the cells (CC_{20}) at 0.2 and 0.15 U/mL of ICRP for CEM and L5178Y-R cells, respectively, meanwhile 50% of the cells were dead (CC_{50}) at 0.6 and 0.3 U/mL of ICRP (Figure 1A), respectively. On the other hand, CTX CC_{20} was 15 mM for both cell lines while 20 mM CTX was required to induce cell death in 50% of the cell population for both cell lines (Figure 1B). Likewise, DOX CC_{20} was shown at 5 μ M for CEM and 10 μ M for L5178Y-R, whereas DOX CC_{50} was shown at 15 μ M for both cell lines (Figure 1C). Furthermore, EPI CC_{20} was 30 μ M for CEM and 3 μ M for L5178Y-R, whereas EPI CC_{50} was obtained at 40 μ M for CEM and 12 μ M for L5178Y-R (Figure 1D). Additionally, 20 μ M and 40 μ M ETO were the CC_{20} , while 100 μ M and 200 μ M ETO were the CC_{50} of CEM and L5178Y-R, respectively (Figure 1E). CC_{20} and CC_{50} cytotoxic concentrations were found and the sublethal concentration was taken as the highest concentration of each treatment that does not induce notable cell death, for each cell line and treatment. These concentrations are summarized in the table shown in Figure 1F.

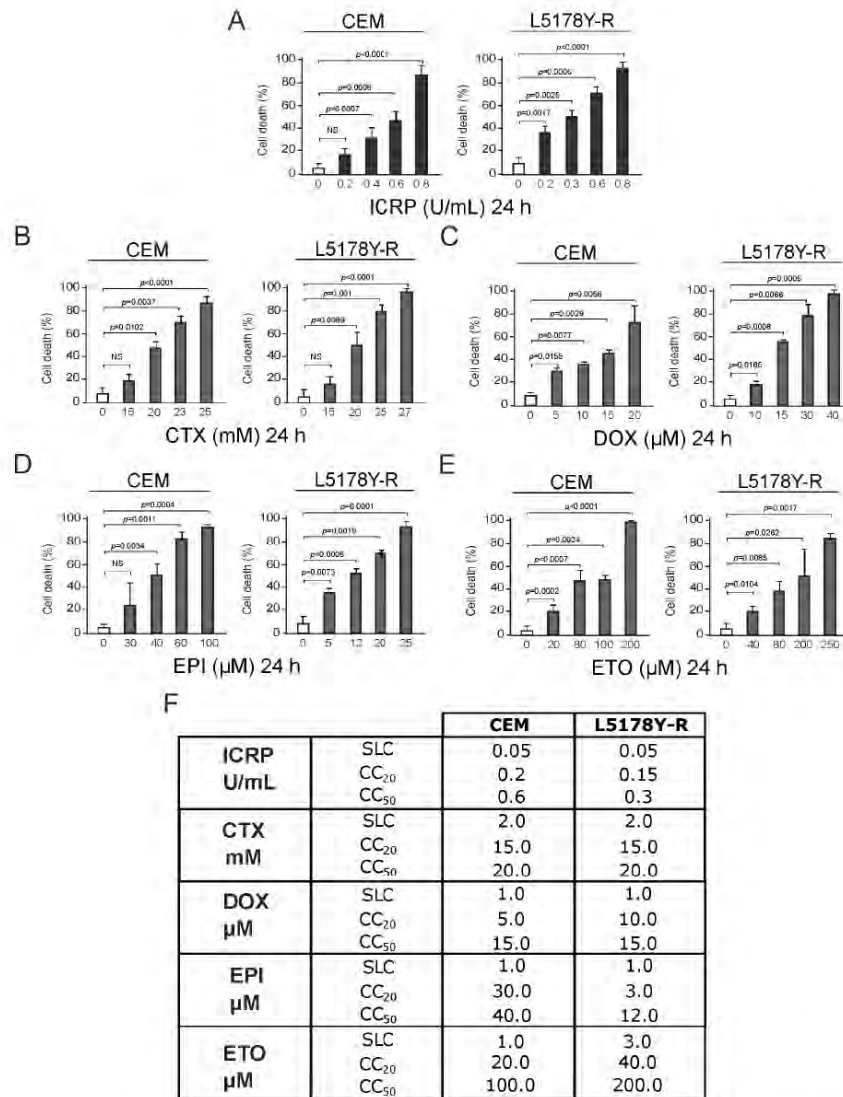


Figure 1. ICRP, CTX, DOX, EPI, and ETO induce cell death in tumoral T-cell lymphoblasts. CEM and L5178Y-R cell lines were treated for 24 h, and biochemical features of cell death were assessed and expressed in percentage (%). Cell death was analyzed by Annexin V/PI staining for (A) ICRP-, (B) CTX-, and (E) ETO-treated cells or only AnnV for (C) DOX and (D) EPI treatments. (F) Sublethal concentration (SLC), cytotoxic concentration that induced cell death of 20% of the cells (CC₂₀) and cytotoxic concentration that induced cell death of 50% of the cells (CC₅₀) found for IMMUNEPOTENT CRP (ICRP), Cyclophosphamide (CTX), Doxorubicin (DOX), Epirubicin (EPI) and Etoposide (ETO) are summarized for CEM and L5178Y-R cell lines. Graphs are the means ± SD of triplicates from at least three independent experiments. NS was assigned to $p > 0.05$.

Although chemotherapies have different mechanisms of action, we proposed that a potentiated cytotoxic effect could be achieved by combining them with ICRP.

2.2. The Combination of ICRP and Chemotherapies Potentiates Cell Death against Tumoral T-Cell Lymphoblasts

Different combination ratios were designed for investigating the effect of several concentrations of ICRP on chemotherapies' cytotoxicity. The chemotherapies for combination studies were chosen from a panel of chemotherapies (with different mechanisms of action such as alkylating agents and topoisomerase inhibitors) that were able to directly induce cell death as monotherapies in the cell lines tested. In contrast, we discarded the antimetabolites Ara-C and Methotrexate as they were unable to induce 50% cell death in L5178Y cells (Figure S1). First, we used a non-cytotoxic concentration (SLC, sublethal) of ICRP, in combination with the CTX, DOX, EPI, and ETO – CC_{50} of each tumoral T-cell lymphoblasts cell line. To investigate whether chemotherapies affect ICRP cell death, we tested the combination of CC_{50} ICRP with SLC CTX, DOX, EPI, and ETO. To examine the combined effect of equipotent concentrations of both treatments, we tested the combination of CC_{20} of ICRP and CTX or the combination of CC_{50} of both treatments. Moreover, to investigate whether ICRP at a low dose affects chemotherapies' cell death, we treated cells with CC_{20} ICRP + CC_{50} CTX, DOX, EPI, and ETO.

As Figure 2A shows, a significant increase in CEM and L5178Y-R cell death compared to single agents was observed, reaching 85% and 96%, respectively, when combining SLC ICRP + CC_{50} CTX. Results showed a non-significant cell death increase in CEM with the combination of CC_{50} ICRP + SLC CTX, whereas this combination induced a significant increase in L5178Y-R death reaching 69% and 77% cell death, respectively. Cell death assessment showed that CC_{20} ICRP + CC_{20} CTX reached 91% cell death in CEM and L5178Y-R. Likewise, CC_{50} ICRP + CC_{50} CTX showed a significant increase in cell death compared to single treatments, reaching 98% and 95% in CEM and L5178Y-R, respectively, and the combination using CC_{20} ICRP + CC_{50} CTX demonstrated 98% cell death in the two cell lines tested. Furthermore, Figure 2B shows that SLC ICRP + CC_{50} DOX demonstrated a significant increase in CEM cell death compared to single treatments, reaching 93%, whereas L5178Y-R showed no significant increase, reaching 59% cell death. The combination using CC_{50} ICRP + SLC DOX induced 50% cell death in CEM and L5178Y-R. A significant increase in CEM and L5178Y-R cell death compared to single agents was observed, reaching 40% and 43%, respectively, when combining CC_{20} ICRP + CC_{20} DOX. When the combination of CC_{50} ICRP + CC_{50} DOX was used we observed a significant cell death increase in CEM, reaching 94%, whereas this combination reached 58% in L5178Y-R cells. The assessment revealed a significant increase in cell death to 97% in CEM when combining CC_{20} ICRP + CC_{50} DOX. Conversely, this combination showed a non-significant increase in cell death in L5178Y-R cells, with 52%.

Moreover, as shown in Figure 2C, a significant increase in cell death occurs when combining SLC ICRP + CC_{50} EPI, demonstrating 81% and 96% cell death in CEM and L5178Y-R, respectively. Results showed a significant cell death augmentation in CEM with the combination of CC_{50} ICRP + SLC EPI reaching 59%, while this combination in L5178Y-R reached 60%. Cell death assessment induced by CC_{20} ICRP + CC_{20} EPI showed a significant increase compared to single treatments, reaching 89% and 46% in CEM and L5178Y-R, respectively. Likewise, CC_{50} ICRP + CC_{50} EPI showed 87% and 91% cell death in CEM and L5178Y-R, respectively, and the combination using CC_{20} ICRP + CC_{50} EPI demonstrated 97% cell death in CEM and 99% in L5178Y-R.

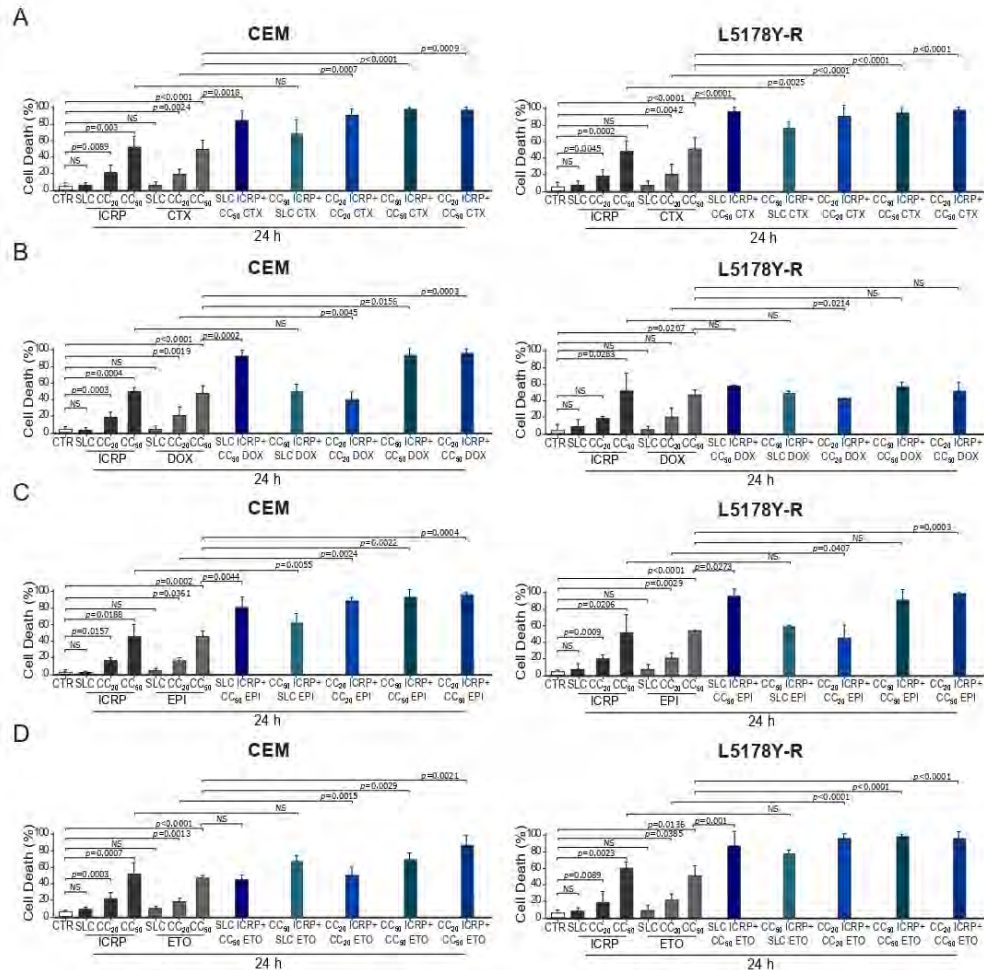


Figure 2. ICRP + chemotherapy-induced cell death in tumoral T-cell lymphoblasts. (A–D) CEM and L5178Y-R were treated for 24 and analyzed by flow cytometry using Ann/PI staining or Ann alone for DOX and EPI. Cell death induced by (A) ICRP, CTX, and its combination, (B) ICRP, DOX, and its combination, (C) ICRP, EPI, and its combination, and (D) ICRP, ETO, and its combination. Graphs are the means \pm SD of triplicates from at least three independent experiments. NS was assigned to $p > 0.05$.

Additionally, Figure 2D shows that SLC ICRP + CC₅₀ ETO showed a non-significant increase in CEM cell death compared to ETO alone, reaching 45%, whereas L5178Y-R showed a significant increase, reaching 88% cell death. The combination using CC₅₀ ICRP + SLC ETO demonstrated an increase in cell death with 68% and 82% values in CEM and L5178Y-R, respectively. When combining CC₂₀ ICRP + CC₂₀ ETO, a significant increase in CEM and L5178Y-R cell death was observed compared to single agents, reaching 51% and 95%, respectively. Results showed a significant cell death augmentation in the two cell lines

tested when the combination of CC₅₀ ICRP + CC₅₀ ETO was used, reaching 70% in CEM and 93% in L5178Y-R. Finally, the assessment showed a significant increase in cell death to 87% in CEM and 96% in L5178Y-R when combining CC₂₀ ICRP + CC₅₀ ETO.

2.3. The Combination of ICRP with Chemotherapy Induces a Synergistic Cytotoxic Effect Allowing a Reduction in Chemotherapy Doses

To correctly define whether the combined effect is superior to the single drugs, we used the combination index (CI) to quantify the drug interaction effect induced by ICRP in combination with each chemotherapy by the software Compusyn. Table 1 shows the CI values obtained from all the tested combinations, revealing a synergistic effect (CI < 1) by all the chemotherapies and ratios tested. Nevertheless, the highest synergic effect, according to the CI values shown in both cell lines, was obtained from the combinations of ICRP with CTX.

Table 1. CI values compilation from the combinations of ICRP with chemotherapies in tumoral T-cell lymphoblasts.

| Cytotoxic Concentration | | Combination Index (CI) | | | |
|-------------------------|------------------|------------------------|----------------|----------|----------------|
| ICRP | CTX | CEM | Interpretation | L5178Y-R | Interpretation |
| SLC | CC ₅₀ | 0.13084 | Synergism | 0.03732 | Synergism |
| CC ₂₀ | CC ₂₀ | 0.11256 | Synergism | 0.11560 | Synergism |
| CC ₂₀ | CC ₅₀ | 0.03383 | Synergism | 0.02743 | Synergism |
| CC ₅₀ | SLC | 0.38717 | Synergism | 0.28102 | Synergism |
| CC ₅₀ | CC ₅₀ | 0.02802 | Synergism | 0.09422 | Synergism |
| ICRP | DOX | CEM | Interpretation | L5178Y-R | Interpretation |
| SLC | CC ₅₀ | 0.08249 | Synergism | 0.45562 | Synergism |
| CC ₂₀ | CC ₂₀ | 0.99682 | Synergism | 0.96383 | Synergism |
| CC ₂₀ | CC ₅₀ | 0.05606 | Synergism | 0.94297 | Synergism |
| CC ₅₀ | SLC | 0.54866 | Synergism | 0.79139 | Synergism |
| CC ₅₀ | CC ₅₀ | 0.11558 | Synergism | 0.96751 | Synergism |
| ICRP | EPI | CEM | Interpretation | L5178Y-R | Interpretation |
| SLC | CC ₅₀ | 0.06456 | Synergism | 0.08965 | Synergism |
| CC ₂₀ | CC ₂₀ | 0.08239 | Synergism | 0.86136 | Synergism |
| CC ₂₀ | CC ₅₀ | 0.02441 | Synergism | 0.00745 | Synergism |
| CC ₅₀ | SLC | 0.47013 | Synergism | 0.76424 | Synergism |
| CC ₅₀ | CC ₅₀ | 0.06537 | Synergism | 0.01220 | Synergism |
| ICRP | ETO | CEM | Interpretation | L5178Y-R | Interpretation |
| SLC | CC ₅₀ | 0.69184 | Synergism | 0.06804 | Synergism |
| CC ₂₀ | CC ₂₀ | 0.47243 | Synergism | 0.02997 | Synergism |
| CC ₂₀ | CC ₅₀ | 0.03856 | Synergism | 0.03988 | Synergism |
| CC ₅₀ | SLC | 0.23747 | Synergism | 0.30940 | Synergism |
| CC ₅₀ | CC ₅₀ | 0.26008 | Synergism | 0.01571 | Synergism |

CI < 1 represents synergism; CI = 1 is additive effect; and CI > 1 indicates antagonism.

Furthermore, when looking for a decreasing toxicity in single drugs, as the combined effect is higher than monotherapy, we calculated the degree of chemotherapy dosage reduction by drug reduction index (DRI). All the chemotherapies tested showed DRI values above 1 reaching up to 1724.07, indicating a favorable dose reduction. DRI values are summarized in Table 2.

Considering CTX demonstrated the greatest synergistic effect across both cell lines and a favorable reduction in DRI values, combinations involving SLC ICRP + CC₅₀ CTX, CC₅₀ ICRP + CC₅₀ CTX and CC₂₀ ICRP + CC₅₀ CTX combinations were chosen to further determine several biochemical features of ICRP + CTX cell death, assessing the main characteristics elicited by each monotherapy.

Table 2. DRI values compilation from the combinations of ICRP with chemotherapies in tumoral T-cell lymphoblasts.

| Cytotoxic Concentration | | Drug Reduction Index (DRI) for the Chemotherapies | | | |
|-------------------------|------------------|---|----------------|----------|----------------|
| ICRP | CTX | CEM | Interpretation | L5178Y-R | Interpretation |
| SLC | CC ₅₀ | 8.42954 | Favorable | 31.1687 | Favorable |
| CC ₂₀ | CC ₂₀ | 17.5163 | Favorable | 18.5702 | Favorable |
| CC ₂₀ | CC ₅₀ | 54.1691 | Favorable | 67.9464 | Favorable |
| CC ₅₀ | SLC | 34.3030 | Favorable | 39.9607 | Favorable |
| CC ₅₀ | CC ₅₀ | 80.3531 | Favorable | 24.2353 | Favorable |
| ICRP | DOX | CEM | Interpretation | L5178Y-R | Interpretation |
| SLC | CC ₅₀ | 12.9454 | Favorable | 2.58459 | Favorable |
| CC ₂₀ | CC ₂₀ | 2.29273 | Favorable | 1.92477 | Favorable |
| CC ₂₀ | CC ₅₀ | 27.4377 | Favorable | 1.94132 | Favorable |
| CC ₅₀ | SLC | 24.6198 | Favorable | 25.6457 | Favorable |
| CC ₅₀ | CC ₅₀ | 15.6821 | Favorable | 2.48874 | Favorable |
| ICRP | EPI | CEM | Interpretation | L5178Y-R | Interpretation |
| SLC | CC ₅₀ | 20.4730 | Favorable | 14.0321 | Favorable |
| CC ₂₀ | CC ₂₀ | 71.7907 | Favorable | 2.87026 | Favorable |
| CC ₂₀ | CC ₅₀ | 340.605 | Favorable | 369.487 | Favorable |
| CC ₅₀ | SLC | 194.782 | Favorable | 14.4692 | Favorable |
| CC ₅₀ | CC ₅₀ | 133.968 | Favorable | 369.487 | Favorable |
| ICRP | ETO | CEM | Interpretation | L5178Y-R | Interpretation |
| SLC | CC ₅₀ | 1.59690 | Favorable | 21.5251 | Favorable |
| CC ₂₀ | CC ₂₀ | 13.5184 | Favorable | 1139.71 | Favorable |
| CC ₂₀ | CC ₅₀ | 280.660 | Favorable | 171.687 | Favorable |
| CC ₅₀ | SLC | 1582.31 | Favorable | 507.816 | Favorable |
| CC ₅₀ | CC ₅₀ | 19.9247 | Favorable | 1724.07 | Favorable |

DRI < 1 represents not favorable dose reduction; DRI = 1 is not dose reduction; and DRI > 1 indicates favorable dose reduction.

2.4. The Combination of ICRP with CTX Induces Mitochondrial Alterations in Tumoral T-Cell Lymphoblasts

The right panel of Figure 3A shows a significant increase in the loss of mitochondrial membrane potential assessment by SLC ICRP + CC₅₀ CTX in CEM and L5178Y-R reaching 75% and 82%, respectively, whereas L5178Y-R also showed a significant increase with CC₅₀ ICRP + CC₅₀ CTX and CC₂₀ ICRP + CC₅₀ CTX-treatment (86–88%) compared to CTX monotherapy. Likewise, CEM CC₂₀ ICRP + CC₅₀ CTX-treated cells showed 55% ROS production, and L5178Y-R at all the combination ratios showed a significant increase in ROS production compared to CTX alone, demonstrated by up to 82% HE+ cells (Figure 3B). Additionally, a significant increase in caspase activation was observed after SLC ICRP + CC₅₀ CTX, CC₅₀ ICRP + CC₅₀ CTX, and CC₂₀ ICRP + CC₅₀ CTX treatment in CEM and L5178Y-R, compared to single agents (Figure 3C).

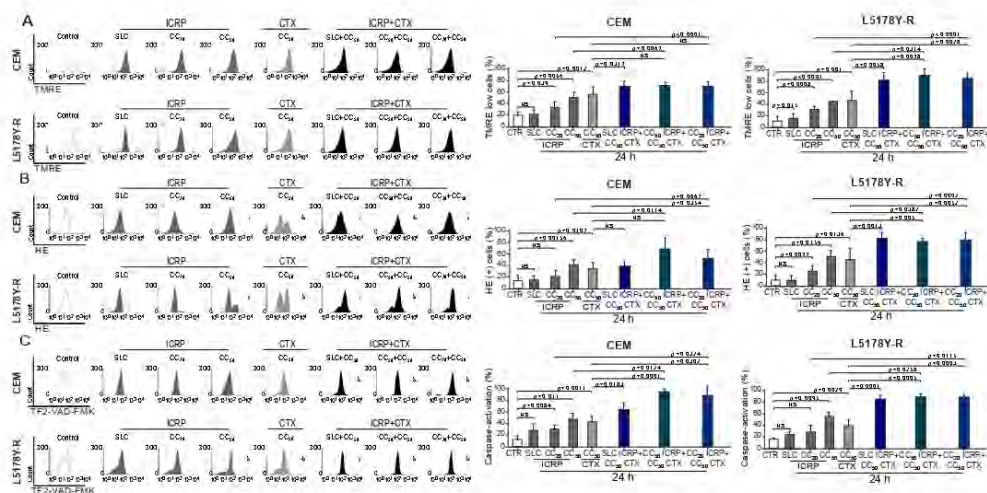


Figure 3. ICRP + CTX cell death-induced mitochondrial alterations in tumoral T-cell lymphoblasts. Cells were treated with ICRP + CTX in distinct ratios for 24 h and analyzed by flow cytometry. Representative histograms and graphs from (A) loss of mitochondrial membrane potential, (B) ROS production, and (C) caspase activation measured using TMRE, HE, and TF2-VAD-FMK staining, respectively, in CEM and L5178Y-R. Graphs are the means \pm SD of triplicates from at least three independent experiments. NS was assigned to $p > 0.05$.

2.5. The Combination of ICRP with CTX Induces Cell Death Involving Caspases, ROS Production, and Calcium Augmentation in Tumoral T-Cell Lymphoblasts

We aimed to investigate the effectors of ICRP + CTX cell death. For this, we analyzed the caspase dependence using the pan-caspase inhibitor QVD. We found that QVD diminished cell death induced by CC_{50} ICRP and CC_{50} CTX in the two cell lines; also in CEM, QVD diminished the cell death in the different combination ratios tested. Whereas, in L5178Y-R, QVD inhibited cell death when cells were treated with SLC ICRP + CC_{50} CTX and CC_{50} ICRP + CC_{50} CTX, but not with the combination CC_{20} ICRP + CC_{50} CTX (Figure 4A). Furthermore, after using the antioxidant NAC, cell death diminished significantly when cells were treated with all the combination ratios tested in both cell lines (Figure 4B). Additionally, pre-treatment with the extracellular calcium chelator BAPTA decreased cell death induced by CC_{50} ICRP and CC_{50} CTX, as well as all the combination ratios tested in both cell lines (Figure 4C).

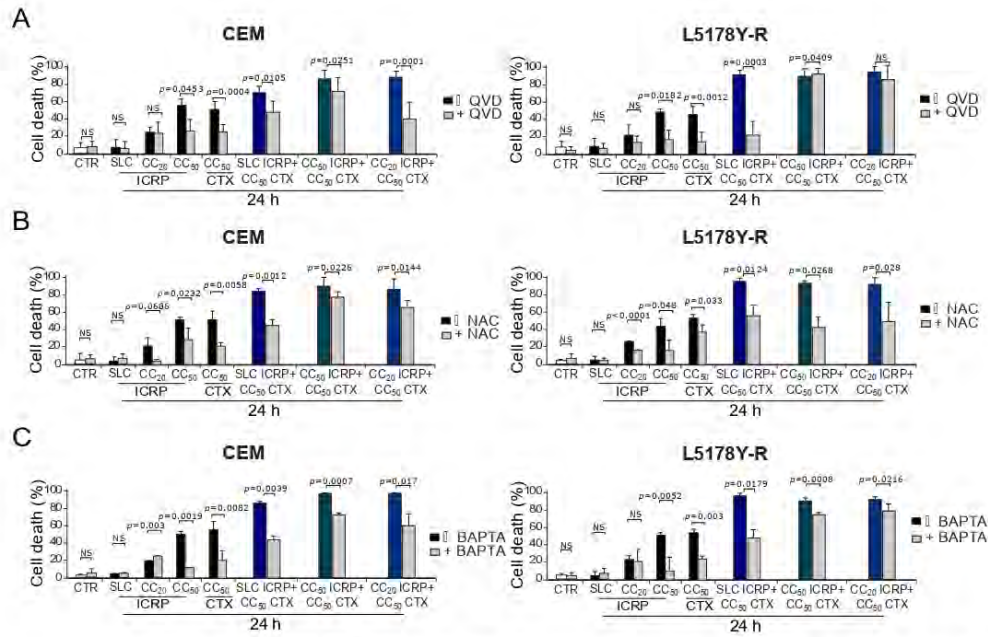


Figure 4. ICRP + CTX cell death effectors in tumoral T-cell lymphoblasts. Cells were treated with (A) QVD, (B) NAC, or (C) BAPTA for 30 min before treatment with ICRP + CTX in distinct ratios for 24 h, and cell death was analyzed by flow cytometry. Graphs from AnnV/PI measurement of CEM (left panel) and L5178Y-R (right panel). Bars are the means \pm SD of triplicates from at least three independent experiments. NS was assigned to $p > 0.05$.

2.6. The Combination of ICRP with CTX Does Not Potentiate CTX Cell Death in Non-Tumoral Immune System Cells and Protects Bone Marrow Cells from CTX Cell Death

To evaluate if the combination of ICRP with CTX could also potentiate the cytotoxicity of non-tumoral immune system cells, we chose the highest cytotoxic concentration used in the tumoral cells to investigate the cytotoxicity of this combination in peripheral blood mononuclear cells (PBMC), splenocytes, and bone marrow cells. As Figure 5 shows, ICRP is not cytotoxic to PBMC (Figure 5A), spleen (Figure 5B), and bone marrow cells (Figure 5C) as only a low relative cell viability reduction was observed at CC₅₀ ICRP of CEM (0.6 U/mL, 17% reduction). In contrast, CC₅₀ CTX (20 mM) induced a strong reduction in cell viability in all the non-tumoral immune system cells, ranging from 57% to 94% reduction. Interestingly, any of the combination ratios tested increased this reduction in cell viability. Importantly, we observed a significant increase in the relative cell viability of bone marrow cells when treated with all the combination ratios tested, compared to CTX alone. This indicates that ICRP protects against cell death in bone marrow cells.

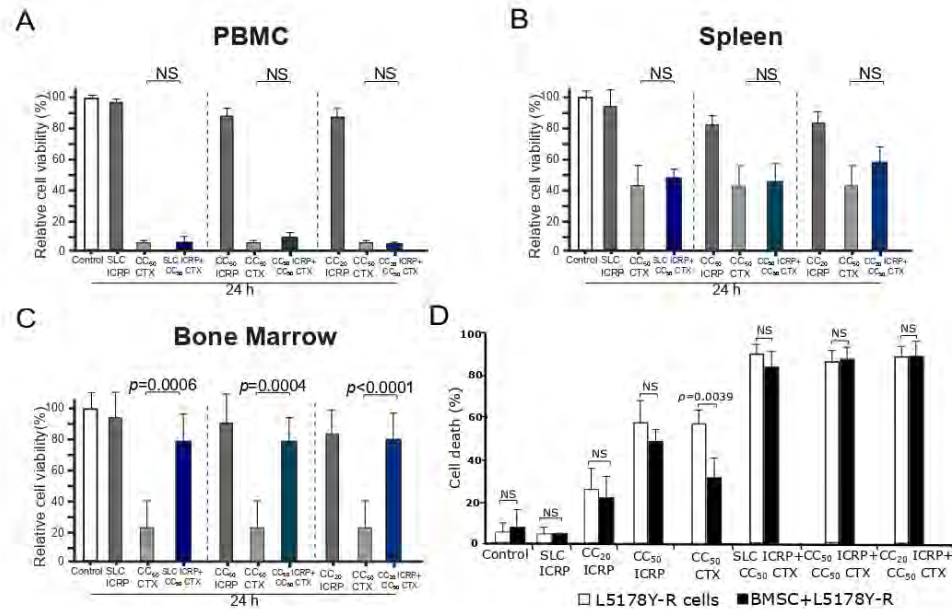


Figure 5. ICRP + CTX cell death in non-tumoral immune system cells and tumoral cells in the presence of BMSC environment. PBMC (A), spleen (B), and bone marrow cells (C) were treated for 24 h with ICRP, CTX, and their combination, analyzed by flow cytometry using Ann V/PI staining, and expressed as relative cell viability by the exclusion of Ann V/PI positive cells considering control cells as 100% cell viability. (D) Cell death induced by ICRP, CTX, and its combination in L5178Y-R co-cultivated with bone marrow stromal cells (BMSC) and analyzed by flow cytometry. NS was assigned to $p > 0.05$.

2.7. The Combination of ICRP with CTX Overcomes Cell Death Resistance Induced by Bone Marrow Stromal Cells

Next, we assessed whether ICRP + CTX-induced cell death could be protected by the survival stimuli provided by the bone marrow microenvironment [25]. In Figure 5D, while cell death induced by CC₂₀ and CC₅₀ ICRP persisted even when L5178Y-R were cocultured with BMSC, the presence of BMSC inhibited cell death in CTX-treated cells. In contrast, the cell death induced by the combination of ICRP + CTX remained unchanged even when using SL concentrations of ICRP (Figure 5D).

2.8. The Combination of ICRP with CTX Has an Antitumor Effect against T-Cell Lymphoma

As Figure 6A shows, female L5178Y-R-bearing mice were treated with a low dose of ICRP, CTX, and their combination. Treatment with two units of ICRP every two days led to a moderate decrease in tumor volume, whereas weekly injections of 125 mg/kg CTX resulted in a significant decrease in tumor volume compared to the control (vehicle-treated group). However, when the low dose of ICRP was combined with CTX, tumor volume significantly diminished compared to CTX monotherapy. This reduction in tumor volume is consistent with the tumor size shown in Figure 6B.

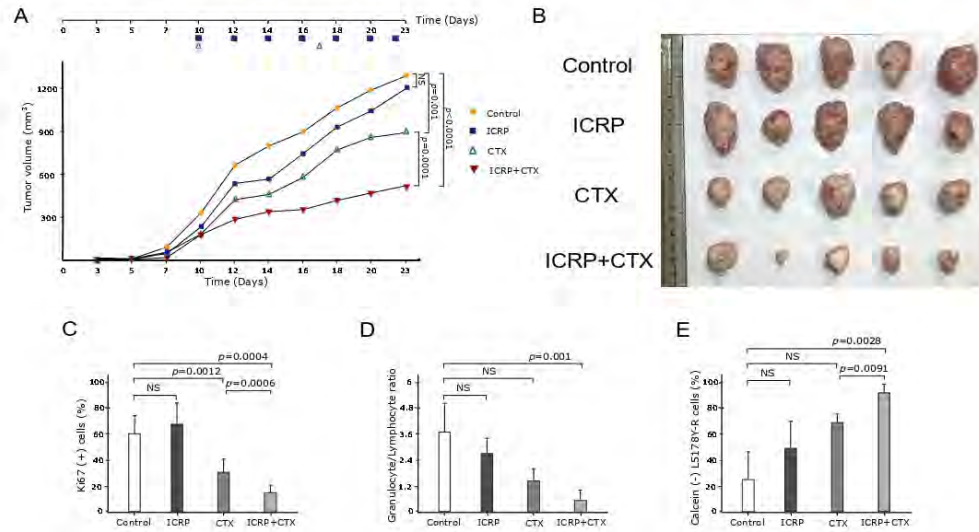


Figure 6. ICRP + CTX induces an antitumor effect against tumoral T-cell lymphoblasts. Female BALB/c mice ($n = 5$ per group) were inoculated s.c. with 1×10^6 L5178Y-R viable cells. When the tumor reached 100–120 mm³ after inoculation, mice were treated with 2 U/mL i.p. ICRP (purple squares) every two days, 125 mg/kg CTX i.p. weekly (green triangles), or the combination of ICRP + CTX (inverted red triangles). Control mice (yellow circles) were treated with 100 μ L sterile water for injection. Data are shown in (A) graph of tumor volume, (B) tumor size photograph, (C) Ki67 in tumor cells analyzed by flow cytometry, (D) granulocyte/lymphocyte ratio obtained from hematic biometry and (E) splenocytes cytotoxicity of mice treated with ICRP, CTX, or its combination against L5178Y-R stained with calcein-AM and analyzed by flow cytometry. NS was assigned to $p > 0.05$.

Additionally, as shown in Figure 6C, tumor cells from the control and ICRP groups exhibited a high percentage of the Ki-67 proliferation marker. In contrast, the CTX group showed a decrease in the percentage of Ki-67, which was further reduced in the ICRP + CTX group compared to CTX monotherapy.

A hematic biometry was conducted after treatment, and the granulocyte/lymphocyte ratio was determined. It was observed that this ratio remained unchanged in the peripheral blood of ICRP- and CTX-treated mice compared to control mice. However, the granulocyte/lymphocyte ratio was significantly decreased only in the ICRP + CTX-treated group (Figure 6D). Furthermore, to analyze the specific cytotoxicity of immune cells against cancer cells after treatment, we assessed the cytotoxicity of splenocytes to L5178Y cells. We observed that only splenocytes obtained from ICRP + CTX-treated mice induced a significant increase in L5178Y-R cell cytotoxicity, as evidenced by the loss of calcein staining (Figure 6E).

3. Discussion

Chemotherapies are well-known apoptosis inducers and exhibit significant immunosuppressive effects on various organs, including bone marrow, spleen, and the central nervous system [5–10]. Immunepotent CRP (ICRP), a bovine dialyzable leukocyte extract, displays selective cytotoxicity against several solid and hematologic cancers by inducing ROS-dependent apoptosis in T-cell acute lymphoblastic leukemia (T-ALL) cells, leading to nuclear and mitochondrial damage [20,26]. This study reported the first use of ICRP in conjunction with chemotherapy to enhance cytotoxicity against T-ALL and T-LBL, which

are often resistant to conventional treatments [27,28]. Our findings revealed that combining ICRP with chemotherapy significantly boosts cytotoxicity in T-cell lymphoblasts, showing potential for enhanced antitumor effects. The concept of combination therapy was pioneered by Frei, Holland, and Freireich, who developed the first chemotherapy regimen for ALL [29]. In subsequent studies, there were combined doses of CC₅₀ cisplatin after 4-hydroperoxycyclophosphamide treatment, achieving up to 85% inhibition of leukemic cell viability [30], similar to our results of 84–96% cell death using sublethal doses of various chemotherapies combined with ICRP.

Our study indicated that synergistic cytotoxic effects are enhanced by combining ICRP with chemotherapy. There have been reported synergistic cytotoxic effects induced by combinations of low doses of chemotherapies with other treatments, such as combinations of CC₁₀ nutlin-3a with CC₂₀ doxorubicin (DOX), CC₂₅ chlorambucil (CLB), or CC₁₅ fludarabine (FLU), which showed 50% to 65% cell death in B-cell chronic lymphocytic leukemia patient's samples [31]. These results are similar to our findings when using sublethal doses of CTX, DOX, EPI, or ETO, combined with CC₅₀ ICRP, where cell death reached 50% to 82%. On the other hand, using a sublethal inhibitory concentration of nelarabine (nela) in combination with the inhibitory concentration 15 (IC₁₅) of ZSTK-474, induced a 25% cell viability inhibition of T-ALL patient's samples [32]. These results are different from the ones observed when we combined suboptimal (CC₂₀) concentrations of ICRP and CTX, DOX, EPI, or ETO as these combinations reached up to 95% cell death, demonstrating a synergistic effect of CI values lower than 1.0. Furthermore, improved efficacy in terms of cytotoxicity was obtained by treatment using CC₂₀ nela plus CC₅₀ ZSTK-474, inducing 60% cell viability inhibition. Remarkably, CC₂₀ ICRP plus CC₅₀ CTX, DOX, EPI, or ETO improved the cell death induced by monotherapies, showing 87% to 98%. These data underline the potential of ICRP in potentiating chemotherapy-induced cell death, even when used at non-lethal or suboptimal concentrations.

Combinations of several agents such as BV6, a bivalent SMAC mimetic, and nela, with chemotherapies at ratios using equipotent concentrations of both treatments, revealed higher cytotoxicity induced by ICRP plus CTX, DOX, EPI, or ETO. For instance, IC₅₀ BV6 combined with IC₅₀ CTX showed a decrease in cell viability to 20% in primary ALL cells [12]. On the other hand, a combination that included CC₄₀ nela and CC₄₀ ZSTK-474 against ALL cells reached 70% inhibition of cell viability. When we combined CC₅₀ ICRP + CC₅₀ of each chemotherapy, our results produced up to 98% cell death, leading to CI values representing a synergistic cytotoxic effect [32].

Combination therapy with synergistic or additive effects may produce a more potent cytotoxic effect in lower doses of each monotherapy. We observed CI values reaching 0.00745–0.99682, showing a stronger synergism as well as more favorable DRI values (1.59690–1724.07) than shown previously by Hosseini M. and colleagues which combined different ratios of carfilzomib (cfz) and dexamethasone (Dex) against MOLT-4, a T-ALL cell line, and obtained 0.983–0.749 in CI values and 2.243–41.951 [33]. Furthermore, our results regarding the CI and DRI values are also different from the ones reported by Hassani S et al., who combined azidothymidine (AZT) and arsenic trioxide (ATO) in different ratios and found a reduction in the ATO cytotoxicity, showing an antagonistic effect with CI values of 1.21–5.54 and non-favorable or non-dose-reduction for ATO with 0.46–1.32 DRI values [34]. These data emphasize the potential of ICRP in boosting the effectiveness of existing chemotherapy protocols in T-ALL and T-LBL, particularly at suboptimal concentrations that are less toxic to healthy cells.

A synergistic effect could be triggered by actions on multiple targets that reside in the same or different pathways, negative regulation of counteractive actions, facilitating actions, or due to complementary actions [15]. Our data showed that both ICRP and CTX induce the loss of mitochondrial membrane potential, an increase in ROS production, and caspase activation. These effects were significantly augmented when the treatments were combined, compared to each treatment alone, in most of the combination ratios tested in both cell lines. Therefore, it seems that the increased cytotoxic effects of ICRP + CTX

could be at least in some part due to the enhancement of mitochondrial alterations which can initiate cell death, similar to the results previously reported by combining Cfz + Dex which showed a significant increase in caspase 3, BAX and BCL2 gene expression in a T-ALL cell line compared to monotherapy [33]. Moreover, we further identified the role of caspase activation, ROS production, and intracellular calcium overload during cell death. As previously reported, ICRP and CTX cell death rely on caspase activation and ROS production, whereas ICRP cell death also depends on the increase in intracellular calcium levels in T-ALL [5,6,20,35]. Yet, here we first reported the relevance of an increase in the intracellular calcium for CTX-mediated cell death as it was previously described for cardiomyocyte toxicity [36]. ICRP + CTX showed mostly caspase-dependent, ROS-dependent, and Calcium-dependent cell death. However, we could note that even if ICRP alone induces caspase-dependent cell death, caspases were dispensable when using CC₂₀ ICRP alone, such independence was maintained in the combination CTX + ICRP CC₂₀ in L5178Y-R cells. We previously demonstrated that in breast cancer cell lines (MCF-7, MDA-MB231, and 4T1 cells) ICRP induces caspase-independent cell death, and the combination of ICRP + CTX maintains such caspase-independent cell death; however, ROS dependence was not assessed [37]. Other ROS- and caspases-dependent cell death modalities have been shown by the combination of bortezomib with PCI-24781 (an HDAC inhibitor) synergized against a Hodgkin and a non-Hodkin lymphoma cell line [38]. The combination of phytosphingosine and ionizing radiation in a T-cell lymphoma cell line resistant to radiation also involved the loss of mitochondrial membrane potential and resulted in a caspase-independent mechanism [39].

Conventional chemotherapies can be toxic to healthy cells, leading to multiple side effects, including a reduction in the immune system by affecting lymphoid organs such as bone marrow and the spleen [5–9]. Although combination therapy can be toxic, the low therapeutic dosage required of each drug may prevent the toxic effects on healthy cells, while potentiating the cytotoxic effects on cancer cells. This may occur if one drug in the combination regimen is non-cytotoxic to healthy cells [19], as is the case in several immunotherapies, which show immunomodulatory activities but also present cytotoxic activities against cancer cells [40]. Although CTX induced variable cytotoxic effects in non-tumoral immune system cells, ICRP was not toxic. When combining both treatments using the concentrations and combination ratios tested in tumoral cells, ICRP + CTX did not demonstrate an increase in the cytotoxic effect of CTX in PBMC and spleen cells, but also, ICRP inhibited the CTX toxicity induced in bone marrow cells. This cytoprotection observed in bone marrow cells is in accordance with previous reports of our research group, where it was demonstrated that ICRP was able to induce *in vivo* bone marrow cell protection after 5-Fluorouracil treatment by reducing ROS production [41]. Other naturally derived products, such as a mixture of honeybee compounds, showed the *in vivo* amelioration of the cytotoxic effects of CTX in bone marrow cells, sperm, and the liver when used in combination with CTX [42]. However, the Janus-like effect of ICRP, where on one hand it is cytotoxic to cancerous cells and cytoprotective to bone marrow cells, could be related to its capacity to induce ER stress. This was demonstrated in T-ALL, where it induces ER stress through ER-Ca²⁺ mobilization and prosurvival autophagosome formation [35]. It has been demonstrated that depending on the duration and intensity of the stress, ER stress can switch from protection to cell death induction [43], and even in the presence of autophagy, the same molecular cascades that initially support the cytoprotection shift to a cytotoxic mode and ultimately promote cell death [44]. Here, we observed that Ca²⁺ mobilization in CTX + ICRP treatment is important for cell death induction, and it has been demonstrated that T-ALL cells upregulate the machinery and signaling molecules associated with ER stress and autophagy [43,45,46]. On the other hand, autophagosomes usually serve as a cell antioxidant pathway [47], which can be linked to the antioxidant activity previously observed in bone marrow cells of mice treated with ICRP. Thus, it is plausible that the mechanism induced by ICRP is in the tightrope between cytoprotective effects in bone marrow cells and the cytotoxic effect observed in cancer cells. This overexpressed

ER stress machinery in leukemic cells, which usually promotes pro-survival mechanisms when activated by ICRP treatment, could trigger perturbations that exceed cellular repair capacities leading to cell death. However, further studies on the precise role of ICRP in cytoprotection and the comparison between non-tumor and tumor cells must be performed to better understand this Janus-like role.

Bone marrow niches support stem cells and their progeny, protecting malignant cells from chemotherapy and ultimately contributing to the recurrence of hematological malignancies [25]. Our results revealed that CTX cell death is modulated by BMSC; in contrast, ICRP-induced cell death remained unchanged under these conditions. Also, ICRP + CTX overcame this CTX resistance, even when the combination included SL concentrations of ICRP. Similar results were reported by the peptide RCP168 which partially inhibited stroma-mediated resistance of Jurkat cells (T-ALL) to cytarabine (Ara-C) cell death [48]. Further analysis should be performed to identify the molecular mechanism by which ICRP + CTX overcomes the BMSC-mediated CTX resistance.

The combination strategies are based on sequential or concurrent therapy [49]. Our results show that concurrent therapy, initiating the administration of ICRP when beginning chemotherapy treatment, improved the tumor volume and the proliferation marker reduction induced by CTX alone in T-cell lymphoblastic lymphoma-bearing mice. A previous clinical trial in non-small cell lung cancer ICRP was administered on the third day after chemotherapy and cisplatin treatment. In this study, no changes in tumor size were observed when ICRP was administered, with respect to conventional treatment alone, although ICRP showed a beneficial effect in lymphocyte numbers and improved the Karnofsky score in patients [50]. Later, a clinical trial in breast cancer patients was performed using ICRP starting with 1-week administration prior to chemotherapy, with continued administration during the chemotherapy cycle and up to 1 month after the completion of chemotherapy. ICRP also showed a beneficial effect in lymphocyte numbers and improved Karnofsky score, but this schema also achieved better complete response percentages in stage III and IV patients, and the regression of metastatic lesions was obtained in less time than in the control group [24]. These results point out that administering ICRP at the same time as or before chemotherapy could be the best option in a conventional treatment for T-ALL or T-LBL. However, clinical trials must be performed to confirm this.

In previous research, when CTX was combined with Interferon type I (IFN-I) *in vivo*, it delayed tumor development and prevented 60% of mice bearing two types of T-cell lymphoma, whereas CTX or IFN alone did not prevent tumor-bearing mice [51]. Furthermore, mice surviving after IFN + CTX could generate immunologic memory, as hypothesized by our results as splenocytes from mice treated with ICRP + CTX showed cytotoxic capacity against the T-LBL cell line. Additionally, the significant decrease in the granulocyte/lymphocyte ratio shown by ICRP + CTX indicates a better anti-tumor efficiency as an elevated ratio seems to be associated with tumor progression and metastasis, perhaps because granulocytes compromise the natural anti-tumor function of lymphocytes [52].

Overall, throughout this study, we demonstrated that combining ICRP with chemotherapy synergistically enhances cytotoxicity against T-cell lymphoblasts even when ICRP was used at non-lethal or suboptimal concentrations, whereas ICRP + CTX overcomes the bone marrow-induced resistance to CTX cell death. Furthermore, ICRP improves the CTX anti-tumor effect *in vivo* and promotes cancer cell killing by splenocytes *ex vivo* (Figure 7). These results set the basis for further research into the clinical application of ICRP in combination with chemotherapeutic regimens for improving outcomes in T-cell malignancies.

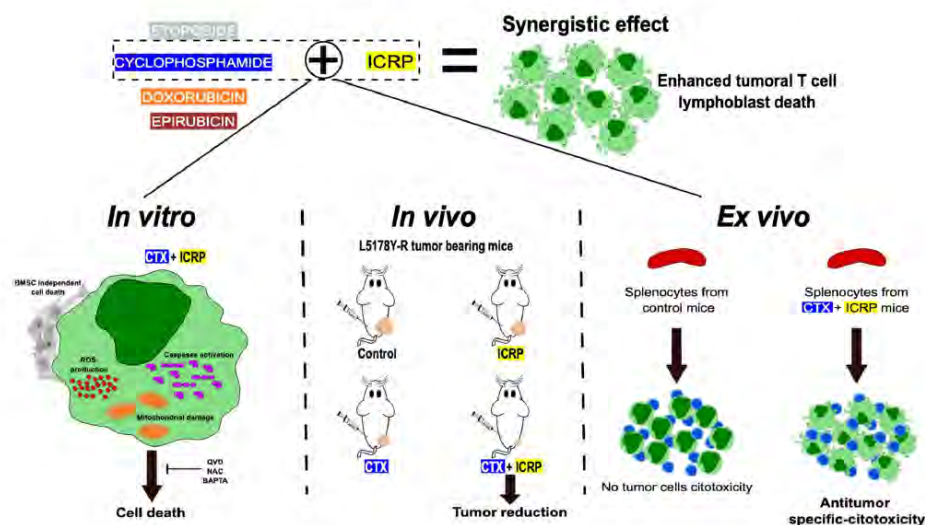


Figure 7. Immunepotent CRP synergistic enhances chemotherapy-induced cell death against tumoral T-cell lymphoblasts. When Immunepotent CRP (ICRP) is combined with Cyclophosphamide (CTX) it enhances ROS production, caspase activation, mitochondrial damage and induces cell death even in the presence of protecting bone marrow stromal cells. The cell death induced depends on caspases, ROS, and calcium. In vivo, the combination of ICRP and Cyclophosphamide enhance the reduction in tumor volume, leading ex vivo to the specific antitumor cytotoxicity induced by splenocytes of the treated mice.

4. Materials and Methods

4.1. Cytotoxic Agents, Cell Culture Mediums, and Inhibitors

Cells were cultured in RPMI-1640 supplemented with heat-inactivated-10% fetal bovine serum (FBS) and 1% penicillin-streptomycin (GIBCO by Life Technologies, Grand Island, NY, USA) referred to now as complete RPMI. The Laboratory of Immunology and Virology from the School of Biological Sciences produced IMMUNEPOTENT CRP (ICRP). One unit of ICRP contains 24 mg of peptides obtained from 15×10^8 leukocytes. The general characterization of ICRP was previously reported [53–55], where physical, bromatological, chemical, and in silico analyses were reported. ICRP and Cyclophosphamide (Cryofaxol from Cryofarma; Tlajomulco de Zuñiga, Jalisco, Mexico) were dissolved in complete RPMI. Doxorubicin (DOX), Epirubicin (EPI) (Farmorubicin RD[®], purchased from Pfizer, Mexico City, Mexico), and Etoposide (ETO, Cavep[®] from Accord Farma, Mexico City, Mexico) were dissolved in sterile water for injection as appropriate. The antioxidant, N-acetyl-L-cysteine (NAC), was dissolved in water to a final concentration of 500 mM. The pan-caspase inhibitor, QVD.opH (QVD, 1 mM), and the extracellular calcium chelator, BAPTA (50 μ M), were dissolved in dimethyl sulfoxide (DMSO) and were incubated for 30 min before treatment. All the solutions were wrapped in foil and stored according to the manufacturer's instructions.

4.2. Cell Culture

The CEM cell line, female human T-cell acute lymphoblastic leukemia (ATCC CCL-119), and L5178Y-R, murine T-cell lymphoblasts (ATCC CRL-1722), were obtained from the American Type Culture Collection (ATCC) and maintained according to its standards in a

humidified incubator at 37 °C and 5% CO₂. Cells were maintained in 25 cm³ cell culture flasks (CORNING Enterprises, Corning, NY, USA) containing complete RPMI.

4.3. Ethical Consideration

All experiments were reviewed and approved by the Ethical Committee (CEIBA) of the College of Biological Sciences at the UANL: CEIBA-2020-015. For animal samples, all experiments were performed following the Mexican regulation NOM-062-ZOO-1999 and were designed according to the Arrive guidelines for animal care and protection [56]. The procedures in our study involving human samples were conducted in accordance with the Helsinki Declaration.

4.4. Animals

The animal house at the Universidad Autónoma de Nuevo León, Mexico, supplied female BALB/c mice (eight-to-ten-week-old; 25 ± 5 g weight). Mice were housed in plastic cages in groups of five, and seven days were given to acclimate to the housing facility. Animals were maintained at 21 ± 3 °C, 55% ± 10% humidity, and 12 h light/dark cycle. Mice were provided with rodent maintenance food (LabDiet, St. Louis, MO, USA) and water ad libitum, and health status was monitored daily. Mice were randomly assigned to different groups for all the studies.

4.5. Lymphoid Cell Isolation

Male mice (n = 4) were anesthetized using 100 mg/kg sodium pentobarbital (CHEMI-NOVA, Mexico City, Mexico) and sacrificed by cervical dislocation. Then, the spleen, femur, and tibia were obtained. The spleen was filtered through a cell strainer (70 µm) with PBS. Bone marrow cells were obtained by flushing the femur and tibia into complete RPMI. All cells were maintained at 2 × 10⁵ per well in complete RPMI at 37 °C in a 5% CO₂ atmosphere.

4.6. Peripheral Blood Mononuclear Cells (PBMC) Isolation

After obtaining written informed consent, human PBMC isolation from healthy donors was performed by gradient centrifugation using Ficoll-Paque™ PLUS (GE Healthcare, Chicago, IL, USA). Cell layers were obtained from which the population corresponding to PBMC was taken. Cells were maintained in complete RPMI at 2 × 10⁵ cells per well at 37 °C in a 5% CO₂ atmosphere.

4.7. Cell Death Analysis

Cells (5 × 10⁵ cells/mL) were exposed to ICRP (0.2–0.8 U/mL), CTX (15–27 mM), DOX (5–40 µM), EPI (5–100 µM), ETO (20–250 µM), and the cytotoxic concentrations (CC) used for the combination treatment were obtained. For the following assays, different combination ratios of ICRP + CTX, ICRP + DOX, ICRP + EPI, and ICRP + ETO were used to treat cells for 24 h in 96-well dishes (Life Sciences, Darmstadt, Germany). After incubation, cells were collected and washed with PBS and suspended in 100 µL of binding buffer (10 mM HEPES/NaOH pH 7.4, 140 mM NaCl, 2.5 mM CaCl₂) containing Annexin-V-APC (AnnV, 1 µg/mL, BD Pharmingen, San Jose, CA, USA) and propidium iodide staining (PI, 0.5 µg/mL, MilliporeSigma, Eugene, OR, USA) to measure cell death with BD Accuri c6 flow cytometer (Becton Dickinson, Franklin Lakes, NJ, USA) and analyzed using FlowJo 10.7.2 Software (BD Biosciences, Ashland, OR, USA).

4.8. Pharmacological Inhibition of Cell Death Analysis

Before treatment with ICRP + CTX, cells were treated for 30 min with or without 1.5 µM QVD, 0.25 mM NAC, or 50 µM BAPTA for cell death inhibition. After 24 h, cells were obtained and washed with PBS twice, and suspended in 100 µL of binding buffer (10 mM HEPES/NaOH pH 7.4, 140 mM NaCl, 2.5 mM CaCl₂) containing Annexin-V-APC (1 µg/mL, BD Pharmingen, San Jose, CA, USA) and 0.5 µg/mL propidium iodide (PI,

MilliporeSigma, Eugene, OR, USA) to determine cell death using a BD Accury c6 flow cytometer (Becton Dickinson, Franklin Lakes, NJ, USA). FlowJo Software was used to analyze data (BD Biosciences).

4.9. Stromal Bone Marrow Cells' Protection Analysis

Bone marrow cells were obtained as mentioned above and plated in a flat plate for 48 h. Adherent cells were taken as stromal cells. L5178Y-R was then incubated with the bone marrow stromal cells (BMSC) and its supernatant at a 1:10 ratio (tumor to BMSC) prior to ICRP, CTX, and ICRP + CTX treatment as mentioned above. Cell death was then measured as described previously.

4.10. ROS Production Analysis

Quantification of ROS production was performed using 2.5 μM Hydroethidine (HE) staining (Invitrogen, St. Louis, MO, USA). Cells (5×10^5 cells/mL) were exposed to ICRP, CTX, and their combination in 96-well dishes (CORNING) for 24 h. Cells were then harvested and washed with PBS before staining incubation. HE was incubated for 30 min at 37 °C and then washed with PBS for assessment by flow cytometry and analyzed as described above.

4.11. Mitochondrial Membrane Potential Analysis

In 5×10^5 cells/mL plated in 96-well dishes (CORNING), treated as mentioned before, and then collected, we performed tetramethyl rhodamine ethyl ester staining analysis (TMRE, 125 nM, Sigma-Aldrich, St. Louis, MO, USA) which was incubated at 37 °C for 30 min to determine loss of mitochondrial membrane potential. Then, cells were washed with PBS to measure the loss of TMRE-fluorescence by flow cytometry as described above.

4.12. Caspase Activity Assay

TF2-VAD-FMK, the Generic Caspase Activity FMK staining kit staining (Abcam, Cambridge, UK) was used to assess caspase activity in cells (5×10^5 cells/mL) that were treated with ICRP, CTX, and ICRP + CTX-combinations for 24 h, according to manufacturer's instructions. Analyses were performed by flow cytometry as described above.

4.13. Tumor Establishment and Treatment

L5178Y-R cells (1×10^6) were suspended in 100 μL PBS and injected into the female mice left hind s.c. Three times per week, the tumor volume and mice weight were measured using a caliper (Digimatic Caliper Mitutoyo Corporation, Kanagawa, Japan) and a digital scale (American Weigh Scale-600-BLK, Atlanta, GA, USA). When the tumor reached 100–120 mm^3 after inoculation, mice ($n = 5$ per group, assigned randomly) were injected with 2 U i.p. every two days, 125 mg/kg CTX i.p., weekly, or the combination of ICRP + CTX. Control mice were treated with 100 μL sterile water for injection. All treatments were dissolved in sterile water for injection. The following formula was used to determine tumor volume: tumor volume (mm^3) = (Length \times width²)/2. Twenty-three days after inoculation of tumor cells, mice were anesthetized as mentioned above, blood was obtained by cardiac puncture for hematic biometry, from which the granulocyte/lymphocyte ratio was determined, and mice were then euthanized by cervical dislocation. Tumor and spleen were obtained and weighed.

4.14. Splenocytes + L5178Y-R Co-Culture

L5178Y-R was stained with 0.1 mg/mL Calcein-AM (BD biosciences, San José, CA, USA) for 30 min at 37 °C and 5% CO_2 . Cells were then washed twice with PBS. Thus, splenocytes (obtained as previously described) were added in a 44:1 (splenocytes to tumor) ratio. Co-culture was maintained at 37 °C and 5% CO_2 for 24 h and calcein-negative L5178Y-R cells were measured by flow cytometry.

4.15. Ki67 Analysis

Dissected tumors were macerated and filtered through a cell strainer (70 μ M) with PBS and tumor cells (1×10^6) were fixed then in ethanol dropwise gradient (50% to 70%) while vortexing and incubated at -20 °C overnight. Cells were washed twice and analyzed using Ki-67 (Alexa Fluor 647 anti-human Ki-67 Antibody, BioLegend, San Diego, CA, USA).

4.16. Statistical Analysis

Triplicate determinations from at least three independent experiments were presented as means \pm SD in graphs. Results were analyzed by GraphPad Prism software (San Diego, CA, USA), using paired Student's *t*-tests for in vitro studies, and two-tailed unpaired Student's *t*-tests and Mann–Whitney tests for the ex vivo and in vivo studies, considering statistical significance as $p < 0.05$.

Supplementary Materials: The following supporting information can be downloaded at <https://www.mdpi.com/article/10.3390/ijms25147938/s1>.

Author Contributions: A.L.R.-L., K.M.C.-R., M.I.-R. and A.C.M.-T.: planned experiments; A.L.R.-L., K.M.C.-R. and M.I.-R.: performed experiments; A.L.R.-L., K.M.C.-R., M.I.-R., J.M.V.-G., A.C.M.-T. and C.R.-P.: analyzed and interpreted data; A.C.M.-T. and C.R.-P.: contributed with reagents or other essential material; A.L.R.-L. and A.C.M.-T.: wrote the paper; A.C.M.-T.: conceived, designed, and supervised the work; A.L.R.-L., K.M.C.-R., M.I.-R., J.M.V.-G., A.C.M.-T. and C.R.-P.: reviewed the work; A.L.R.-L., K.M.C.-R., M.I.-R., J.M.V.-G., A.C.M.-T. and C.R.-P.: revised and approved the final version. All authors have read and agreed to the published version of the manuscript.

Funding: This research received no external funding.

Institutional Review Board Statement: All experiments involving animals were reviewed and approved by the Ethical Committee (CEIBA) of the School of Biological Sciences at the UANL: CEIBA-2020-015. For animal samples, all experiments were performed following the Mexican regulation NOM-062-ZOO-1999 and were designed according to the Arrive guidelines for animal care and protection [56]. The procedures in our study involving human samples were conducted in accordance with the Helsinki Declaration.

Informed Consent Statement: Informed consent was obtained from all subjects involved in the study.

Data Availability Statement: Data is contained within the article or Supplementary Material.

Acknowledgments: Authors thank Alejandra Arreola-Triana for english language editing, and the Laboratory of Immunology and Virology at the UANL for the infrastructure provided to achieve this work. A.L.R.-L., M.I.-R., and K.M.C.-R. are thankful for the scholarship provided by CONAHICYT. A.L.R.-L., K.M.C.-R., A.C.M.-T., and C.R.-P. thank ECOS-NORD, ANUIES CONAHICYT.

Conflicts of Interest: All authors have read the journal's policy on disclosure of potential conflicts of interest. The authors declare no conflicts of interest. C.R.P. is an employee of LONGEVEDEN SA de CV; the company had no role in the design of the study, in the collection, analyses, or interpretation of data; in the writing of the manuscript; or in the decision to publish the results.

References

1. Network, H.M.R. (n.d.). Classification of Haematological Malignancies. Network, Haematological Malignancy Research. Available online: <https://hmrn.org/about/classification> (accessed on 15 July 2024).
2. Intermesoli, T.; Weber, A.; Leoncin, M.; Frison, L.; Skert, C.; Bassan, R. Lymphoblastic Lymphoma: A Concise Review. *Curr. Oncol. Rep.* **2022**, *24*, 1–12. [CrossRef]
3. Fleischer, L.C.; Spencer, H.T.; Raikar, S.S. Targeting T cell malignancies using CAR-based immunotherapy: Challenges and potential solutions. *J. Hematol. Oncol.* **2019**, *12*, 141. [CrossRef]
4. Kroeze, E.; Loeffen, J.L.C.; Poort, V.M.; Meijerink, J.P.P. T-cell lymphoblastic lymphoma and leukemia: Different diseases from a common premalignant progenitor? *Blood Adv.* **2020**, *4*, 3466–3473. [CrossRef]
5. Emadi, A.; Jones, R.J.; Brodsky, R.A. Cyclophosphamide and cancer: Golden anniversary. *Nat. Reviews. Clin. Oncol.* **2009**, *6*, 638–647. [CrossRef] [PubMed]
6. Zhang, Z.; Pan, T.; Liu, C.; Shan, X.; Xu, Z.; Hong, H.; Lin, H.; Chen, J.; Sun, H. Cyclophosphamide induced physiological and biochemical changes in mice with an emphasis on sensitivity analysis. *Ecotoxicol. Environ. Saf.* **2021**, *211*, 111889. [CrossRef] [PubMed]

7. Tacar, O.; Sriamornsak, P.; Dass, C.R. Doxorubicin: An update on anticancer molecular action, toxicity and novel drug delivery systems. *J. Pharm. Pharmacol.* **2013**, *65*, 157–170. [CrossRef]
8. Khasraw, M.; Bell, R.; Dang, C. Epirubicin: Is it like doxorubicin in breast cancer? A clinical review. *Breast* **2012**, *21*, 142–149. [CrossRef]
9. Wood, L.J.; Nail, L.M.; Perrin, N.A.; Elsea, C.R.; Fischer, A.; Druker, B.J. The cancer chemotherapy drug etoposide (VP-16) induces proinflammatory cytokine production and sickness behavior-like symptoms in a mouse model of cancer chemotherapy-related symptoms. *Biol. Res. Nurs.* **2006**, *8*, 157–169. [CrossRef] [PubMed]
10. Hannun, Y.A. Apoptosis and the dilemma of cancer chemotherapy. *Blood* **1997**, *89*, 1845–1853. [CrossRef]
11. Hanahan, D.; Weinberg, R.A. Hallmarks of cancer: The next generation. *Cell* **2011**, *144*, 646–674. [CrossRef]
12. Sadeghi, M.; Hamdi Hajibaba, H.; Valizadeh, Y.; Movasaghpour Akbari, A.A.; Hosseinpour Feizi, A.A.; Aghebati-Maleki, L.; Jadidi-Niaragh, F. Combinational therapy of acute lymphoblastic leukemia with cyclophosphamide and BV6 synergistically induces apoptosis in leukemic cells. *ImmunoAnalysis* **2022**, *2*, 9. [CrossRef]
13. Smith, A.L.; Pal, D.; Martínez-Rico, R.; Eiken, A.P.; Durden, D.L.; Kutateladze, T.G.; El-Gamal, D. Preclinical activity of a novel multi-axis inhibitor in aggressive and indolent B-cell malignancies. *Leuk. Lymphoma* **2023**, *64*, 2333–2337. [CrossRef] [PubMed]
14. Barreca, M.; Lang, N.; Tarantelli, C.; Spriano, F.; Barraja, P.; Bertoni, F. Antibody-drug conjugates for lymphoma patients: Preclinical and clinical evidences. *Explor. Target. Anti-Tumor Ther.* **2022**, *3*, 763–794. [CrossRef] [PubMed]
15. Zhang, J.; Zhu, F.; Ma, X.; Cao, Z.; Cao, Z.W.; Li, Y.; Li, Y.X.; Chen, Y.Z. Mechanisms of drug combinations: Interaction and network perspectives. *Nat. Rev. Drug Discov.* **2009**, *8*, 111–128. [CrossRef]
16. Pemovska, T.; Bigenzahn, J.W.; Superti-Furga, G. Recent advances in combinatorial drug screening and synergy scoring. *Curr. Opin. Pharmacol.* **2018**, *42*, 102–110. [CrossRef] [PubMed]
17. Chou, T.; Talalay, P. Analysis of combined drug effects: A new look at a very old problem. *Trends Pharmacol. Sci.* **1983**, *4*, 450–454. [CrossRef]
18. Correia, A.S.; Gärtner, F.; Vale, N. Drug combination and repurposing for cancer therapy: The example of breast cancer. *Heliyon* **2021**, *7*, e05948. [CrossRef] [PubMed]
19. Bayat Mokhtari, R.; Homayouni, T.S.; Baluch, N.; Morgatskaya, E.; Kumar, S.; Das, B.; Yeager, H. Combination therapy in combating cancer. *Oncotarget* **2017**, *8*, 38022–38043. [CrossRef] [PubMed]
20. Lorenzo-Anota, H.Y.; Martínez-Torres, A.C.; Scott-Algara, D.; Tamez-Guerra, R.S.; Rodríguez-Padilla, C. Bovine Dialyzable Leukocyte Extract IMMUNEPOTENT-CRP Induces Selective ROS-Dependent Apoptosis in T-Acute Lymphoblastic Leukemia Cell Lines. *J. Oncol.* **2020**, *2020*, 1598503. [CrossRef]
21. Lorenzo-Anota, H.Y.; Martínez-Loria, A.B.; Tamez-Guerra, R.S.; Scott-Algara, D.; Martínez-Torres, A.C.; Rodríguez-Padilla, C. Changes in the natural killer cell repertoire and function induced by the cancer immune adjuvant candidate IMMUNEPOTENT-CRP. *Cell. Immunol.* **2022**, *374*, 104511. [CrossRef]
22. Santana-Krinskaya, S.E.; Franco-Molina, M.A.; Zárate-Triviño, D.G.; Prado-García, H.; Zapata-Benavides, P.; Torres-Del-Muro, F.; Rodríguez-Padilla, C. IMMUNEPOTENT CRP plus doxorubicin/cyclophosphamide chemotherapy remodel the tumor microenvironment in an air pouch triple-negative breast cancer murine model. *Biomed. Pharmacother.* **2020**, *126*, 110062. [CrossRef]
23. Rodríguez-Salazar, M.D.C.; Franco-Molina, M.A.; Mendoza-Gamboa, E.; Martínez-Torres, A.C.; Zapata-Benavides, P.; López-González, J.S.; Coronado-Cerda, E.E.; Alcocer-González, J.M.; Tamez-Guerra, R.S.; Rodríguez-Padilla, C. The novel immunomodulator IMMUNEPOTENT CRP combined with chemotherapy agent increased the rate of immunogenic cell death and prevented melanoma growth. *Oncol. Lett.* **2017**, *14*, 844–852. [CrossRef] [PubMed]
24. Lara, H.H.; Turrent, L.I.; Garza-Treviño, E.N.; Tamez-Guerra, R.; Rodríguez-Padilla, C. Clinical and immunological assessment in breast cancer patients receiving anticancer therapy and bovine dialyzable leukocyte extract as an adjuvant. *Exp. Ther. Med.* **2010**, *1*, 425–431. [CrossRef]
25. Méndez-Ferrer, S.; Bonnet, D.; Steensma, D.P.; Hasserjian, R.P.; Ghobrial, I.M.; Gribben, J.G.; Andreeff, M.; Krause, D.S. Bone marrow niches in haematological malignancies. *Nat. Rev. Cancer* **2020**, *20*, 285–298. [CrossRef]
26. Reyes-Ruiz, A.; Calvillo-Rodríguez, K.M.; Martínez-Torres, A.C.; Rodríguez-Padilla, C. The bovine dialyzable leukocyte extract IMMUNEPOTENT CRP induces immunogenic cell death in breast cancer cells leading to long-term antitumour memory. *Br. J. Cancer* **2021**, *124*, 1398–1410. [CrossRef]
27. Follini, E.; Marchesini, M.; Roti, G. Strategies to Overcome Resistance Mechanisms in T-Cell Acute Lymphoblastic Leukemia. *Int. J. Mol. Sci.* **2019**, *20*, 3021. [CrossRef]
28. Savage, P. Chemotherapy Curability in Leukemia, Lymphoma, Germ Cell Tumors and Gestational Malignancies: A Reflection of the Unique Physiology of Their Cells of Origin. *Front. Genet.* **2020**, *11*, 426. [CrossRef] [PubMed]
29. Frei, E., 3rd; Karon, M.; Levin, R.H.; Freireich, E.J.; Taylor, R.J.; Hananian, J.; Selawry, O.; Holland, J.F.; Hoogstraten, B.; Wolman, I.J.; et al. The effectiveness of combinations of antileukemic agents in inducing and maintaining remission in children with acute leukemia. *Blood* **1965**, *26*, 642–656. [CrossRef] [PubMed]
30. Peters, R.H.; Stuart, R.K. Synergism between 4-hydroperoxycyclophosphamide and cisplatin: Importance of incubation sequence and measurement of cisplatin accumulation. *Biochem. Pharmacol.* **1990**, *39*, 607–609. [CrossRef]
31. Coll-Mulet, L.; Iglesias-Serret, D.; Santidrián, A.F.; Cosiáls, A.M.; de Frias, M.; Castaño, E.; Campàs, C.; Barragán, M.; de Sevilla, A.F.; Domingo, A.; et al. MDM2 antagonists activate p53 and synergize with genotoxic drugs in B-cell chronic lymphocytic leukemia cells. *Blood* **2006**, *107*, 4109–4114. [CrossRef]

32. Lonetti, A.; Cappellini, A.; Bertaina, A.; Locatelli, F.; Pession, A.; Buontempo, F.; Evangelisti, C.; Evangelisti, C.; Orsini, E.; Zamboni, L.; et al. Improving nelarabine efficacy in T cell acute lymphoblastic leukemia by targeting aberrant PI3K/AKT/mTOR signaling pathway. *J. Hematol. Oncol.* **2016**, *9*, 114. [[CrossRef](#)] [[PubMed](#)]
33. Hosseini, M.S.; Mohammadi, M.H.; Vahabpour Roudsari, R.; Jafari, L.; Mashati, P.; Gharehbaghian, A. Proteasome Inhibition by Carfilzomib Induced Apoptosis and Autophagy in a T-cell Acute Lymphoblastic Leukemia Cell Line. *Iran. J. Pharm. Res.* **2019**, *18* (Suppl. 1), 132–145. [[CrossRef](#)]
34. Hassani, S.; Ghaffari, S.H.; Zaker, F.; Mirzaee, R.; Mardani, H.; Bashash, D.; Zekri, A.; Yousefi, M.; Zaghal, A.; Alimoghaddam, K.; et al. Azidothymidine hinders arsenic trioxide-induced apoptosis in acute promyelocytic leukemia cells by induction of p21 and attenuation of G2/M arrest. *Ann. Hematol.* **2013**, *92*, 1207–1220. [[CrossRef](#)]
35. Lorenzo-Anota, H.Y.; Reyes-Ruiz, A.; Calvillo-Rodríguez, K.M.; Mendoza-Reveles, R.; Urdaneta-Peinado, A.P.; Alvarez-Valadez, K.M.; Martínez-Torres, A.C.; Rodríguez-Padilla, C. IMMUNEPOTENT CRP increases intracellular calcium through ER-calcium channels, leading to ROS production and cell death in breast cancer and leukemic cell lines. *EXCLI J.* **2023**, *22*, 352–366. [[CrossRef](#)]
36. Iqbal, A.; Iqbal, M.K.; Sharma, S.; Ansari, M.A.; Najmi, A.K.; Ali, S.M.; Ali, J.; Haque, S.E. Molecular mechanism involved in cyclophosphamide-induced cardiotoxicity: Old drug with a new vision. *Life Sci.* **2019**, *218*, 112–131. [[CrossRef](#)] [[PubMed](#)]
37. Rivera-Lazarin, A.L.; Martínez-Torres, A.C.; de la Hoz-Camacho, R.; Guzmán-Aguillón, O.L.; Franco-Molina, M.A.; Rodríguez-Padilla, C. The bovine dialyzable leukocyte extract, immunepotent CRP, synergically enhances cyclophosphamide-induced breast cancer cell death, through a caspase-independent mechanism. *EXCLI J.* **2023**, *22*, 131–145. [[CrossRef](#)]
38. Bhalla, S.; Balasubramanian, S.; David, K.; Sirisawad, M.; Buggy, J.; Mauro, L.; Prachand, S.; Miller, R.; Gordon, L.I.; Evens, A.M. PCI-24781 induces caspase and reactive oxygen species-dependent apoptosis through NF-kappaB mechanisms and is synergistic with bortezomib in lymphoma cells. *Clin. Cancer Res.* **2009**, *15*, 3354–3365. [[CrossRef](#)] [[PubMed](#)]
39. Park, M.T.; Kim, M.J.; Kang, Y.H.; Choi, S.Y.; Lee, J.H.; Choi, J.A.; Kang, C.M.; Cho, C.K.; Kang, S.; Bae, S.; et al. Phytosphingosine in combination with ionizing radiation enhances apoptotic cell death in radiation-resistant cancer cells through ROS-dependent and -independent AIF release. *Blood* **2005**, *105*, 1724–1733. [[CrossRef](#)]
40. Calvillo-Rodríguez, K.M.; Lorenzo-Anota, H.Y.; Rodríguez-Padilla, C.; Martínez-Torres, A.C.; Scott-Algara, D. Immunotherapies inducing immunogenic cell death in cancer: Insight of the innate immune system. *Front. Immunol.* **2023**, *14*, 1294434. [[CrossRef](#)]
41. Coronado-Cerda, E.E.; Franco-Molina, M.A.; Mendoza-Gamboa, E.; Prado-García, H.; Rivera-Morales, L.G.; Zapata-Benavides, P.; Rodríguez-Salazar Mdel, C.; Caballero-Hernandez, D.; Tamez-Guerra, R.S.; Rodríguez-Padilla, C. In Vivo Chemoprotective Activity of Bovine Dialyzable Leukocyte Extract in Mouse Bone Marrow Cells against Damage Induced by 5-Fluorouracil. *J. Immunol. Res.* **2016**, *2016*, 6942321. [[CrossRef](#)]
42. Fahmy, M.; Hassan, N.; El-Fiky, S.; Elalfy, H. A mixture of honey bee products ameliorates the genotoxic side effects of cyclophosphamide. *Asian Pac. J. Trop. Dis.* **2015**, *5*, 638–644. [[CrossRef](#)]
43. Féral, K.; Jaud, M.; Philippe, C.; Di Bella, D.; Pyronnet, S.; Rouault-Pierre, K.; Mazzolini, L.; Touriol, C. ER Stress and Unfolded Protein Response in Leukemia: Friend, Foe, or Both? *Biomolecules* **2021**, *11*, 199. [[CrossRef](#)] [[PubMed](#)]
44. Kroemer, G.; Galassi, C.; Zitvogel, L.; Galluzzi, L. Immunogenic cell stress and death. *Nat. Immunol.* **2022**, *23*, 487–500. [[CrossRef](#)] [[PubMed](#)]
45. Huang, F.L.; Yu, S.J.; Li, C.L. Role of Autophagy and Apoptosis in Acute Lymphoblastic Leukemia. *Cancer Control* **2021**, *28*, 10732748211019138. [[CrossRef](#)] [[PubMed](#)]
46. Xie, S.Z.; Garcia-Prat, L.; Voisin, V.; Ferrari, R.; Gan, O.I.; Wagenblast, E.; Kaufmann, K.B.; Zeng, A.G.X.; Takayanagi, S.I.; Patel, I.; et al. Sphingolipid Modulation Activates Proteostasis Programs to Govern Human Hematopoietic Stem Cell Self-Renewal. *Cell Stem Cell* **2019**, *25*, 639–653. [[CrossRef](#)]
47. Li, D.; Ding, Z.; Du, K.; Ye, X.; Cheng, S. Reactive Oxygen Species as a Link between Antioxidant Pathways and Autophagy. *Oxidative Med. Cell. Longev.* **2021**, *2021*, 5583215. [[CrossRef](#)]
48. Zeng, Z.; Samudio, I.J.; Munsell, M.; An, J.; Huang, Z.; Estey, E.; Andreeff, M.; Konopleva, M. Inhibition of CXCR4 with the novel RCP168 peptide overcomes stroma-mediated chemoresistance in chronic and acute leukemias. *Mol. Cancer Ther.* **2006**, *5*, 3113–3121. [[CrossRef](#)]
49. Kwon, M.; Jung, H.; Nam, G.H.; Kim, L.S. The right Timing, right combination, right sequence, and right delivery for Cancer immunotherapy. *J. Control. Release* **2021**, *331*, 321–334. [[CrossRef](#)]
50. Franco-Molina, M.A.; Mendoza-Gamboa, E.; Zapata-Benavides, P.; Vera-García, M.E.; Castillo-Tello, P.; García de la Fuente, A.; Mendoza, R.D.; Garza, R.G.; Tamez-Guerra, R.S.; Rodríguez-Padilla, C. IMMUNEPOTENT CRP (bovine dialyzable leukocyte extract) adjuvant immunotherapy: A phase I study in non-small cell lung cancer patients. *Cytotherapy* **2008**, *10*, 490–496. [[CrossRef](#)]
51. Schiavoni, G.; Sistigu, A.; Valentini, M.; Mattei, F.; Sestili, P.; Spadaro, F.; Sanchez, M.; Lorenzi, S.; D'Urso, M.T.; Belardelli, F.; et al. Cyclophosphamide synergizes with type I interferons through systemic dendritic cell reactivation and induction of immunogenic tumor apoptosis. *Cancer Res.* **2011**, *71*, 768–778. [[CrossRef](#)]
52. Liu, H.; Tabuchi, T.; Takemura, A.; Kasuga, T.; Motohashi, G.; Hiraishi, K.; Katano, M.; Nakada, I.; Ubukata, H.; Tabuchi, T. The granulocyte/lymphocyte ratio as an independent predictor of tumour growth, metastasis and progression: Its clinical applications. *Mol. Med. Rep.* **2008**, *1*, 699–704. [[CrossRef](#)] [[PubMed](#)]
53. García Coronado, P.L.; Franco Molina, M.A.; Zárate Triviño, D.G.; Menchaca Arredondo, J.L.; Zapata Benavides, P.; Rodríguez Padilla, C. Putative Wound Healing Induction Functions of Exosomes Isolated from IMMUNEPOTENT CRP. *Int. J. Mol. Sci.* **2023**, *24*, 8971. [[CrossRef](#)] [[PubMed](#)]

54. Franco-Molina, M.A.; Santana-Krimskaya, S.E.; Zarate-Triviño, D.G.; Zapata-Benavides, P.; Hernández-Martínez, S.P.; Cervantes-Wong, F.; Rodríguez-Padilla, C. Bovine Dialyzable Leukocyte Extract IMMUNEPOTENT CRP: Evaluation of Biological Activity of the Modified Product. *Appl. Sci.* **2021**, *11*, 3505. [[CrossRef](#)]
55. Franco-Molina, M.A.; Santana-Krimskaya, S.E.; Coronado-Cerda, E.E.; Hernández-Luna, C.E.; Zarate-Triviño, D.G.; Zapata-Benavides, P.; Rodríguez-Padilla, C. Increase of the antitumour efficacy of the biocompound IMMUNEPOTENT CRP by enzymatic treatment. *Biotechnol. Biotechnol. Equip.* **2018**, *32*, 1028–1035. [[CrossRef](#)]
56. Percie du Sert, N.; Ahluwalia, A.; Alam, S.; Avey, M.T.; Baker, M.; Browne, W.J.; Clark, A.; Cuthill, I.C.; Dirnagl, U.; Emerson, M.; et al. Reporting animal research: Explanation and elaboration for the ARRIVE guidelines 2.0. *PLoS Biol.* **2020**, *18*, e3000411. [[CrossRef](#)]

Disclaimer/Publisher's Note: The statements, opinions and data contained in all publications are solely those of the individual author(s) and contributor(s) and not of MDPI and/or the editor(s). MDPI and/or the editor(s) disclaim responsibility for any injury to people or property resulting from any ideas, methods, instructions or products referred to in the content.

**CHAPTER 2. STUDY OF THE CYTOTOXIC EFFECT INDUCED
BY IMMUNEPOTENT CRP IN COMBINATION WITH
CHEMOTHERAPIES IN IMMUNE SYSTEM CELLS**

**2.1 CYCLOPHOSPHAMIDE AND EPIRUBICIN INDUCE HIGH
APOPTOSIS IN MICROGLIA CELLS WHILE EPIRUBICIN
PROVOKES DNA DAMAGE AND MICROGLIAL ACTIVATION
AT SUB-LETHAL CONCENTRATIONS**

Original article:

CYCLOPHOSPHAMIDE AND EPIRUBICIN INDUCE HIGH APOPTOSIS IN MICROGLIA CELLS WHILE EPIRUBICIN PROVOKES DNA DAMAGE AND MICROGLIAL ACTIVATION AT SUB-LETHAL CONCENTRATIONS

Rafael de la Hoz-Camacho^a, Ana Luisa Rivera-Lazarín^a, Jose Manuel Vázquez-Guillen^a, Diana Caballero-Hernández^a, Edgar Mendoza-Gamboa^a, Ana Carolina Martínez-Torres^{a,*}, Cristina Rodríguez-Padilla^{a,b,+}

^a Universidad Autónoma de Nuevo León, Facultad de Ciencias Biológicas, Laboratorio de Inmunología y Virología, Monterrey 66455, México

^b LONGEVEDEN S.A. de C.V.

⁺ These authors share equal co-seniorship.

* **Corresponding author:** Ana Carolina Martínez-Torres, Universidad Autónoma de Nuevo León, Facultad de Ciencias Biológicas, Laboratorio de Inmunología y Virología, Monterrey 66455, México. Tel +52 8 121 4115. Fax +52 818 352 4212. E-mail: ana.martinezto@uanl.edu.mx

<https://dx.doi.org/10.17179/excli2021-4160>

This is an Open Access article distributed under the terms of the Creative Commons Attribution License (<http://creativecommons.org/licenses/by/4.0/>).

ABSTRACT

Chemotherapy Related Cognitive Impairment (CRCI), also called chemobrain, diminishes cancer patient's life quality. Breast cancer (BC) patients have been described to be importantly affected, however, the mechanism leading to CRCI has not been fully elucidated. Recent research proposes microglia as the main architect of CRCI, thus dysregulations in these cells could trigger CRCI. The aim of this research was to evaluate the effects of two drugs commonly used against breast cancer, cyclophosphamide (CTX) and epirubicin (EPI), on the microglia cell line SIM-A9, using the BC cell line, 4T1, as a control. Our results show that CTX and EPI decrease microglia-cell viability and increase cell death on a concentration-dependent manner, being 5 and 2 times more cytotoxic to microglia cell line than to breast cancer 4T1 cells, respectively. Both chemotherapies induce cell cycle arrest and a significant increase in p53, p16 and γ -H2AX in breast cancer and microglia cells. Furthermore, mitochondrial membrane potential ($\Delta\Psi_m$) diminishes as cell death increases, and both chemotherapies induce reactive oxygen species (ROS) production on SIM-A9 and 4T1. Moreover, caspase activation increases with treatments and its pharmacological blockade inhibits CTX and EPI induced-cell death. Finally, low concentrations of CTX and EPI induce γ -H2AX, and EPI induces cytokine release, NO production and Iba-1 overexpression. These findings indicate that microglia cells are more sensitive to CTX and EPI than BC cells and undergo DNA damage and cell cycle arrest at very low concentrations, moreover EPI induces microglia activation and a pro-inflammatory profile.

Keywords: Microglia, breast cancer, neurotoxicity, chemotherapy, chemobrain, apoptosis

INTRODUCTION

Breast cancer (BC) is one of the main causes of death among women worldwide (American Cancer Society, 2017). Treatments

include surgery, radiotherapy, and chemotherapy. There are different types of drugs used as chemotherapy, of which two commonly used are anthracyclines and alkylating

agents, such as epirubicin (EPI) and cyclophosphamide (CTX) (Feng et al., 2016; Wu et al., 2016). Most chemotherapies induce regulated cell death (RCD), a mechanism by which the cell activates its own machinery to self-destruct (Galluzzi et al., 2018). Both chemotherapies, EPI and CTX, have similar action mechanisms that include DNA damage (Taymaz-Nikerel et al., 2018), cell cycle arrest (Xiong et al., 2016), mitochondrial alterations and oxidative stress (Prasad et al., 2010), in different tumoral cell lines and some non-neoplastic cell lines (Standish et al., 2008). Even though chemotherapies are effective against cancer cells, they also induce secondary effects, such as nausea, alopecia (Uchida et al., 2018), hepatotoxicity, and cardiotoxicity (Wu et al., 2016), directly diminishing patient's quality life. Immune cells are frequently damaged by cancer treatments (Verma et al., 2016), either around the body or in specific organs, such as liver, lungs and recently associated, brain (Matsos et al., 2017).

In this regard, studies show that around 23 % of surviving chemotherapy-treated BC patients present cognitive impairment (de Ruiter et al., 2012; Selamat et al., 2014; Shen et al., 2019; Ongnok et al., 2020). Chemotherapy related cognitive impairment (CRCI) is known to appear after chemotherapy treatment of non-central nervous system (non-CNS) tumors, and recent studies propose microglia as the main architect of CRCI (Gibson et al., 2019). Microglia are tissue resident macrophages that play vital functions on the central nervous system (CNS), such as homeostatic maintenance, release of neurotrophic factors and protection against pathogens. Because of their macrophage nature, microglia cells produce cytokines and regulate neuroinflammation, which has been associated with different neuropathologies, such as Parkinson's disease, Alzheimer's disease, and cognitive impairment (McLeary et al., 2019). Studies have shown a decrease in white matter density in patients after chemotherapy, leading to further investigation on cell death in central nervous system cells (Matsos et al.,

2017). There is a gap in knowledge regarding the susceptibility of central nervous system cells to chemotherapies directed at non-CNS tumors. Although the central nervous system is protected by the blood brain barrier (BBB), increasing cytokines and ROS levels associated with cancer-induced inflammation have been proposed to augment its permeability (Yarlagadda et al., 2009). Increased permeability of the BBB may allow the direct interaction between circulating drugs and central nervous system cells during cancer therapy. Thus, the aim of this study was to assess the sensibility of microglia cells to the antitumor drugs epirubicin and cyclophosphamide to provide evidence supporting role for chemotherapy in CRCI.

METHODS

Reagents

Cells were maintained in DMEM-F12 and RPMI-1640 supplemented with 10 % fetal bovine serum (FBS) and 1 % penicillin-amphotericin-streptomycin (GIBCO by Life Technologies, Grand Island, NY) referred as complete DMEM-F12 or RPMI. FACS buffer is composed of 2 % of fetal bovine serum (FBS) in phosphate buffer saline 1X (PBS) at pH 7.4. Epirubicin (Farmorubicin RD®), EPI, was purchased from Pfizer (Ciudad de México, México) and was dissolved in sterile water for injection. Cyclophosphamide (Cryofaxol®), CTX, was purchased from Cryopharma (Tlajomulco de Zuñiga, Jalisco, México) and was dissolved in complete DMEM-F12 or RPMI. All stock solutions were wrapped in aluminum foil and stored at -20°C .

Cell culture

Murine microglia SIM-A9 (ATCC® HTB-22™) and murine breast cancer 4T1 (ATCC® HTB-26™) cells were purchased from the American Type Culture Collection (ATCC) and cultured in complete DMEM-F12 or RPMI for 4T1 and were routinely grown in 25-cm³ cell culture flasks (CORNING Enterprises, Corning, NY), following

ATCC instructions. Cells were maintained in a humidified incubator containing 5 % CO₂ at 37 °C.

Cell viability assessment

Cell growth inhibition was determined with Alamar blue (resazurin test). Cells (5x10³) were seeded in flat bottomed-96-well microtiter plates and exposed to different concentrations of EPI and CTX for 24 h. According to manufacturer's instructions, 20 µL of resazurin solution (0.15 mg/mL, Sigma-Aldrich, St. Louis, MO) was added to each well and incubated for 4 hours at 37 °C, after which, fluorescence was measured at 590 nm using a microplate reader (Varioskan Lux, ThermoFisher®).

Cell death analysis

For cell death induction, 5x10⁴ cells were seeded in 24-well plates (CORNING). Cells were treated with the indicated concentrations of EPI or CTX and incubated for 24 hours at 37 °C. SIM-A9 cells were then detached using glucose (1 mg/mL), EDTA (1 mM) and EGTA (1 mM) solution trypsin (GIBCO) was used for 4T1 cells. Subsequently, cells were washed with PBS and resuspended in 100 µL of annexin binding buffer (100 mM HEPES pH 7.4, 1.4 M NaCl, and 25 mM CaCl₂) staining cells with annexin-V-APC (0.1 µg/mL, BD Biosciences). Cells were then assessed with BD Accury 6 flow cytometer and analyzed using FlowJo Software.

Cell cycle analysis

In brief, 2x10⁵ cells in 6-well dishes (CORNING) were incubated with the indicated concentrations of EPI or CTX for 24 h. Cells were then washed and fixed in 70 % ethanol (30 % PBS). Cells were washed again, and cell cycle distribution was determined by DNA staining. Cells were treated simultaneously with 25 µg/mL propidium iodide (PI) and 50 µg/mL RNase at 37 °C for 20 min. For DNA degradation, we analyzed the SubG1 population obtained from cell cycle analysis using flow cytometry. Cell DNA contents were then analyzed using FlowJo Software.

Cell death-morphology analysis

After 5x10⁴ cells were seeded in 24-well dishes (CORNING) and treated with both chemotherapies at CC₅₀ for 24 hours, cells were then observed in an inverted microscope (Nikon Eclipse TS100) and images were captured for assessing changes in morphology (Lumiera INFINITY 1-2 CMOS 2.0 MP Camera) with 20x objective in bright-field.

γ-H2AX, p53 and p16 assessment

Cells were seeded (2x10⁵) in 6-well dishes (CORNING) and incubated after treatment with cytotoxic concentration 50 (CC₅₀) for 24 hours. After incubation, cells were detached, washed with PBS, and fixed with 80 % methanol (20 % PBS) and stored overnight at -20 °C. Subsequently, cells were washed with 2 % FACS buffer and then rehydrated with 10 % FACS buffer and cells were placed at 4 °C for 30 minutes.

For γ-H2AX, p53 and p16 assessment, ab26350 mouse monoclonal [9F3] to gamma H2A.X (phospho S139. Abcam, Cambridge, UK) antibody, sc-126 DO-1 antibody (Santa Cruz, TX, USA) or p16 INK4a (ab108349), respectively, were incubated in 2 % FACS buffer in constant agitation for 1 hour and washed with 2 % FACS buffer. Therefore, a secondary antibody Alexa Fluor 488 (ab150077) for γ-H2AX and p16 or Alexa Fluor 488 (A11001. Thermo Fisher Scientific, Waltham, MA, USA) for p53 were added in constant agitation for 30 minutes and washed with 2 % FACS buffer. Cells were then assessed with BD Accury 6 flow cytometer and analyzed as mentioned before.

Loss of mitochondrial membrane potential analysis

For this assessment, 5x10⁴ cells were seeded in 24-well dishes (CORNING) and then treated with CC₅₀ of CTX or EPI during 24 h. Cells were then harvested and washed with PBS. DIOC₆ (0.1 µM) (Invitrogene) staining was used by incubating cells at 37 °C for 30 min and washing them twice with PBS. Cells were then assessed by flow cytometry and analyzed using FlowJo Software.

ROS production analysis

Cells were seeded (5×10^4) in 24-well dishes (CORNING) and incubated with each chemotherapy at CC_{50} for 24 hours. Cells were then collected and washed with PBS. ROS generation was measured using DCFDA-AM (20 mM) (Thermo Fisher Scientific) staining that was incubated at 37 °C for 30 min. To evaluate the role of ROS in cell death, cells were pre-treated with N-acetylcysteine (NAC) for 30 minutes, then, cells were treated with CC_{50} of EPI or CTX. After 24 hours, cells were detached and resuspended in 100 μ L of annexin binding buffer (100 mM HEPES pH 7.4, 1.4 M NaCl, and 25 mM $CaCl_2$) staining cells with annexin-V-APC, after which, cell death was evaluated by flow cytometry.

Autophagy assessment

SIM-A9 and 4T1 cells were seeded in 24-well dishes (CORNING) at a confluence of 5×10^4 cells/well, and incubated with CC_{50} of EPI or CTX alone or pre-treated for 30 min with spautin-1 (Abcam) (autophagy inhibitor). Cells were then harvested and stained using CYTO ID (ENZO technologies) following the manufacturer's instructions. Cells were then evaluated by flow cytometry and analyzed using FlowJo Software.

Caspase activation assessment

SIM-A9 and 4T1 cultures were prepared by seeding 5×10^4 cells/well in 24-well dishes (CORNING), then incubated with EPI or CTX alone or pre-treated for 30 min with 10 mM QVD-Oph (Abcam) (pan caspase inhibitor). Cells were then detached and stained using a General Caspase Activation Kit (TF2-VAD-FMK) (Abcam) following the manufacturer's instructions. Caspase activity was determined by flow cytometry and analyzed using FlowJo Software.

NO production analysis

For NO assessment, cells were treated with sub-lethal concentrations of EPI, after 24 h cells were detached and incubated at 37 °C for 30 minutes with DAF-FM (ThermoFisher

Scientific) and washed twice with PBS. Increases in cell fluorescence were measured by flow cytometry and analyzed using FlowJo Software.

Cytokine quantification

Cytokines in supernatants were analyzed with the CBA Mouse Inflammation kit (Beckman Dickinson and Company, Franklin Lakes, NJ) according to the manufacturer instructions. SIM-A9 cells, were seeded at a confluence of 5×10^4 cells/well in 24-well dishes (CORNING) subsequently incubated for 24 h with sub-lethal concentrations of EPI. Supernatants were then collected and analyzed by flow cytometry using BD Accury 6 flow cytometer and were quantified using Cytometric Bead Array Analysis Software (FCAP) (Beckman Dickinson and Company).

Iba-1 expression assessment

Cells were seeded (2×10^5) in 6-well dishes (CORNING) and treated with both chemotherapies at CC_{50} for 24 hours. After incubation, cells were detached, washed with PBS and fixed with 80 % methanol (20 % PBS) and stored overnight at -20 °C. Subsequently, cells were washed with 2 % FACS buffer and then rehydrated with 10 % FACS buffer and cells were placed at 4 °C for 30 minutes. For Iba-1 expression polyclonal antibody (PA5-27436 Invitrogen, Thermo Fisher Scientific, Waltham, MA, USA) was incubated in 2 % FACS buffer in constant agitation for 1 hour and washed with 2 % FACS buffer. Then, a secondary antibody Alexa Fluor 488 (ab150077) was added in constant agitation for 30 minutes and washed with 2 % FACS buffer. Cells were then assessed with BD Accury 6 flow cytometer and analyzed as mentioned before.

Statistical analysis

Results represent the mean \pm SD of at least triplicate determinations from three independent experiments. Significant differences were considered if $p < 0.05$ using paired student's t-test. Data was analyzed using GraphPad Prism (San Diego, CA).

RESULTS

Microglia cells are more sensitive to chemotherapy than breast cancer cells

EPI and CTX have been shown to suppress cell viability in several tumor cell lines (Trebunova et al., 2012; Xiong et al., 2016). However, their effect on cell viability and cell death on microglia cells has not been assessed, thus, we determined the effect of CTX and EPI in murine SIM-A9 microglia cells using 4T1, murine BC cells, as a control. Our results show that EPI and CTX decreased the viability of SIM-A9 and 4T1 cells in a dose-dependent manner (Figure 1A), however a higher concentration of chemotherapy was necessary to induce the same cytotoxic effect on BC cells.

We further evaluated cell death by assessing phosphatidylserine (PS) exposure (Figure 1B). In healthy cells, PS is generally restricted to the inner leaflet of the cell membrane, and the exposure of phosphatidylserine on the outer leaflet is an effect that is commonly observed during cell death (Reyes-Ruiz et al., 2015). We determined PS externalization by flow cytometry of Annexin-V-APC-labelled cells that were treated with EPI and CTX at different doses for 24 h. As shown in Figure 1B, EPI and CTX induced cell death on SIM-A9 at significantly lower doses compared to 4T1 cells according to population of Annexin-V positive. Furthermore, as expected with resazurin results, EPI and CTX induced cell-death in a concentration-dependent manner. EPI induced cell death in 50 % of the cells (CC_{50}) at 1.0 μ M in microglia cells, and 5 μ M in breast cancer cells, while CTX induced 50 % of cell death (CC_{50}) at 15 mM in SIM-A9 and 30 mM in 4T1 cells. The CC_{50} for both chemotherapies were confirmed by trypan-blue staining (see Supplementary information). Moreover, morphological assessment showed a reduction of cell confluence and alterations in cell morphology that were visible after 24 hours of EPI and CTX treatment (Figure 1C).

EPI and CTX induce DNA damage and cell cycle arrest

Once we observed cell death induction in SIM-A9 and 4T1 cells after EPI and CTX treatment, we decided to elucidate the mechanism. First, to evaluate if DNA damage was taking place after chemotherapy treatment of microglia cells, we first assessed H2AX phosphorylation (γ -H2AX). DNA damage can lead to γ -H2AX, the first step in recruiting and localizing DNA repair proteins (Mah et al., 2010), which can initiate cell cycle arrest, followed by cell death and DNA degradation. We found that treatment with EPI and CTX increase the percentage of γ -H2AX-positive cells from 3 % to 40 % and 33 % respectively in SIM-A9 (left) and from 2 % to 61 % and 33 % respectively in 4T1 (right) cells (Figure 2A), indicating that both treatments induce DNA damage. Furthermore, we assessed p53 expression, and results show an increase on p53 expression for both treatments in SIM-A9, from 5 % to 48 % and 37 % for EPI and CTX, respectively (Figure 2B), by the time that p16 assessment showed a significant increase in CTX treatment in SIM-A9 cells (from 3 % to 13 %), while in 4T1, EPI and CTX treatment respectively, from 3 % to 36 % and 15 % (Figure 2C).

We then assessed cell cycle in microglia and breast cancer cells using PI staining. Our analysis shows that EPI induces cell cycle arrest on G2 in SIM-A9 and G1 and G2 in 4T1 cells, by the time that CTX induces cell cycle arrest on G1 in SIM-A9 and G2 in 4T1 cells, compared to control cells (Figure 2D).

As DNA degradation is a recurrent feature of cell death, especially after DNA damage (Kawane et al., 2014), we analyzed DNA degradation by quantification of sub-G1 population in microglia and breast cancer cells treated with EPI and CTX. Results exhibit 22 % and 45 % of DNA degradation in SIM-A9 corresponding to EPI and CTX-24 hours treatment, respectively. In 4T1 cells DNA degradation relation was 17 % for EPI and 65 % in CTX for 24 hours treatment (Figure 2E). DNA degradation has been reported as a

feature of apoptosis, hence, we decided to inquire in other apoptotic features such as loss of mitochondrial membrane potential and caspase activation.

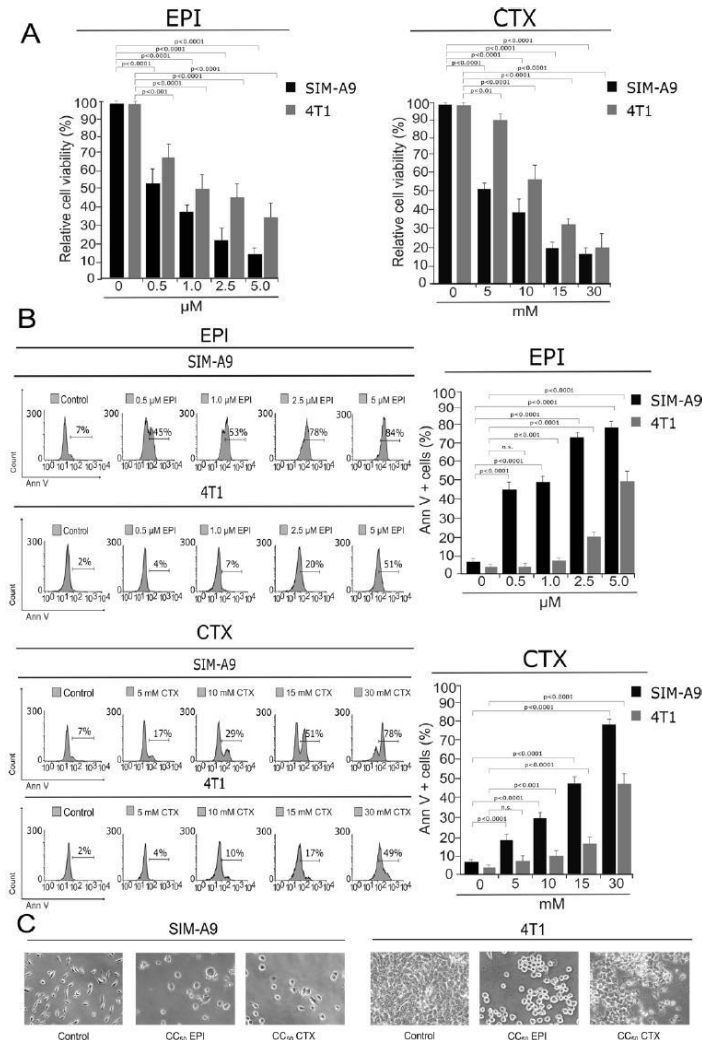


Figure 1: Cytotoxicity induced by EPI and CTX in SIM-A9 and 4T1 cells. SIM-A9 and 4T1 cells were treated with various concentrations (0.5, 1.0, 2.5 and 5.0 μ M) of EPI, and 5, 10, 15 and 30 mM of CTX for 24 hours. **A)** Cell viability was measured by resazurin assay represented as percentage of control (non-treated cell viability = 100 %) presenting means \pm SD. **B)** Cell death was measured by flow cytometry through Annexin-V staining. The histograms refer to Annexin-V positive cells analyzed by FlowJo software (left) and the bar graphs represent the mean (\pm SD) (right). **C)** Morphology assessment was performed with Nikon Eclipse TS100 using 20x objective.

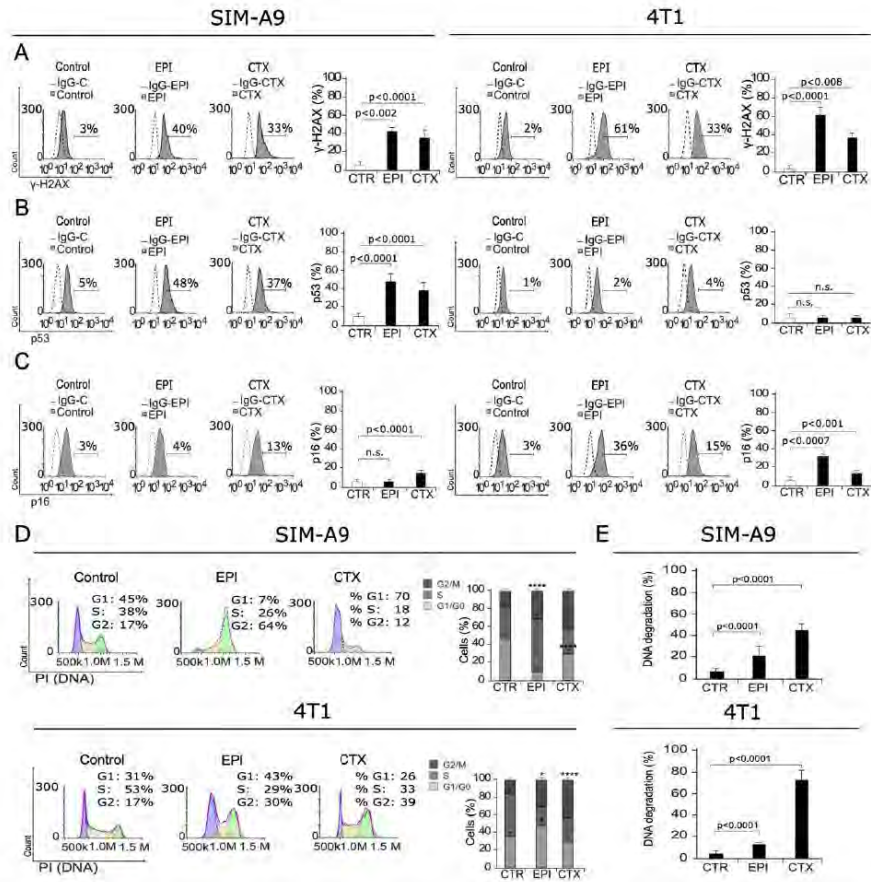


Figure 2: DNA damage and cell cycle arrest. SIM-A9 and 4T1 cells were treated for 24 h with CC_{50} of EPI or CTX and assessed by flow cytometry. Representative histograms of nuclear damage analysis and quantification measured through **A)** γ -H2AX assessment, **B)** p53 expression, **C)** p16 expression, and **D)** Cell cycle analysis. Bars at right represent the mean \pm SD. **E)** DNA degradation was evaluated using propidium iodide (PI) staining as in D, and SubG1 population was analyzed and mean (\pm SD) was presented in bar graphs.

EPI and CTX induce loss of mitochondrial membrane potential and ROS production

The role of mitochondria in cell death is widely known, as they play a central role in cellular metabolism and cell death signaling. Furthermore, mitochondrial dysfunction

leads to reactive-oxygen species (ROS) production (Vakifahmetoglu-Norberg et al., 2017). We assessed whether EPI and CTX were able to induce loss of mitochondrial membrane potential ($\Delta\Psi_m$) and ROS production, through 3,3'-Dihexyloxycarbocyanine Iodide (DIOC6) and 2',7'-dichlorofluorescin diacetate (DCFDA) staining, respectively,

followed by flow cytometric analysis. As shown in Figure 3A, EPI and CTX induce $\Delta\Psi_m$ loss and ROS production, as shown by flow cytometry (Figure 3B) in both cell lines. We also found a correlation between ROS production and PS exposure, because approximately 50 % of the cells display these two features (Figure 3C). Then, we used the antioxidant N-acetyl-L-cysteine (NAC), which increases intracellular glutathione (GSH) levels and possesses thiol-disulfide exchange activity (Xie et al., 2018), to determine if ROS were playing a role in chemotherapies-induced cell death, pre-treating cells with NAC. As shown in Figure 3C, NAC was able to inhibit EPI induced cell death in SIM-A9 cells, as observed by the reduction of Annexin V+ staining. These results show that EPI and CTX induce $\Delta\Psi_m$ loss and ROS production, and particularly after EPI treatment we observed ROS-dependent cell death in SIM-A9. On the other hand, we observed ROS production in 4T1 cells treated with CC_{50} of EPI and

CTX. Using NAC, we determined ROS dependency for cell death in 4T1 cells after CTX treatment, but not after EPI's treatment.

EPI and CTX induce autophagy

It has been proven that ROS and $\Delta\Psi_m$ loss could lead to autophagy, a protective mechanism that helps cells survive and has been previously described as a regulatory mechanism in microglia cells (Plaza-Zabala et al., 2017). In this regard, we assessed autophagosome formation in microglia cells after treatment with EPI and CTX. As shown in Figure 4A, both chemotherapies induce autophagy at CC_{50} . Furthermore, we evaluated cell death in cells pre-treated with spautin-1 (SP-1) an autophagy inhibitor by enhancing degradation of beclin-1 (Schott et al., 2018), to confirm if the autophagy was playing a protective role. We observed that SP-1 pre-treatment increased the cell death induced by the CC_{50} of both chemotherapies (Figure 4B).

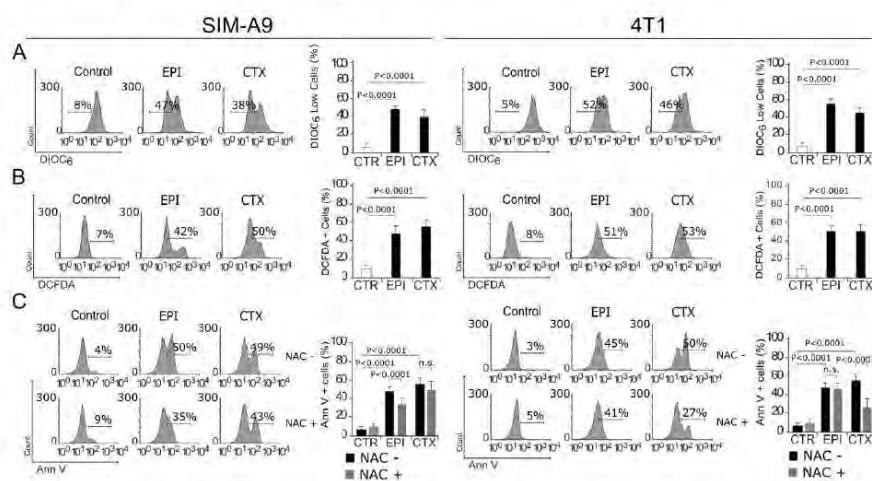


Figure 3: Mitochondrial alterations and ROS production. SIM-A9 and 4T1 cells were left without treatment (control) or treated with CC_{50} of EPI and CTX for 24 h and assessed by flow cytometry. **A)** Representative histogram of mitochondrial membrane potential measured by DIOC6 staining (left), bars represent the mean \pm SD (right). **B)** Representative histogram of ROS production measured with DCFDA (left), bars represent the mean \pm SD (right). **C)** Representative histogram of Annexin V staining, in cells pre-treated or not with the antioxidant NAC and then treated with EPI or CTX (left), bars represent the mean \pm SD (right).

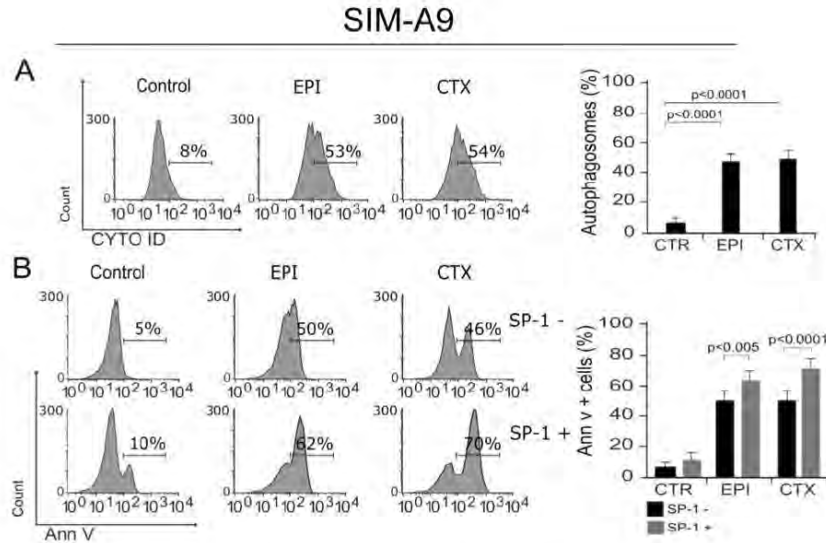


Figure 4: Autophagosome formation and cell death. **A)** Representative histogram of autophagy, measured by flow cytometry using Cyto-ID staining in SIM-A9 cells treated with EPI and CTX for 24 hours (left), bars represent the mean \pm SD (right). **B)** Representative histograms showing autophagy involvement in cell death, assessed by pre-treating SIM-A9 cells with the autophagy inhibitor, SP-1, and measuring cell death by Ann V-positive cells after 24 hours of treatment with EPI or CTX (CC₅₀) (left), bars represent the mean \pm SD (right).

EPI and CTX induce caspase activation

To evaluate if the main molecular regulators of apoptosis were activated by EPI and CTX, we assessed caspase activity (McIlwain et al., 2015) after treatment. As shown in Figure 5, EPI and CTX induce caspase activation, as determined by the detection of TF2-VAD-FMK (Figure 5A). To determine if this type of cell death was dependent on caspase activity, we used the pan-caspase inhibitor, QVD-Oph (Keonie and Brown, 2015). As Figure 5A shows, QVD was able to inhibit caspase activation in SIM-A9 and 4T1 cells. Furthermore, we found that chemotherapies-induced cell death was diminished in presence of QVD (Figure 5B). This result shows that EPI and CTX induce caspase-dependent cell death in both cell lines.

EPI's low concentration induces DNA damage and cell cycle arrest

Studies show that EPI and CTX have limited to none ability to cross blood brain barrier (BBB) (Guo et al., 2011), a selective protective membrane that covers blood vessels that cross the central nervous system (Vieira and Gamarra, 2016), however, anthracyclines and alkylating agents are able to disrupt BBB after a certain number of chemotherapy cycles (Ren et al., 2019). Considering the quantity of chemotherapy needed to achieve CC₅₀, we decided to test low concentrations of EPI and CTX to determine whether these concentrations induce DNA damage and further cell cycle arrest. For this, we used sub-lethal (SL) concentrations and CC₂₀ of EPI (SL of 0.1 μ M

and CC₂₀ of 0.25 μM), and CTX (SL of 2 mM and CC₂₀ of 5 mM) in microglia cells.

Our results show that EPI can induce DNA damage (Figure 6A) and cell cycle arrest (Figure 6B) at SL and CC₂₀. On the other

hand, CTX did induce DNA damage at SL concentration (Figure 6A), but no cell cycle arrest was observed, although G1 arrest was observed at CC₂₀ (Figure 6B).

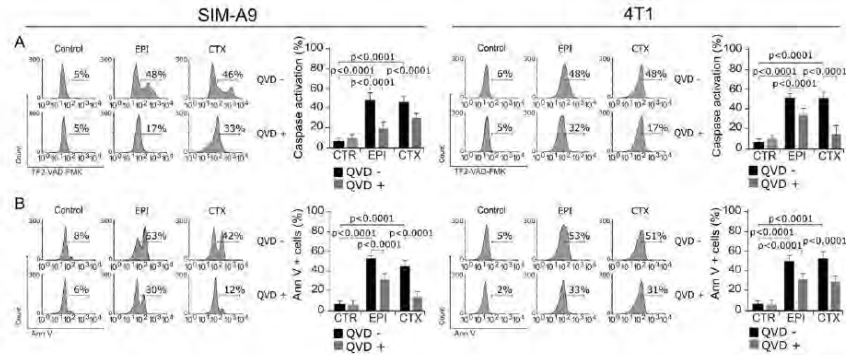


Figure 5: Activation and role of caspases in cell death. A) Representative histograms of caspase activation measured by flow cytometry using TF2-VAD-FMK in SIM-A9 and 4T1 cells treated with EPI and CTX for 24 hours (left). Bars at right represent the mean ± SD. B) Cells were pretreated with the pan-caspase inhibitor QVD-Oph and then treated with EPI or CTX (CC₅₀) for 24 hours and Ann V positive SIM-A9 or 4T1 cells were assessed. Representative histograms (left) and bar graphs presenting mean ± SD (right) are shown.

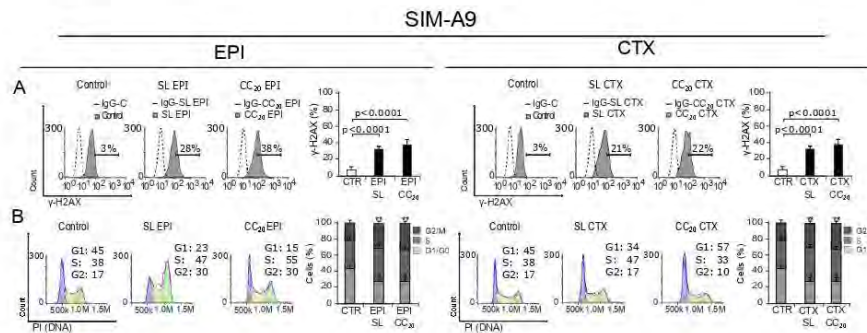


Figure 6: DNA damage and cell cycle arrest induced by low concentrations of EPI and CTX. A) Representative histograms of nuclear damage analysis and quantification measured through γ-H2AX. Bars at right represent the mean ± SD. B) Cell cycle analysis by propidium iodide (PI) staining after treatment with SL or CC₂₀ of EPI or CTX in SIM-A9 for 24 h. Representative histograms (left) and bar graphs presenting mean ± SD (right) are shown.

EPI induces microglia activation

As our results show DNA damage and cell cycle arrest from a sub-lethal concentration, we decided to evaluate if EPI was also able to induce the production of the neuroinflammatory mediator, nitric oxide (NO) (Frank et al., 2019). In Figure 7A, we can observe an increase in NO production in cells treated with EPI at a SL concentration and EPI CC₂₀. Then, as cytokines are key players in neuroinflammation, and as an increase in p16 and γ -H2AX have been related to cytokine production by microglia (Marques et al., 2020) we next assessed cytokine release after EPI (SL

and CC₂₀) treatment. Our results show that EPI induces a significant increase in TNF- α and IL-6 release at SL and CC₂₀ (Figure 7B). These results led to the idea that microglia cells could have been activated by EPI treatment, to solve that we assessed Iba-1 (ionized calcium-binding adapter molecule 1) expression, as its overexpression is correlated to microglia activation (Zhao et al., 2019). In Figure 7C we observe that EPI increases Iba-1 expression in cells treated with SL and CC₂₀ concentrations, indicating that EPI's treatment induces microglia activation.

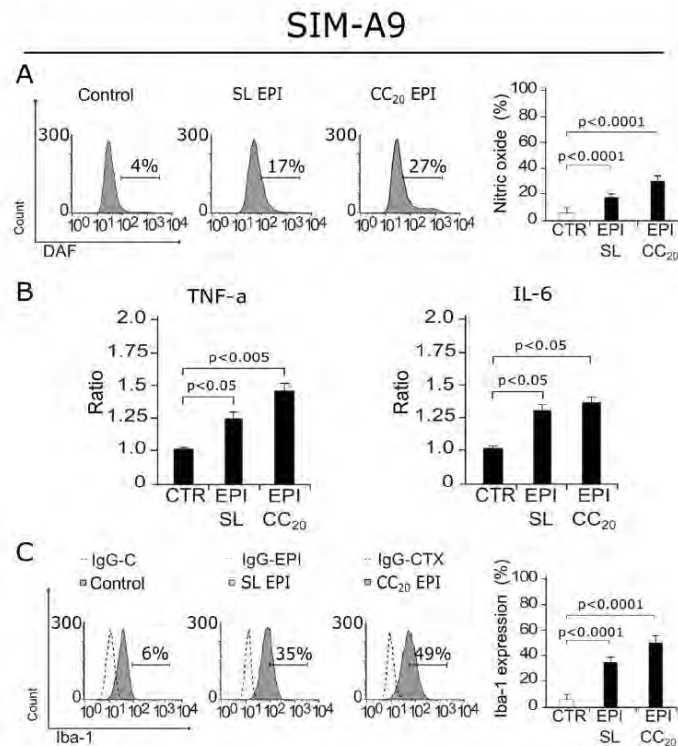


Figure 7: NO production, cytokine release and Iba-1 expression after SIM-A9 treatment with EPI. **A)** Representative histograms of Nitric oxide (NO) (left) production measured through DAF staining, bar graphs presenting mean \pm SD (right) are shown. **B)** Bar graphs displaying mean \pm SD of TNF- α and IL-6 cytokine release assessed in SIM-A9 cells treated for 24 hours with sub-lethal (SL) concentration of EPI or EPI CC₂₀. **C)** Representative histograms of Iba-1 (left) expression assessed by anti-Iba-1 antibody, bar graphs presenting mean \pm SD (right) are shown.

DISCUSSION

The objective of this study was to analyze the effects induced by EPI and CTX in microglia cells, comparing sensitivity and cell death mechanisms between both cell types. The results shown in this study were noteworthy, starting with the fact that SIM-A9 cells are highly susceptible to EPI and CTX, approximately five times more for EPI and two times more for CTX than 4T1. There have been several studies showing the response of microglia with chemotherapies, but none for them had addressed the type of cell death induced by EPI and CTX. Here we show that both chemotherapies induce DNA damage, as shown by γ H2AX, an histone variant that respond to double strand breaks (Kitazumi and Tsukahara, 2011), that has also been described as a senescent marker (Noren Hooten and Evans, 2017). To assess activation of repair genes, p53 and p16 were evaluated, since 4T1 cells are p53 null (Yerlikaya et al., 2012), hence p16 assessment was important to compare proteins capable of inducing cell cycle arrest. Increase in p53 activation and in p16 was observed in SIM-A9 cells, according to cell cycle arrest in G1 and in G2 phase by EPI and CTX-treatment, respectively. Some chemotherapies are able to activate and produce p53 and p16 (Marques et al., 2020) in microglia, however, p16 and γ H2AX are also senescent markers, pointing out that more research must be made to determine if EPI and CTX induce senescence in microglia cells, which is known that can lead to neurodegeneration (Angelova and Brown, 2019).

It is well known that most chemotherapies are able to disrupt mitochondrial membrane potential (Gorini et al., 2018), our findings suggest that $\Delta\psi_m$ loss in microglia occurs and could lead to oxidative stress, which is known to occur in microglia and in tissue of *in vivo* models treated with doxorubicin (DOX) (Cruzado et al., 2014), methotrexate (MTX) (Gibson et al., 2019), and some other chemotherapies (Gaman et al., 2016), but the role of ROS in cell death has not been described before. We observed a dependence of ROS for

cell death in SIM-A9 treated with EPI. Anthracyclines increase ROS production to induce cell death but, oxidative stress could lead to a direct disruption in CNS homeostasis, generating neurotoxicity and diminishing cognitive performance in patients (Bergamini et al., 2018; Solleiro-Villavicencio and Rivas-Arancibia 2018; Misra et al., 2020). As we demonstrated autophagy induction after chemotherapy treatment (Figure 4), cytotoxicity of both chemotherapeutic agents could be reduced by pro-survival autophagy inductors as it has been described before in *in vivo* studies (Yi et al., 2020). Also, our assessment of caspase activity showed evidence of caspase activation in both treatments over microglia and breast cancer cells, as well as their dependency for cell death. These results lead to the conclusion that apoptotic cell death was happening in microglia after 24 hours of EPI CC₅₀ and CTX CC₅₀ treatment.

Although it is widely known that CTX is not able to cross BBB, there is no information for EPI, however, DOX has limited capacity to penetrate BBB (Vieira and Gamarra, 2016). Although scarce, there is evidence supporting chemotherapy increase BBB permeability, allowing the direct interaction between chemotherapies and microglia (Ren et al., 2017). By analyzing how much chemotherapy is needed to achieve 50 % of cytotoxicity (CC₅₀), we asked ourselves what would happen if lower concentrations of chemotherapy interact with microglia. Hence, we used sub-lethal (non-lethal) concentrations and CC₂₀ of both agents. Results of γ H2AX analysis show that both chemotherapies induce DNA damage at SL concentration and CC₂₀. Furthermore, as some chemotherapies can disrupt the cell cycle at low concentrations, we evaluated if DNA damage could lead to cell cycle arrest, indeed, cells treated with EPI from SL concentrations to CC₅₀ were found arrested in G2, whereas for CTX treated cells arrest G1 was observed at CC₂₀ and CC₅₀. These findings suggest that EPI's negative effects in microglia occur before cytotoxicity. Similar findings have been reported with DOX in microglia cells (Marques et al., 2020).

Because EPI's negative effects in microglia were evident from SL concentrations, we decided to assess NO production at the lowest concentration of EPI where cell death was not observed. Increases in NO have been associated with neuroinflammation and augmenting oxidative stress in CNS (Frank et al., 2019). As we observed, EPI at SL and CC₂₀ can increase NO production. It has also been described that increases in TNF- α and IL-6 could be hurtful for the CNS and there is evidence of their induction by some chemotherapies (Ren et al., 2017). As microglia cells are capable of releasing cytokines depending on their activation pathway, we assessed cytokine release in response to chemotherapy stimuli. We observed and increase in TNF- α and IL-6, at SL of EPI after 24 hours of treatment, this has been proven in microglia cells treated with DOX and could mean that these chemotherapies could have the capability to activate microglia and dysregulate cytokines in CNS that could potentially initiate neurodegeneration *in vivo* (Marques et al., 2020). However, other microglial activation markers had to be assessed to conclude activation, hence, we assessed Iba-1 expression (ionized calcium-binding adapter molecule 1), as its overexpression is correlated with microglia activation (Zhao et al., 2019). We observed that EPI's treatment induced Iba-1 overexpression. This result, along with NO production and pro-inflammatory cytokine release led us to conclude that EPI's treatment induces microglia activation, which has been associated with neurodegeneration and it's believed to be one of the mechanisms of CRCI (Monje and Dietrich, 2012; Cerulla et al., 2019; Gibson and Monje, 2019; Du et al., 2021).

It is also noteworthy that a very low concentration of EPI is needed to damage microglia or to induce their activation. Apoptosis induced by TNF- α released by activated microglia in progenitor neural cells (NPC) has been observed (Guadagno et al., 2013), as well as cognitive decline in LPS stimulated-

mice in *in vivo* models (Zhao et al., 2019). Finally, IL-6 has not only been associated with neurodegeneration and senescence, but with loss of lean body and fat mass in tumor-free mice (Elsea et al., 2015), suggesting the importance of assessing cytokine release by peripheral immune cells treated with chemotherapy and moreover, the interaction between the peripheral and central immune system. Thus, although further research must be done to assess these effects *in vivo*, here we demonstrate that EPI and CTX induce important cell effects in microglia, causing DNA damage since sub-lethal concentrations, while EPI induces microglia activation and a pro-inflammatory phenotype at low concentrations.

CONCLUSIONS

In summary, the present research demonstrates that microglia cells are more susceptible to CTX and EPI than breast cancer cells (approximately two to five times with CTX and EPI respectively) and both chemotherapies induced DNA damage, cell cycle arrest, and apoptosis (Figure 8). Interestingly, low concentrations of EPI induced microglia activation, as demonstrated by NO production, pro-inflammatory cytokines release, IL-6 and TNF- α , and the overexpression of Iba-1 (Figure 8). Further research is needed to evaluate if this could happen *in vivo*. Also, this work opens the door to the study of new agents that can diminish microglia cell death and activation, as well as the identification of the mechanisms leading to these effects.

Declaration of competing interest

The authors have no conflicts of interest to declare.

Acknowledgments

This work was funded by PAICYT (UANL) (grant CN1563-21) and the Laboratorio de Inmunología y Virología (UANL).

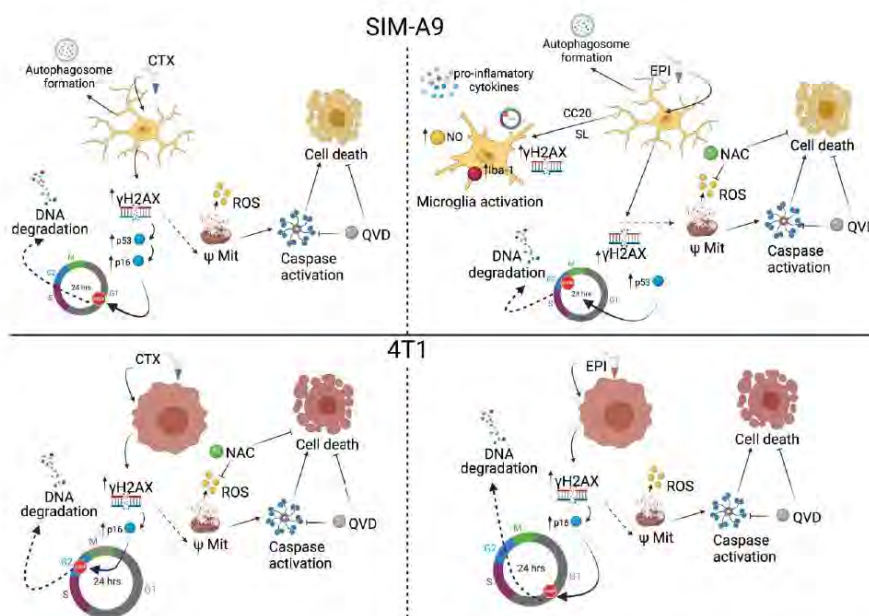


Figure 8: Chemotherapy effect in microglia and breast cancer cells. CTX induces DNA damage and cell cycle arrest, as well as mitochondrial alterations and increase in ROS production leading to ROS-dependent cell death in breast cancer cells (down left), but not in microglia cells (upper left). Caspase activation and caspase-dependent cell death are also observed in both cell lines. In microglia, CTX treatment induces autophagosome formation. EPI induces DNA damage and cell cycle arrest, as well as mitochondrial alterations and increase in ROS production leading to ROS-dependent cell death in microglia (upper right), but not in breast cancer cells (down right). Caspase activation and caspase-dependent cell death are also observed in both cell lines. Furthermore, EPI also induces autophagosome formation in microglia. Finally, CC₂₀ and sub-lethal concentrations of EPI induce DNA damage, cell cycle arrest and microglia activation, increasing nitric oxide production and pro-inflammatory cytokine release in SIM-A9 cells.

REFERENCES

- American Cancer Society. What is breast cancer? Am Cancer Soc Cancer Facts Fig Atlanta, Ga. Am Cancer Soc. 2017;1-19. <http://www.cancer.org/cancer/breast-cancer/about/what-is-breast-cancer.html>.
- Angelova DM, Brown DR. Microglia and the aging brain: are senescent microglia the key to neurodegeneration? *J Neurochem*. 2019;151:676-88.
- Bergamini G, Mechtersheimer J, Azzinnari D, Sigris H, Buerge M, Dallmann R, et al. Chronic social stress induces peripheral and central immune activation, blunted mesolimbic dopamine function, and reduced reward-directed behaviour in mice. *Neurobiol Stress*. 2018;8:42-56.
- Cerulla N, Arcusa À, Navarro JB, de la Osa N, Garolera M, Enero C, et al. Cognitive impairment following chemotherapy for breast cancer: The impact of practice effect on results. *J Clin Exp Neuropsychol*. 2019;41:290-9.
- Cruzado JA, López-Santiago S, Martínez-Marín V, José-Moreno G, Custodio AB, Feliu J. Longitudinal study of cognitive dysfunctions induced by adjuvant chemotherapy in colon cancer patients. *Support Care Cancer*. 2014;22:1815-23.

- de Ruiter MB, Reneman L, Boogerd W, Veltman DJ, Caan M, Douaud G, et al. Late effects of high-dose adjuvant chemotherapy on white and gray matter in breast cancer survivors: converging results from multimodal magnetic resonance imaging. *Hum Brain Mapp.* 2012; 33:2971-83.
- Du J, Zhang A, Li J, Liu X, Wu S, Wang B, et al. Doxorubicin-induced cognitive impairment: the mechanistic insights. *Front Oncol.* 2021;11:1-10.
- Elsa CR, Kneiss JA, Wood LJ. Induction of IL-6 by cytotoxic chemotherapy is associated with loss of lean body and fat mass in tumor-free female mice. *Biol Res Nurs.* 2015;17:549-57.
- Feng H, Dong Y, Wu J, Qiao Y, Zhu G, Jin H, et al. Epirubicin pretreatment enhances NK cell-mediated cytotoxicity against breast cancer cells in vitro. *Am J Transl Res.* 2016;8:473-84.
- Frank MG, Fonken LK, Watkins LR, Maier SF. Microglia: Neuroimmune-sensors of stress. *Semin Cell Dev Biol.* 2019;94:176-85.
- Galluzzi L, Vitale I, Aaronson SA, Abrams JM, Adam D, Agostinis P, et al. Molecular mechanisms of cell death: Recommendations of the Nomenclature Committee on Cell Death 2018. *Cell Death Differ.* 2018;25:486-541.
- Gaman AM, Uzoni A, Popa-Wagner A, Andrei A, Petcu EB. The role of oxidative stress in etiopathogenesis of chemotherapy induced cognitive impairment (CICD)-"Chemobrain". *Aging Dis.* 2016;7: 307-17.
- Gibson EM, Monje M. Emerging mechanistic underpinnings and therapeutic targets for chemotherapy-related cognitive impairment. *Curr Opin Oncol.* 2019; 31:531-9.
- Gibson EM, Nagaraja S, Ocampo A, Tam LT, Wood LS, Pallegar PN, et al. Methotrexate chemotherapy induces persistent tri-glial dysregulation that underlies chemotherapy-related cognitive impairment. *Cell.* 2019;176:43-55.e13.
- Gorini S, De Angelis A, Berrino L, Malara N, Rosano G, Ferraro E. Chemotherapeutic drugs and mitochondrial dysfunction: Focus on doxorubicin, trastuzumab, and sunitinib. *Oxid Med Cell Longev.* 2018;2018: 7582730.
- Guadagno J, Xu X, Karajgikar M, Brown A, Cregan SP. Microglia-derived TNF α induces apoptosis in neural precursor cells via transcriptional activation of the Bcl-2 family member Puma. *Cell Death Dis.* 2013;4(3):e538.
- Guo L, Fan L, Pang Z, Ren J, Ren Y, Li J, et al. TRAIL and doxorubicin combination enhances anti-glioblastoma effect based on passive tumor targeting of liposomes. *J Control Release.* 2011;154:93-102.
- Kawane K, Motani K, Nagata S. DNA degradation and its defects. *Cold Spring Harb Perspect Biol.* 2014;6:1-14.
- Keoni CL, Brown TL. Inhibition of apoptosis and efficacy of pan caspase inhibitor, Q-VD-OPh, in models of human disease. *J Cell Death.* 2015;8:1-7.
- Kitazumi I, Tsukahara M. Regulation of DNA fragmentation: The role of caspases and phosphorylation. *FEBS J.* 2011;278:427-41.
- Mah LJ, El-Osta A, Karagiannis TC. γ H2AX: A sensitive molecular marker of DNA damage and repair. *Leukemia.* 2010;24:679-86.
- Marques L, Johnson AA, Stolzing A. Doxorubicin generates senescent microglia that exhibit altered proteomes, higher levels of cytokine secretion, and a decreased ability to internalize amyloid β . *Exp Cell Res.* 2020;395:112203.
- Matsos A, Loomes M, Zhou I, Macmillan E, Sabel I, Rotziokos E, et al. Chemotherapy-induced cognitive impairments: White matter pathologies. *Cancer Treat Rev.* 2017;61:6-14.
- McIlwain DR, Berger T, Mak TW. Caspase functions in cell death and disease. *Cold Spring Harb Perspect Biol.* 2015;5(4):a008656.
- McLeary F, Davis A, Rudrawar S, Perkins A, Anoopkumar-Dukie S. Mechanisms underlying select chemotherapeutic-agent-induced neuroinflammation and subsequent neurodegeneration. *Eur J Pharmacol.* 2019;842:49-56.
- Misra UK, Singh SK, Kalita J, Kumar A. Astrocyte activation following nitrous oxide exposure is related to oxidative stress and glutamate excitotoxicity. *Brain Res.* 2020;1730:146645.
- Monje M, Dietrich J. Cognitive side effects of cancer therapy demonstrate a functional role for adult neurogenesis. *Behav Brain Res.* 2012;227:376-9.
- Noren Hooten N, Evans MK. Techniques to induce and quantify cellular senescence. *J Vis Exp.* 2017;2017:1-14.
- Ongnok B, Chattipakorn N, Chattipakorn SC. Doxorubicin and cisplatin induced cognitive impairment: The possible mechanisms and interventions. *Exp Neurol.* 2020;324:113118.

- Plaza-Zabala A, Sierra-Torre V, Sierra A. Autophagy and microglia: Novel partners in neurodegeneration and aging. *Int J Mol Sci.* 2017;18:598.
- Prasad SB, Rosangkima G, Nicol BM. Cyclophosphamide and ascorbic acid-mediated ultrastructural and biochemical changes in Dalton's lymphoma cells in vivo. *Eur J Pharmacol.* 2010;645:47–54.
- Ren X, St Clair DK, Butterfield DA. Dysregulation of cytokine mediated chemotherapy induced cognitive impairment. *Pharmacol Res.* 2017;117:267–73.
- Ren X, Boriero D, Chaiswing L, Bondada S, St Clair DK, Butterfield DA. Plausible biochemical mechanisms of chemotherapy-induced cognitive impairment ("chemobrain"), a condition that significantly impairs the quality of life of many cancer survivors. *Biochim Biophys Acta - Mol Basis Dis.* 2019;1865:1088–97.
- Reyes-Ruiz A, Benitez-Londoño M, Martínez-Torres AC, Rodríguez-Padilla C. Análisis del mecanismo citotóxico inducido por el IMMUNEPOTENT CRP sobre células HELA. *Revista de Ciencias Farmaceuticas y Biomedicina.* 2015;1(Ed. Esp. 1):16. http://www.fcq.uanl.mx/wp-content/uploads/2016/05/15RC-DF_AR.pdf.
- Schott CR, Ludwig L, Mutsaers AJ, Foster RA, Wood GA. The autophagy inhibitor spautin-1, either alone or combined with doxorubicin, decreases cell survival and colony formation in canine appendicular osteosarcoma cells. *PLoS One.* 2018;13:7–10.
- Selamat MH, Loh SY, Mackenzie L, Vardy J. Chemobrain experienced by breast cancer survivors: A meta-ethnography study investigating research and care implications. *PLoS One.* 2014;9(9):e108002.
- Shen CY, Chen VCH, Yeh DC, Huang SL, Zhang XR, Chai JW, et al. Association of functional dorsal attention network alterations with breast cancer and chemotherapy. *Sci Rep.* 2019;9:104.
- Solleiro-Villavicencio H, Rivas-Arancibia S. Effect of chronic oxidative stress on neuroinflammatory response mediated by CD4+T cells in neurodegenerative diseases. *Front Cell Neurosci.* 2018;12:114.
- Standish LJ, Sweet ES, Novack J, Wenner CA, Bridge C, Nelson A, et al. Breast cancer and the immune system. *J Soc Integr Oncol.* 2008;6:158–68.
- Taymaz-Nikerel H, Karabekmez ME, Eraslan S, Kırdar B. Doxorubicin induces an extensive transcriptional and metabolic rewiring in yeast cells. *Sci Rep.* 2018;8:13672.
- Trebunova M, Laputkova G, Slaba E, Lacjakova K, Verebova A. Effects of docetaxel, doxorubicin and cyclophosphamide on human breast cancer cell line MCF-7. *Anticancer Res.* 2012;32:2849–54.
- Uchida M, Nakamura T, Shima T, Yoshimoto G, Kato K, Hosohata K, et al. Comparative quantification of chemotherapy-induced nausea and emesis between the common terminology criteria for adverse events and the multinational association of supportive care in cancer antiemesis tool. *Biol Pharm Bull.* 2018;41:1667–71.
- Vakifahmetoglu-Norberg H, Uchida AT, Norberg E. The role of mitochondria in metabolism and cell death. *Biochem Biophys Res Commun.* 2017;482:426–31.
- Verma R, Foster RE, Horgan K, Mounsey K, Nixon H, Smalle N, et al. Lymphocyte depletion and repopulation after chemotherapy for primary breast cancer. *Breast Cancer Res.* 2016;18(1):10.
- Vieira DB, Gamarra LF. Getting into the brain: Liposome-based strategies for effective drug delivery across the blood-brain barrier. *Int J Nanomedicine.* 2016;11:5381–414.
- Wu J, Xue X, Zhang B, Cao H, Kong F, Jiang W, et al. Enhanced antitumor activity and attenuated cardiotoxicity of Epirubicin combined with Paeonol against breast cancer. *Tumor Biol.* 2016;37:12301–13.
- Xie C, Yi J, Lu J, Nie M, Huang M, Rong J, et al. N-Acetylcysteine reduces ROS-mediated oxidative DNA damage and PI3K/Akt pathway activation induced by *Helicobacter pylori* infection. *Oxid Med Cell Longev.* 2018;2018:1874985.
- Xiong J, Fan F, Zhang Y, Chen W, Mao W. Epirubicin inhibits proliferation of breast cancer cells through upregulating p21cip1 expression. *Int J Clin Exp Med.* 2016;9:22764–72.
- Yarlagadda A, Alfson E, Clayton AH. The blood brain barrier and the role of cytokines in neuropsychiatry. *Psychiatry.* 2009;6:18–22.
- Yerlikaya A, Okur E, Ulukaya E. The p53-independent induction of apoptosis in breast cancer cells in response to proteasome inhibitor bortezomib. *Tumor Biol.* 2012;33:1385–92.
- Yi LT, Dong SQ, Wang SS, Chen M, Li CF, Geng D, et al. Curcumin attenuates cognitive impairment by enhancing autophagy in chemotherapy. *Neurobiol Dis.* 2020;136:104715.
- Zhao J, Bi W, Xiao S, Lan X, Cheng X, Zhang J, et al. Neuroinflammation induced by lipopolysaccharide causes cognitive impairment in mice. *Sci Rep.* 2019;9:5790.

2.2 IMMUNEPOTENT CRP PROTECTS MICROGLIA CELLS FROM EPIRUBICIN-INDUCED DAMAGE

2.2.1 INTRODUCTION

Before chemotherapy emerged in the early twentieth century, cancer was primarily treated with surgery or radiation. In the early 1900s, Paul Ehrlich coined the term “chemotherapy” to describe the use of chemicals to combat cancer (DeVita V. & Chu E., 2008). Due to its effectiveness in targeting rapidly dividing cells, a key hallmark of cancer, chemotherapy remains a fundamental treatment option even with the advent of newer therapies (Bianna & Lee S., 2023). These drugs are categorized based on their type; examples include alkylating agents, alkaloids, antibiotics, and antimetabolites. They disrupt cell growing by targeting nucleic acids and metabolic pathways. Antimetabolites act on enzymes involved in purine or pyrimidine metabolism, while alkaloids target β -tubulin in the cytoskeleton and mitosis (Schirmacher V., 2019). Because chemotherapy circulates throughout the body, it impacts both cancerous and healthy cells indiscriminately. This can lead to a range of side effects, varying in severity depending on the specific drugs used, dosage, and individual patient response. (Bianna & Lee S., 2023; Hanahan D. & Weinberg R., 2011). Common side effects include nephro-, hepato-, neuro-, cardio-, and ototoxicity, as well as impact on bone marrow and immune system cells (van den Boogaard, W. M. C. et al., 2022).

Additionally, up to approximately 70% of cancer survivor soften face persistent challenges with cognition, including memory, focusing, attention, processing speed, and problem-solving abilities, collectively known as cancer therapy-related cognitive impairment (CRCI) (Demos-Davies, K. et al., 2023). Recent studies on the mechanisms underlying CRCI indicate disruptions to the structure and function of neural circuits, highlighting the role of microglia, the specialized immune cells of the central nervous system (CNS), in the neural dysfunction following cancer treatments (Gibson, E. M., & Monje, M., 2021). Research on CRCI suggests that some chemotherapeutic drugs generate reactive oxygen species (ROS) and inflammatory cytokines that compromise the blood-brain barrier (BBB), leading to neuroinflammation, oxidative stress, and microglial activation, which in turn result in neurocognitive changes (Santos & Pyter, 2018; Ren et al., 2019).

To face this issue, recently much attention has been paid to the use of immunotherapies (Schirmacher V., 2019). IMMUNEPOTENT CRP (ICRP), a dialyzed extract of leukocytes from bovine origin has been shown to modulate LPS-induced nitric oxide (NO) and ROS overproduction in murine peritoneal macrophages and peripheral blood mononuclear cells (Franco Molina et al., 2011; 2005b). On the other hand, in a murine model treated with 5-Flurouracilo (5-FU), an elevation in bone marrow cell count and a decrease in ROS generation by ICRP were reported (Coronado Cerda et al., 2016). However, until now it has not been studied whether ICRP can protect from the damage caused by chemotherapeutic agents on immune system cells from CNS, such as the microglia cells. This work aimed to evaluate the protective effect of ICRP on microglial cells against a stimulus of damage induced by chemotherapies.

2.2.2 METHODS

Cell culture mediums and reagents

Cells were maintained in either DMEM-F12 or RPMI-1640, based on the cell line, with both media fortified with 10% fetal bovine serum (FBS) inactivated by heating and 1% penicillin-streptomycin (GIBCO by Life Technologies, Grand Island, NY), termed complete DMEM or complete RPMI. The Laboratorio de Inmunología y Virología at Facultad de Ciencias Biológicas developed IMMUNEPOTENT CRP[©] (ICRP), which was dissolved in the appropriate complete medium. One unit of ICRP is derived from 1×10^8 leukocytes. Doxorubicin (DOX) was sourced from Accord and Epirubicin (EPI) (Farmorubicin RD[®]) from Pfizer (Ciudad de México, México), both reconstituted in sterile water for injection. Cyclophosphamide (CTX, Cryofaxol[®]) was obtained from Cryopharma (Tlajomulco de Zuñiga, Jalisco, México) and dissolved in the respective complete medium. N-acetyl-L-cysteine (NAC) was prepared in water to a final concentration of 500 mM, and QVD.opH (QVD, 1 mM) was prepared in dimethyl sulfoxide (DMSO). All prepared solutions were wrapped in foil and stored as per the manufacturer's guidelines.

Cell culture

SIM-A9, murine microglia (ATCC[®] HTB-22TM) was bought to the American Type Culture Collection (ATCC) and maintained according to its lineaments in a cell culture incubator set at 37°C with 5% CO₂. Cells were cultured in 25-cm³ flasks (CORNING Enterprises, Corning, NY) containing complete DMEM-F12.

Animals

All animal procedures were executed in compliance with the NOM-062-ZOO-1999, which specifies the Mexican technical standards for the production, care, and use of laboratory animals. The experimental strategy was reviewed and approved by the Animal Research and Welfare Ethics Committee (CEIBA) at the Facultad de Ciencias Biológicas, with registration number CEIBA-2021-016.

Female BALB/c mice, aged eight to ten weeks and weighing 25 ± 5 grams, were supplied by the animal facility at the Universidad Autónoma de Nuevo León, Mexico. The mice were kept in plastic enclosures in cohorts of 5 and given a 7-day adaptation period in the facility. They were maintained at a temperature of $21 \pm 3^\circ\text{C}$, with $55\% \pm 10\%$ humidity, and cycles of 12-hour light/dark. They were provided unrestricted access to rodent maintenance diet (LabDiet, St. Louis, MO) and water. Their health status was monitored daily. For all experiments, the mice were allocated randomly into distinct groups.

Lymphoid and peripheral blood mononuclear cells (PBMC) isolation and death

Mice were anesthetized and sacrificed, followed by the collection of blood samples, spleen, femur, and tibia. PBMC isolation was carried out through centrifugation and separation based on density gradient using Ficoll-Paque[™] PLUS (GE Healthcare, Chicago, Illinois), from which the PBMC population was collected. The spleen was processed through a 70 μM cell strainer with PBS, and bone marrow cells were extracted by flushing the femur and tibia into complete RPMI. All cells were cultured at 2×10^5

cells/well in complete RPMI at 37°C in an atmosphere of 5% CO₂. Cells were exposed to the cytotoxic concentrations of tumoral cells for 24 hours, and cell death was assessed as described in the corresponding section.

Cell death analysis

Cells were treated with ICRP (0.25 U/mL), DOX (0.1-20 µM), EPI (0.1-5 µM), or CTX (2-20 mM) to determine cytotoxic concentrations (CC) for combination analysis. For subsequent experiments, cells were exposed to combinations of ICRP+DOX, ICRP+EPI, or ICRP+CTX for 24 hours in plates of 24 wells (Life Sciences). After treatment, cells were collected, rinsed with PBS, and then resuspended in 100 µL of binding buffer (10 mM HEPES/NaOH pH 7.4, 140 mM NaCl, 2.5 mM CaCl₂) containing Annexin-V-APC (1 µg/mL, BD Pharmingen, San Jose, CA) to measure cell death using a BD Accuri 6 flow cytometer (Becton Dickinson, Franklin Lakes, NJ) and analyzed with FlowJo Software (LCC, Ashland, OR).

ROS production analysis

Bone marrow and spleen were seeded at a concentration of 2x10⁶ cells/mL, using U-bottom 96-well plates (CORNING®), whereas SIM-A9 was seeded at a concentration of 3.5x10⁴. EPI (5 µM), DOX (20 µM), and CTX (20 mM) were added to the peripheral immune system cells, and EPI (1 µM), DOX (1 µM), and CTX (15 mM) were added to SIM-A9, along with their combination with ICRP (0.25 U/mL). The cultures were incubated at 37°C for 24 hours in controlled humidity with 5% CO₂. Harvested cells were treated with 0.02 mM DCFDA, followed by a 30-minute incubation at 37°C. After washing, ROS levels were measured using flow cytometry as mentioned above.

NO production analysis

SIM-A9 was seeded as mentioned above. EPI (1 µM), ICRP (0.25 U/mL), and their combinations were added. Treatments were incubated as mentioned above. At the end, harvested cells were stained for 30 minutes using 1.3 µM DAF-FM at 37°C. Cells were then rinsed using PBS two times, and the amount of NO was determined by flow cytometry using the Accuri C6 cytometer (BD Biosciences).

Cell death inhibition

SIM-A9 was seeded as mentioned above. SP-1 (15 µM) was added for 30 minutes before treatment with EPI (1 µM) and its combination with 0.25 U/mL ICRP following previously mentioned incubation conditions. Cells were then collected and AnnV staining was used for quantification of the cell death-percentage obtained through flow cytometry.

Statistical analysis

Data is displayed as graphs showing the mean ± SD of triplicate measurements from a minimum of three independent experiments. GraphPad Prism software was used to analyze the data (San Diego, CA). For *in vitro* studies, paired Student's t-tests was used, while unpaired Student's t-tests was applied for cytotoxicity studies in PBMCs. A statistical significance was assigned to results with a p-value below 0.05.

2.2.3 RESULTS

EPI, DOX, and CTX are cytotoxic in bone marrow, spleen, PBMC, and microglia

We have previously demonstrated the cytotoxic effect induced by EPI, CTX, and DOX in breast and hematologic cancer cells (de la Hoz Camacho et al. 2022; Rivera Lazarin et al., 2024 in revision). Thus, to assess the cytotoxicity induced by these chemotherapies in immune system cells, we determined the cytotoxicity induced by the CC₅₀ of cancer cells in the immune system and microglia cells. Our results show that EPI, DOX-induced 30% cell death, and CTX 80%-cell death in bone marrow (Fig. 1A) and spleen (Fig. 1B). On the other hand, treatments induced 10-50% of PBMC death (Fig. 1C). However, higher cell death was induced in SIM-A9 by all the chemotherapies tested showing 60-80% microglia cell death (Fig. 1D).

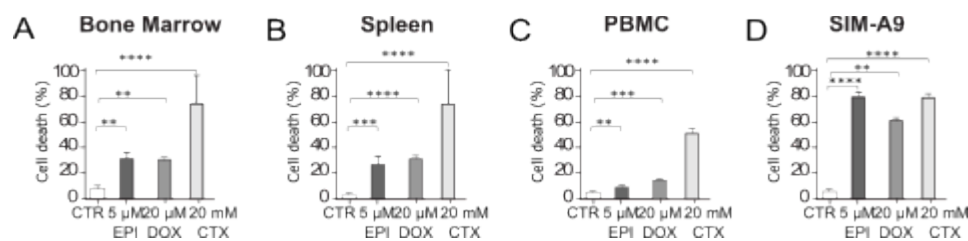


Figure 1. The cytotoxic effect induced by EPI, DOX, and CTX in bone marrow, spleen, PBMC, and SIM-A9. Murine bone marrow (A), spleen (B), PBMC (C), and SIM-A9 (D) were treated for 24 hours with 5 μM epirubicin, 20 μM doxorubicin, and 20 mM cyclophosphamide. The percentage of cell death was evaluated using the exclusion of trypan blue staining. The graphs represent the average ± standard deviation from a minimum of three separate experiments, each executed in triplicate. * (p < 0.05), ** (p < 0.01), *** (p < 0.001), **** (p < 0.0001).

Given the cytotoxicity induced by chemotherapies in non-tumoral immune system cells, we decided to evaluate whether ICRP could reverse this effect.

For this purpose, we evaluated several concentrations of ICRP in combination with EPI, to find an optimal concentration in which ICRP could exhibit a protective effect. Our results showed that the concentration of 0.25 U/mL was optimal for use in combination, as it was the maximum concentration at which a decrease in EPI-cytotoxicity was observed (Supplementary Fig. 1S).

Sublethal doses of ICRP protect bone marrow, spleen, and microglia cells

Figure 2A illustrates a significant reduction in the cell death proportion in bone marrow cells treated with 5 μM EPI, 20 μM DOX, and 20 mM CTX of about 10% in combination with 0.25 U/mL ICRP. Likewise, this effect is seen in spleen cells treated with EPI and DOX in combination with ICRP of approximately 50% (Fig. 2B). However, Figure 2C shows no significant decrease in the percentage of PBMC-cell death when treated with EPI, DOX, and CTX in combination with ICRP. Additionally, a reduction of about 30% was induced by the treatment with 1 μM EPI, 1 μM DOX, and 15 mM CTX (the CC₅₀ of each chemotherapy in SIM-A9 as these cells resulted highly sensitive to cancer-cytotoxic concentrations. Supplementary Fig. 2S) in combination with ICRP (Fig. 2D).

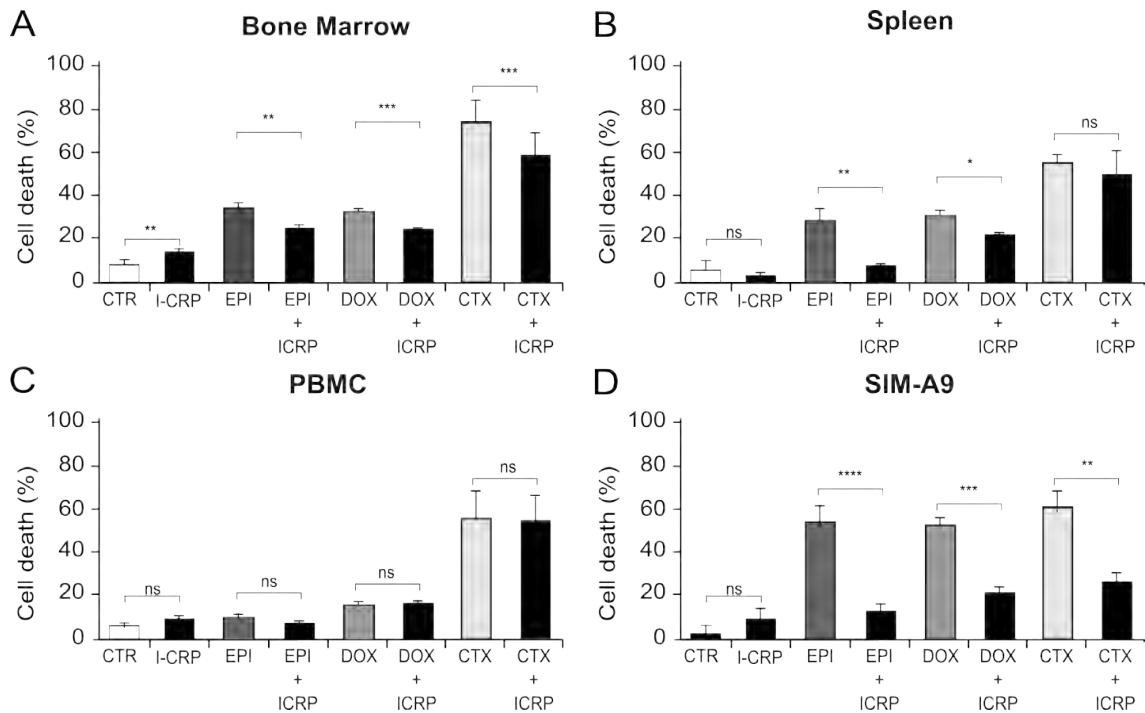


Figure 2. The protective effect induced by ICRP in bone marrow, spleen, PBMCs, and SIM-A9 against CC₅₀ EPI, DOX, and CTX-cytotoxicity. Murine bone marrow (A), spleen (B), PBMCs (C), and SIM-A9 (D) were treated for 24 hours with EPI (5 μ M), DOX (20 μ M), CTX (20 mM), and 0.25 U/mL ICRP, as well as their combinations. Cell death percentage was assessed using the trypan blue exclusion method. The graphs illustrate the mean \pm standard deviation from a minimum of three separate experiments, each executed in triplicate. Statistical analysis was performed, where ns indicates not significant, * indicates $p < 0.05$, ** indicates $p < 0.01$, *** indicates $p < 0.001$, and **** indicates $p < 0.0001$.

Once we demonstrated the potential of ICRP to protect lymphoid immune system cells against chemotherapy-cytotoxicity, we used microglia cells (the main cell orchestrating CRCI) to further identify the mechanism by which this protection occurs, using EPI as it has previously been reported to induce ROS and NO production, as well as microglia activation (de la Hoz Camacho et al., 2022).

ICRP decreases ROS and NO production in microglia cells treated with EPI

Analysis showed that EPI and ICRP increased DCFDA+ SIM-A9 cells, which was diminished by combining EPI+ICRP (Fig. 3 left panel). This reduction in ROS production induced by combining EPI+ICRP is significantly lower than EPI-monotherapy (Fig. 3 right panel).

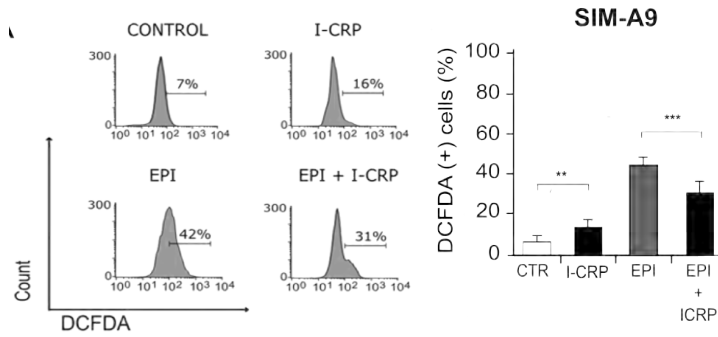


Figure 3. Antioxidant effect of ICRP with EPI in SIM-A9. SIM-A9 was treated with the CC₅₀ EPI (1 μ M) and ICRP (0.25 U/mL) for 24 hours. ROS production was measured using DCFDA. Representative histograms obtained by flow cytometry and graphs representing the average \pm SD. * (p < 0.05), ** (p < 0.01), *** (p < 0.001), **** (p < 0.0001).

Furthermore, cells exhibited a significant reduction in NO production when treated with the combination of CC₅₀ EPI with ICRP (Fig. 4).

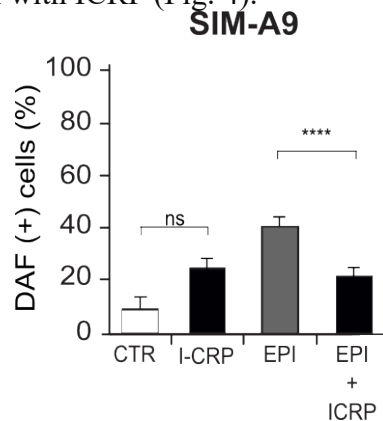


Figure 4. Modulatory effect of ICRP with EPI in SIM-A9. SIM-A9 was treated with 1 μ M EPI and ICRP (0.25 U/mL) for 24 hours and analyzed through flow cytometry. NO production was measured using DAF. The graph represents the average \pm SD. * (p < 0.05), ** (p < 0.01), *** (p < 0.001), **** (p < 0.0001).

ICRP triggers autophagy in microglial cells as a protective response

Recent studies suggest that autophagy could decrease activation markers and play a neuroprotective role against cytotoxic agents such as chemotherapy in microglia cells. Therefore, we decided to evaluate the formation of autophagosomes as a protective mechanism. Figure 5A demonstrates that both ICRP and EPI significantly enhance autophagosome formation compared to the control. However, Combining ICRP with EPI significantly induced a higher production of autophagosomes compared to either treatment by itself. Furthermore, inhibiting autophagosome formation with SP-1 led to a significant increase in cell death induced by EPI, ICRP, and their combination, suggesting that autophagy has a protective role.

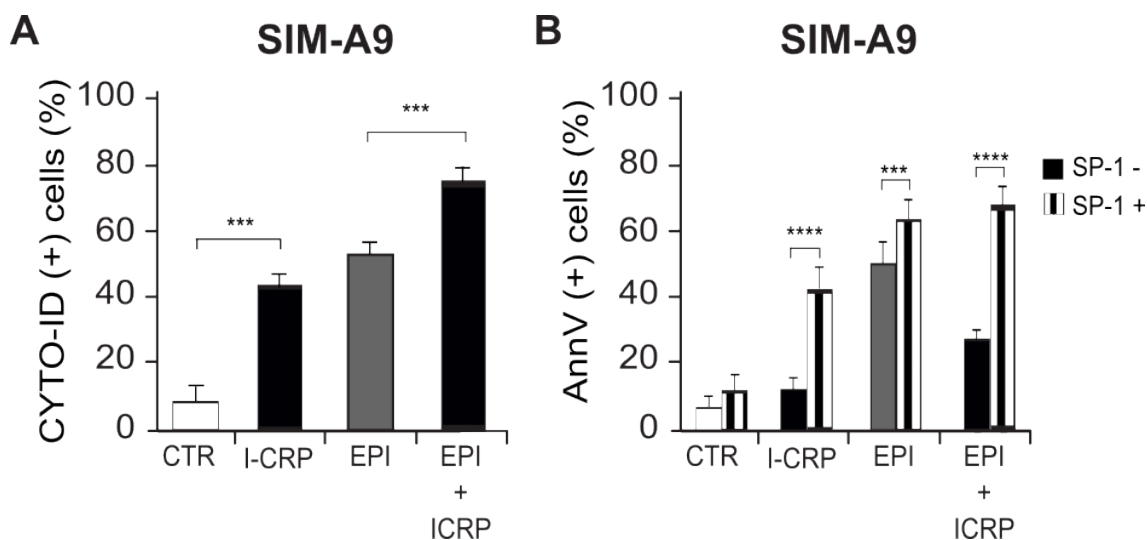


Figure 5. ICRP-mediated autophagosome formation as a protective mechanism against EPI-induced cytotoxicity. SIM-A9 was treated with or without SP-1, followed by 24 hours incubation with the CC_{50} of EPI and ICRP (0.25 U/mL) and analysis by flow cytometry. A) Autophagosome formation was evaluated using CYTO-ID. B) AnnV staining used for cell death analysis. Graphs illustrate the average \pm SD. * ($p < 0.05$), ** ($p < 0.01$), *** ($p < 0.001$), **** ($p < 0.0001$).

2.2.4 DISCUSSION

While chemotherapies are effective against tumors, they also cause side effects by indiscriminately targeting non-cancerous tissues. Immune system cells are frequently substantially damaged by cancer treatment, affecting the entire body (Verma R. et al., 2016) or different organs like the liver, and lungs, and recently reported for causing chemotherapy-induced cognitive impairment (CRCI), suggesting microglia as the main contributor to this issue (Matsos A. et al., 2017; Gibson E. M. et al., 2019).

Throughout this work, our objective was to assess whether ICRP shields against chemotherapy-induced damage.. The findings in this study were noteworthy, particularly highlighting that SIM-A9 cells exhibited the highest susceptibility to EPI, DOX, and CTX-induced cytotoxicity when tested at the CC_{50} in tumor cells. Previously it has been reported that microglia in the central nervous system are often more metabolically active than macrophages (Deng Y. et al., 2024), which let us hypothesize that this feature increases their susceptibility to the oxidative stress and therefore apoptosis triggered by chemotherapy as demonstrated by DOX in murine lymphocytes and EPI and CTX in microglia cells (Kim H.S. et al., 2009; de la Hoz-Camacho et al., 2022).

An important objective of combinatorial therapy is to reduce chemotherapy toxicity. Ideally, drugs used to mitigate toxic effects should not cause side effects themselves (Panchenko et al., 2018). From this overview, we decided to evaluate whether ICRP could reduce the cell death caused by chemotherapy. Our results showed that ICRP protects the spleen, bone marrow, and SIM-A9 cells. Similar results were reported before by combining Angelica polysaccharide (ASP) with 5-FU, which inhibited 5-FU-induced hepatocyte apoptosis presumptively by enhancing the transcriptional activity of Nrf2 and

by reducing the upregulation of Keap1 expression triggered by 5-FU (Zeng D. et al., 2021). Moreover, Immunepotent CRP, in combinational treatment with 5-FU, generates protection for bone marrow by reducing ROS/superoxide formation and Nrf2 activation (Coronado-Cerda et al., 2016), thus a reduction in ROS production could also be a mechanism implicated in the ICRP-mediated protection observed in spleen cells.

Since studies have shown that excessive ROS levels surpassing cellular regulatory mechanisms may harm microglia and result in cellular demise (Li J. et al., 2022), we decided to analyze whether a reduction in ROS generation could be a mechanism involved in the ICRP protection to microglia-cell death. Our results demonstrate that ICRP in combination with EPI could reduce ROS and NO production in microglia cells. Similarly, H₂O₂-induced microglia-cell death could be alleviated by cotreatment with polysaccharides obtained from *Polygonatum cyrtonema* Hua (PCP), which alleviated the ROS overload triggered through H₂O₂ (Li J. et al., 2022). Another research using a *Physalis alkekengi* L. var. francheti fruit extract (PAFE) decreased NO production in a microglia cell line and primary microglia without reducing cell viability by decreasing iNOS and COX-2 expression under a LPS-stimulus (Park B. H. et al., 2021).

Recently, limited research has explored autophagy's function in microglia and the potential consequences of its dysregulation on cell survival (Plaza-Zavala A. et al., 2017). Here we showed that ICRP combined with EPI protects microglia from cell death through an autophagosome-formation-dependent mechanism. This protection of microglia cells against a damaging stimulus that relies on autophagosome formation was also previously reported by the use of ferulic acid (FA) which enhance autophagy flux at both the gene and protein levels while also inhibiting the expression of inflammatory proteins. (Chen X et al., 2023). Altogether the results of this work highlight ICRP as an agent that protects healthy cells against the damage induced by chemotherapy for improving CRCI outcomes.

2.2.5 REFERENCES

Brianna, & Lee, S. H. (2023). Chemotherapy: how to reduce its adverse effects while maintaining the potency?. *Medical oncology* (Northwood, London, England), 40(3), 88. <https://doi.org/10.1007/s12032-023-01954-6>

Chen, X., Zhou, X., Cheng, X., Lin, L., Wang, Q., Zhan, R., Wu, Q., & Liu, S. (2023). Protective effect of ferulic acid on lipopolysaccharide-induced BV2 microglia inflammation via AMPK/mTOR signaling pathway. *Molecules*, 28(8), 3482. <https://doi.org/10.3390/molecules28083482>

Coronado-Cerda, E. E., Franco-Molina, M. A., Mendoza-Gamboa, E., Prado-García, H., Rivera-Morales, L. G., Zapata-Benavides, P., Rodríguez-Salazar, M.delC., Caballero-Hernandez, D., Tamez-Guerra, R. S., & Rodríguez-Padilla, C. (2016). In Vivo Chemoprotective Activity of Bovine Dialyzable Leukocyte Extract in Mouse Bone

Marrow Cells against Damage Induced by 5-Fluorouracil. *Journal of immunology research*, 2016, 6942321. <https://doi.org/10.1155/2016/6942321>

de la Hoz-Camacho, R., Rivera-Lazarín, A. L., Vázquez-Guillen, J. M., Caballero-Hernández, D., Mendoza-Gamboa, E., Martínez-Torres, A. C., & Rodríguez-Padilla, C. (2022). Cyclophosphamide and epirubicin induce high apoptosis in microglia cells while epirubicin provokes DNA damage and microglial activation at sub-lethal concentrations. *EXCLI journal*, 21, 197–212. <https://doi.org/10.17179/excli2021-4160>

Demos-Davies, K., Lawrence, J., Rogich, A., Lind, E., & Seelig, D. (2023). Cancer treatment induces neuroinflammation and behavioral deficits in mice. *Frontiers in behavioral neuroscience*, 16, 1067298. <https://doi.org/10.3389/fnbeh.2022.1067298>

Deng, Y., Chen, Q., Wan, C., Sun, Y., Huang, F., Hu, Y., & Yang, K. (2024). Microglia and macrophage metabolism: a regulator of cerebral gliomas. *Cell & bioscience*, 14(1), 49. <https://doi.org/10.1186/s13578-024-01231-7>

DeVita, V. T., Jr, & Chu, E. (2008). A history of cancer chemotherapy. *Cancer research*, 68(21), 8643–8653. <https://doi.org/10.1158/0008-5472.CAN-07-6611>

Franco-Molina, M. A., Mendoza-Gamboa, E., Castillo-León, L., Tamez-Guerra, R. S., & Rodríguez-Padilla, C. (2005). Bovine dialyzable leukocyte extract modulates the nitric oxide and pro-inflammatory cytokine production in lipopolysaccharide-stimulated murine peritoneal macrophages in vitro. *Journal of medicinal food*, 8(1), 20–26. <https://doi.org/10.1089/jmf.2005.8.20>

Franco-Molina, M. A., Mendoza-Gamboa, E., Mir, D. F., Sierra-Rivera, C. A., Zapata-Benavides, P., Vera-García, M. E., Tamez-Guerra, R., & Rodríguez-Padilla, C. (2011). Anti-inflammatory and antioxidant effects of IMMUNEPOTENT CRP in Lipopolysaccharide (LPS)-stimulated human macrophages. *African Journal of Microbiology Research*, 5(26), 3726-3736. doi:10.5897/AJMR11.578

Gibson, E. M., & Monje, M. (2021). Microglia in Cancer Therapy-Related Cognitive Impairment. *Trends in neurosciences*, 44(6), 441–451. <https://doi.org/10.1016/j.tins.2021.02.003>

Hanahan, D., & Weinberg, R. A. (2011). Hallmarks of cancer: the next generation. *Cell*, 144(5), 646–674. <https://doi.org/10.1016/j.cell.2011.02.013>

Kim, H. S., Lee, Y. S., & Kim, D. K. (2009). Doxorubicin exerts cytotoxic effects through cell cycle arrest and Fas-mediated cell death. *Pharmacology*, 84(5), 300–309. <https://doi.org/10.1159/000245937>

Li, J., Wang, X., Zhou, R., Cheng, F., Tang, X., Lao, J., Xu, L., He, W., Wan, D., Zeng, H., & Zhang, S. (2022). *Polygonatum cyrtanema* Hua Polysaccharides Protect BV2 Microglia Relief Oxidative Stress and Ferroptosis by Regulating NRF2/HO-1 Pathway.

Molecules (Basel, Switzerland), 27(20), 7088.
<https://doi.org/10.3390/molecules27207088>

Matsos, A., Loomes, M., Zhou, I., Macmillan, E., Sabel, I., Rotziokos, E., Beckwith, W., & Johnston, I. N. (2017). Chemotherapy-induced cognitive impairments: White matter pathologies. *Cancer treatment reviews*, 61, 6–14.
<https://doi.org/10.1016/j.ctrv.2017.09.010>

Plaza-Zabala, A., Sierra-Torre, V., & Sierra, A. (2017). Autophagy and Microglia: Novel Partners in Neurodegeneration and Aging. *International journal of molecular sciences*, 18(3), 598. <https://doi.org/10.3390/ijms18030598>

Panchenko, A. V., Fedoros, E. I., Pigarev, S. E., Maydin, M. A., Gubareva, E. A., Yurova, M. N., Kireeva, G. S., Lanskih, G. P., Tyndyk, M. L., & Anisimov, V. N. (2018). Effect of the polyphenol composition BP-C3 on haematological and intestinal indicators of 5-fluorouracil toxicity in mice. *Experimental and therapeutic medicine*, 15(3), 3124–3132.
<https://doi.org/10.3892/etm.2018.5782>

Park, B.H., Kwon, O.W., Kim, I.S., & Kim, J. (2021). *Physalis alkekengi L. var. francheti* alleviates neuronal cell death caused by activated microglia in vitro. *Applied Biological Chemistry*, 64, 23. <https://doi.org/10.1186/s13765-021-00594-6>

Ren, X., Boriero, D., Chaiswing, L., Bondada, S., St Clair, D. K., & Butterfield, D. A. (2019). Plausible biochemical mechanisms of chemotherapy-induced cognitive impairment ("chemobrain"), a condition that significantly impairs the quality of life of many cancer survivors. *Biochimica et biophysica acta. Molecular basis of disease*, 1865(6), 1088–1097. <https://doi.org/10.1016/j.bbadis.2019.02.007>

Santos, J. C., & Pyter, L. M. (2018). Neuroimmunology of Behavioral Comorbidities Associated With Cancer and Cancer Treatments. *Frontiers in immunology*, 9, 1195. <https://doi.org/10.3389/fimmu.2018.01195>

Schirmmacher V. (2019). From chemotherapy to biological therapy: A review of novel concepts to reduce the side effects of systemic cancer treatment (Review). *International journal of oncology*, 54(2), 407–419. <https://doi.org/10.3892/ijo.2018.4661>

van den Boogaard, W. M. C., Komninos, D. S. J., & Vermeij, W. P. (2022). Chemotherapy Side-Effects: Not All DNA Damage Is Equal. *Cancers*, 14(3), 627. <https://doi.org/10.3390/cancers14030627>

Verma, R., Foster, R. E., Horgan, K., Mounsey, K., Nixon, H., Smalle, N., Hughes, T. A., & Carter, C. R. (2016). Lymphocyte depletion and repopulation after chemotherapy for primary breast cancer. *Breast cancer research : BCR*, 18(1), 10. <https://doi.org/10.1186/s13058-015-0669-x>

Zeng, D., Wang, Y., Chen, Y., Li, D., Li, G., Xiao, H., Hou, J., Wang, Z., Hu, L., Wang, L., & Li, J. (2021). Angelica Polysaccharide Antagonizes 5-FU-Induced Oxidative Stress

Injury to Reduce Apoptosis in the Liver Through Nrf2 Pathway. *Frontiers in oncology*, 11, 720620. <https://doi.org/10.3389/fonc.2021.720620>

7. CONCLUSIONS

From the results obtained in the present thesis, we can conclude that combining ICRP with several chemotherapies synergically potentiates cell death in breast and hematologic cancer cells. Also, the combination of ICRP+CTX can function even in cells lacking caspases, as its cell death mechanism is caspase-independent in breast cancer and the CC_{50} ICRP+ CC_{50} CTX combination in murine T-cell lymphoblastic lymphoma. Additionally, the combination of ICRP+CTX-improved tumor regression in T-cell lymphoblast tumor-bearing mice model. Furthermore, the combination of ICRP with chemotherapies does not potentiate cell death in non-tumor immune system cells.

The results obtained in this work provide evidence of ICRP as a promising immunotherapy to use in combination with several chemotherapies and different types of cancer and highlight a new approach to the use of dialyzable leukocyte extracts in hematologic cancer treatment.

8. PERSPECTIVES

- To evaluate the antitumor effect of combining ICRP and CTX in breast cancer cells.
- To assess the antitumor efficacy of ICRP combined with DOX, EPI, or ETO against hematologic cancer cells *in vivo*.
- To investigate cell death evoked by ICRP and CTX in caspase-null-breast cancer cells.
- To examine the participation of the immune system in the tumor elimination induced by ICRP and CTX in hematologic cells.
- To determine if ICRP+CTX can induce long-term memory following *in vivo* treatment.
- To assess the combination effect of ICRP+CTX in hematologic cancer cells from patients, confirming its efficacy and potential for clinical trials.
- To elucidate the key regulator of ICRP+CTX-induced cell death.
- To explore the mechanism of overcoming the resistance to CTX-cell death in the presence of BMSC-microenvironment when combined with ICRP.

9. REFERENCES

- Fuchs, Y., & Steller, H. (2015). Live to die another way: modes of programmed cell death and the signals emanating from dying cells. *Nature Reviews Molecular Cell Biology*, 16(6), 329-344.
- Galluzzi, L., Yamazaki, T., & Kroemer, G. (2018). Linking cellular stress responses to systemic homeostasis. *Nature Reviews Molecular Cell Biology*.
- Galluzzi, L., & Vitale, I. (2018). Molecular mechanisms of cell death: recommendations of the Nomenclature Committee on Cell Death 2018. *Cell death & Differentiation*, 25, 486-541.
- Galluzzi, L., & et al. (2012). Molecular definitions of cell death subroutines: recommendations of the Nomenclature Committee on Cell Death 2012. *Cell Death Differentiation*, 19, 107-20.
- Kroemer, G., Galluzzi, L., Vandernabeele, P., Abrams, J., Alnemri, E., Baehrecke, E., . . . Yuan. (2009). Classification of cell death. *Cell Death Differentiation*, 16(1), 3-11.
- Vandernabeele, P., Vanden Berghe, T., & Festjens, N. (2006). Caspase inhibitors promote alternative cell death pathways. *Science's STKE*, 358.
- Organization, W. H. (2020). *Cáncer*. From <https://www.who.int/topics/cancer/es/>
- Hanahan, D., & Weinberg, R. (2011). Hallmarks of cancer. The next generation. *Cell*, 144.
- CIDTA. (n.d.). *TOXICOLOGIA AMBIENTAL*. From https://cidta.usal.es/riesgos/CD1/toxicologia_contaminacion_aire/www.cepis.ops-oms.org/bvsci/e/fulltext/toxicol/leccion3.pdf
- Bayat Mokhtari, R., Homayouni, T., Baluch, N., Morgatskaya, E., Kumar, S., Das, B., & Yeger, H. (2017). Combination therapy in combating cancer. *Oncotarget*, 6(8), 38022-38043.
- Luo, Q., Zhang, L., Luo, C., & Jiang, M. (2019). Emerging strategies in cancer therapy combining chemotherapy with immunotherapy. *Cancer Letters*, 454, 191-203.
- Franco-Molina, M. A., Mendoza-Gamboa, E., Miranda-Hernandez, D., Zapata-Benavides, P., Castillo-Leon, L., Isaza-Brando, C., . . . Rodriguez-Padilla, C.

- (2006). In vitro effects of bovine dialyzable leukocyte extract (bDLE) in cancer cells. *Cytotherapy*, 8(4), 408-414.
- Lorenzo-Anota, H., Martinez-Torres, A. C., Scott-Algara, D., Tamez-Guerra, R. S., & Rodriguez-Padilla, C. (2020). Bovine Dialyzable Leukocyte Extract IMMUNEPOTENT-CRP Induces Selective ROS-Dependent Apoptosis in T-Acute Lymphoblastic Leukemia Cell Lines. *J Oncol*, 1598503.
- Martinez-Torres, A. C., Gomez-Morales, L., Martinez-Loria, A. B., Uscanga-Palomeque, A. C., Vazquez-Guillen, J. M., & Rodriguez-Padilla, C. (2019). Cytotoxic activity of IMMUNEPOTENT CRP against non-small cell lung cancer cell lines. *PeerJ*, 7, e7759.
- Martinez-Torres, A. C., Reyes-Ruiz, A., Benitez-Londoño, M., Franco-Molina, M. A., & Rodriguez-Padilla, C. (2018). IMMUNEPOTENT CRP induces cell cycle arrest and caspase-independent regulated cell death in HeLa cells through reactive oxygen species production. *BMC Cancer*, 18(13), 3954-5.
- Reyes-Ruiz, A., Calvillo-Rodriguez, K. M., Martinez-Torres, A. C., & Rodriguez-Padilla, C. (2021). The bovine dialyzable leukocyte extract IMMUNEPOTENT CRP induces immunogenic cell death in breast cancer cells leading to long-term antitumour memory. *British Journal of Cancer*, 124, 1398–1410.
- Franco-Molina, M. A., Mendoza-Gamboa, E., Zapata-Benavides, P., Vera-Garcia, M. E., Castillo-Tello, P., Garcia de la Fuente, A., . . . Rodriguez-Padilla, C. (2008). IMMUNEPOTENT CRP (bovine dialyzable leukocyte extract) adjuvant immunotherapy: a phase I study in non-small cell lung cancer patients. *Cytotherapy*, 10(5), 490-496.
- Lara, H. H., Ixtepan-Turrent, L., Garza-Treviño, E. N., Tamez-Guerra, R., & Rodriguez-Padilla, C. (2010). Clinical and immunological assessment in breast cancer patients receiving anticancer therapy and bovine dialyzable leukocyte extract as an adjuvant. *Exp Ther Med*, 1(3), 425-431.
- Coronado-Cerda, E. E., Franco-Molina, M. A., Mendoza-Gamboa, E., Prado-Garcia, H., Rivera-Morales, L. G., Zapata-Benavides, P., . . . Tamez-Guerra, R. (2016). In Vivo Chemoprotective Activity of Bovine Dialyzable Leukocyte Extract in Mouse

- Bone Marrow Cells against Damage Induced by 5-Fluorouracil. *J Immunol Res*, 6942321.
- Rodriguez-Salazar, M. d., Franco-Molina, M. A., Mendoza-Gamboa, E., Martinez-Torres, A. C., Zapata-Benavides, P., Lopez-Gonzalez, J. S., . . . Tamez-Guerr. (2017). The novel immunomodulator IMMUNEPOTENT CRP combined with chemotherapy agent increased the rate of immunogenic cell death and prevented melanoma growth. *Oncol Lett*, 14(1), 844-852.
- Santana-Krimskaya, S. E., Franco-Molina, M. A., Zarate-Triviño, D. G., Prado-Garcia, H., Zapata-Benavides, P., Torres-del-Muro, F., & Rodriguez-Padilla, C. (2020). IMMUNEPOTENT CRP plus doxorubicin/cyclophosphamide chemotherapy remodel the tumor microenvironment in an air pouch triple-negative breast cancer murine model. *Biomed Pharmacother*, 110062.
- Organization, W. H. (2020). *WHO*. From Cancer: https://www.who.int/health-topics/cancer#tab=tab_1
- Hanahan, D. (2022). Hallmarks of Cancer: New Dimensions. *Cancer Discov*, 12(1), 31-46.
- Institute, N. C. (2023). *NIH*. Retrieved March, 2024 from Cancer Stat Facts: Cancer Among Adolescents and Young Adults (AYAs) (Ages 15–39): <https://seer.cancer.gov/statfacts/html/aya.html>
- Garcia-Foncillas, J., Bandres, E., Catalan, V., Garcia-Amigot, F., & Zabalegui, N. (2001). Basic concepts in the molecular biology of cancer. *ANALES Sis San Navarra*, 24(1), 31-52.
- Organization, W. H. (2024, February 1). *World Health Organization*. Retrieved March, 2024 from Global cancer burden growing, amidst mounting need for services: <https://www.who.int/news/item/01-02-2024-global-cancer-burden-growing--amidst-mounting-need-for-services>
- Society, A. C. (2019). *ACS*. Retrieved March, 2024 from Breast Cancer Facts & Figures 2019-2020: <https://www.cancer.org/content/dam/cancer-org/research/cancer-facts-and-statistics/breast-cancer-facts-and-figures-2019-2020.pdf>

- Perou, C. M., Sorlie, T., Eisen, M. B., Van de Rijn, M., Jeffrey, S. S., Rees, C. A., . . . Botstein, D. (2000). Molecular portraits of human breast tumours. *Nature*, *406*(6797), 747-752.
- Zhang, N., Wu, J., Wang, Q., Liang, Y., Li, X., Chen, G., . . . Zhou, F. (2023). Global burden of hematologic malignancies and evolution patterns over the past 30 years. *Blood Cancer Journal*, *13*(1), 82.
- Alaggio, R., Amador, C., Anagnostopoulos, I., Attygalle, A. D., de Oliveira Araujo, I. B., Berti, E., . . . Cheuk, W. (2022). The 5th edition of the World Health Organization Classification of Haematolymphoid Tumours: Lymphoid Neoplasms. *Leukemia*, *36*, 1720-1748.
- Vadillo, E., Dorantes-Acosta, E., Pelayo, R., & Schnoor, M. (2018). T cell acute lymphoblastic leukemia (T-ALL): New insights into the cellular origins and infiltration mechanisms common and unique among hematologic malignancies. *Blood Rev*, *32*(1), 36-51.
- Cordo, V., Meijer, M. T., Hagelaar, R., de Goeij-de Haas, R. R., Poort, V. M., Henneman, A. A., . . . Meijerink, J. P. (2022). Phosphoproteomic profiling of T cell acute lymphoblastic leukemia reveals targetable kinases and combination treatment strategies. *Nature Communications*, *13*, 1048.
- Raetz, E. A., & Teachey, D. T. (2016). T-cell acute lymphoblastic leukemia. *Hematology Am Soc Hematol Educ Program*(1), 580-588.
- Terwilinger, T., & Abdul-Hay, M. (2017). Acute lymphoblastic leukemia: a comprehensive review and 2017 update. *Blood Cancer J*, *7*(6), e577.
- Organization, W. H. (2024, March 13). *World Health Organization*. Retrieved April, 2024 from Breast cancer: <https://www.who.int/news-room/fact-sheets/detail/breast-cancer>
- Society, A. C. (2022). *Cancer*. Retrieved April, 2024 from Breast Cancer, facts & figures 2022-2024: <https://www.cancer.org/content/dam/cancer-org/research/cancer-facts-and-statistics/breast-cancer-facts-and-figures/2022-2024-breast-cancer-fact-figures-acf.pdf>
- Bontoux, C., Simonin, M., Garnier, N., Lhermitte, L., Touzart, A., Andrieu, G., . . . Macintyre, E. (2022). Oncogenetic landscape of T-cell lymphoblastic lymphomas

- compared to T-cell acute lymphoblastic leukemia. *Modern Pathology*, 35(9), 1227-1235.
- Lepretre, S., Graux, C., Touzart, A., Macintyre, E., & Boissel, N. (2017). Adult T-type lymphoblastic lymphoma: Treatment advances and prognostic indicators. *Experimental Hematology*, 51, 7-16.
- Kroeze, E., Loeffen, L., Poort, V. M., & Meijerink, J. P. (2020). T-cell lymphoblastic lymphoma and leukemia: different diseases from a common premalignant progenitor? *Blood advances*, 4(14), 3466-3473.
- Ortega Sanchez, M. A., Osnaya Ortega, M. L., & Rosas Barrientos, J. V. (2007). Leucemia linfoblástica aguda. *Medicina Interna de México*, 23(1), 26-33.
- Wu, J., & Waxman, D. J. (2018). Immunogenic chemotherapy: Dose and schedule dependence and combination with immunotherapy. *Cancer Lett*, 419, 210-221.
- Coeffic, D., Antoine, E. C., & Khayat, D. (2002). Quimioterapia antitumoral. *EMC-Tratado de Medicina*, 6(2), 1-7.
- Bayon-Calderon, F., Toribio, M. L., & Gonzalez-Garcia, S. (2020). Facts and Challenges in Immunotherapy for T-Cell Acute Lymphoblastic Leukemia. *Int. J. Mol. Sci*, 21(20), 7685.
- VADEMECUM. (2022, 08 24). *VADEMECUM*. Retrieved 04, 24 from CYCLOPHOSPHAMIDE powder for solution for injection 1 g: <https://www.vademecum.es/estados-unidos/medicamento/28005844/cyclophosphamide-powder-for-solution-for-injection-1-g>
- PLM. (2018). *Medicamentos PLM*. Retrieved 04, 2024 from Cryofaxol: https://www.medicamentosplm.com/Home/productos/cryofaxol_solucion_inyectable/45/101/43709/162
- Ahlmann, M., & Hempel, G. (2016). The effect of cyclophosphamide on the immune system: implications for clinical cancer therapy. *Cancer Chemotherapy and Pharmacology*, 78(4), 661-671.
- Emadi, A., Jones, R. J., & Brodsky, R. A. (2009). Cyclophosphamide and cancer: golden anniversary. *Nature reviews. Clinical oncology*, 6(11), 638-647.

- Liberman, A. C., Drunker, J., Refojo, D., & Arzt, E. (2008). [Molecular mechanisms of action of some immunosuppressive drugs]. *Medicina*, 68(6), 455-464.
- Goldstein, M., Roos, W. P., & Kaina, B. (2008). Apoptotic death induced by the cyclophosphamide analogue mafosfamide in human lymphoblastoid cells: Contribution of DNA replication, transcription inhibition and Chk/p53 signaling. *Toxicology and Applied Pharmacology*, 229(1), 20-32.
- Singh, N., Nigam, M., Ranjan, V., Sharma, R., Kumar Balapure, A., & Kumar Rath, S. (2009). Caspase Mediated Enhanced Apoptotic Action of Cyclophosphamide- and Resveratrol-Treated MCF-7 Cells. *Journal of Pharmacological Sciences*, 109(4), 473-485.
- Pastorczyk, A., Domka, K., Fidyk, K., Poprzeczko, M., & Firczuk, M. (2021). Mechanisms of Immune Evasion in Acute Lymphoblastic Leukemia. *Cancers*, 13(7), 1536.
- Chiarini, F., Lonetti, A., Evangelisti, C., Buontempo, F., Orsini, E., Evangelisti, C., . . . Martelli, A. M. (2016). Advances in understanding the acute lymphoblastic leukemia bone marrow microenvironment: From biology to therapeutic targeting. *Biochimica et biophysica acta*, 1863(3), 449-463.
- Valencia, J., Fernandez-Sevilla, L. M., Fraile-Ramos, A., Sacedon, R., Jimenez, E., Vicente, A., & Varas, A. (2019). Acute Lymphoblastic Leukaemia Cells Impair Dendritic Cell and Macrophage Differentiation: Role of BMP4. *Cells*, 8(7), 722.
- Chou, T., & Talalay, P. (1983). Analysis of combined drug effects: a new look at a very old problem. *Trends in Pharmacology Sciences*, 4(C), 450-454.
- Mokhtari, R. B., Homayouni, T. S., Baluch, N., Morgatskaya, E., Kumar, S., Das, B., & Yeger, H. (2017). Combination therapy in combating cancer. *Oncotarget*, 8(23), 38022-38043.
- Sierra-Rivera, C. A., Franco-Molina, M. A., Mendoza-Gamboa, E., Zapata-Benavides, P., Santaolalla-Tapia, J., Coronado-Cerda, E. E., . . . Rodriguez-Padilla, C. (2016). Effect of bovine dialyzable leukocyte extract on induction of cell differentiation and death in K562 human chronic myelogenous leukemia cells. *Oncology letters*, 12(6), 4449-4460.

10. BIOGRAPHICAL ABSTRACT

Ana Luisa Rivera Lazarín

Candidate for the degree of: PhD in Immunobiology.

Thesis: “Study of the effect of Immunepotent CRP in combination with chemotherapies on cancer cells and immune system cells”

Research field: Cellular Biology

Personal data: Born in Saltillo, Coahuila, México on January 28th 1994. Daughter of Carlos Rivera Rodríguez and Ma. Patricia Lazarín Cierra.

Education: BSc in Chemistry, Pharmacology and Biology with honors at Universidad Autónoma de Coahuila, México. Master of Science with orientation in Immunobiology at Universidad Autónoma de Nuevo León, México.

Awards:

- Recognition as Honor student of the College Degree. Ranked as 1st place in the class. UAdeC, Coahuila, México, 2018.
- Recognition for satisfactory performance in the Examen General de Egresados de Licenciatura (EGEL), 2018.
- Recognition for being the Treasurer of the Student Board in the School of Chemical Sciences, 2017.
- Award as best proposal of Campus Saltillo in the category of Institutional Commitment, UAdeC, 2015.
- Recognition as Honor student of the High School. Ranked as 4th place in the class. UVM, Coahuila, México, 2012.
- Recognition for satisfactory performance in the Centro Nacional de Evaluación para la Educación Superior (CENEVAL) test, 2012

Professional experience:

- Research Stay at UMR 7203-LBM- Laboratoire des biomolécules, Sorbonne Université, 2023-2024.
- Customer service at Snackers Bussiness. Coahuila, México, 2020-2024
- Participation as an evaluator at the II Psychology and Neuroscience student's research event. Nuevo León, México, 2022.
- Participation as bachelor's thesis advisor, Nuevo León, México, 2022.
- Professional Practices at La Concepción Surgical Clinic. Coahuila, México, 2017.
- Research stay at the Department of Biology of the Division of Natural and Exact Sciences at the University of Guanajuato, Guanajuato, México, 2016.

List of Scientific Communications

Scientific publications on Indexed Journals JCR:

- **Rivera-Lazarín, A. L.**, Calvillo-Rodríguez, K. M., Izaguirre-Rodríguez, M., Vázquez-Guillén, J. M., Martínez-Torres, A. C., & Rodríguez-Padilla, C. (2024). Synergistic enhancement of chemotherapy-induced cell death and antitumor efficacy against tumoral T-cell lymphoblasts by IMMUNEPOTENT CRP. *International Journal of Molecular Sciences, 25*(14), 7938. <https://doi.org/10.3390/ijms25147938>
- Calvillo-Rodríguez Kenny Misael, **Rivera-Lazarín Ana Luisa**, Támez-Guerra Reyes, Martínez-Torres Ana Carolina, Rodríguez-Padilla Cristina. (2024). Splenocytes anti-tumor cytotoxicity assessment after prophylactic vaccination or drug treatment of tumor-bearing mice. In revision. International Review of Cell and Molecular Biology
- **Rivera-Lazarín, A. L.**, Martínez-Torres, A. C., de la Hoz-Camacho, R., Guzmán-Aguillón, O. L., Franco-Molina, M. A., & Rodríguez-Padilla, C. (2023). The bovine dialyzable leukocyte extract, immunepotent CRP, synergistically enhances cyclophosphamide-induced breast cancer cell death, through a caspase-independent mechanism. *EXCLI journal*, 22, 131–145. <https://doi.org/10.17179/excli2022-5389>
- de la Hoz-Camacho, R., **Rivera-Lazarín, A. L.**, Vázquez-Guillén, J. M., Caballero-Hernández, D., Mendoza-Gamboa, E., Martínez-Torres, A. C., & Rodríguez-Padilla, C. (2022). Cyclophosphamide and epirubicin induce high apoptosis in microglia cells while epirubicin provokes DNA damage and microglial activation at sub-lethal concentrations. *EXCLI Journal*, 21, 197–212.
- Zugasti-Cruz A, **Rivera-Lazarín AL**, Silva Belmares SY, Alfaro-A. M, Sierra-Rivera CA. (2020). Effect of sodium dichloroacetate as single agent or in combination with cisplatin in normal and human cervical cancer cell lines. *Tropical Journal of Pharmaceutical Research*, 19 (3): 467-474.
- **Rivera-Lazarín AL**, Zugasti-Cruz A, Aldape-de la Peña G, Silva-Belmares SY, Sierra-Rivera CA. (2019) Synergistic cytotoxic effect of sodium dichloroacetate combined with chemotherapeutic drugs on B16F10 murine melanoma cell line. *Biomedical Research*, 30(1): 179-185.

Scientific publications in Arbitrated Journals:

- “El Immunepotent CRP en combinación con ciclofosfamida tiene un efecto citotóxico sinérgico en células de cáncer de mama”. VII Simposio Nacional de Ciencias Farmacéuticas y Biomedicina y V Simposio Nacional de Microbiología Aplicada (2019).
- Study of the Bioaccumulation of Heavy Metals in Candida Species. Jóvenes en la Ciencia, Vol II. No. 4. Pages 496-500 (2017).

Oral and poster presentations:

- Speaker in the panel "Challenges of postgraduate studies". Monterrey, N.L. 2023
- Poster exhibition in 13th European Workshop on Cell death. Fiuggi, Italy. 2023
- Poster exhibition in the ECDO-EATI Joint Annual Conference. Paris, France, 2023.
- Poster exhibition in the Young Researchers in Life Science. Paris, France, 2023.
- Oral presentation in the XXXII National Congress of Medicine Innovation and Research. Monterrey, N.L. 2023
- Poster exhibition in XXII International Medicine Sciences Meeting. León, Gto. 2022
- Poster exhibition in 12th European Workshop on Cell death. Fiuggi, Italy. 2022
- Poster exhibition in Cell la Vie 2021-the online edition. Francia. 2021
- Poster exhibition in 4th Annual UTRGV SOM Research Symposium: International Conference on Cancer Health Disparities. Texas Rio Grande Valley. 2021
- Poster exhibition in XXX National Congress of Medicine Research. Monterrey, N.L. 2019
- Poster exhibition in VII Congress of Reactive Oxygen Species in Biology and Medicine. Ciudad de México, Mex. 2019
- Poster exhibition in VI National Symposium of Pharmaceutical and Biomedicine Sciences and VI National Symposium of Applied Microbiology. 2018
- Poster exhibition in 10th Meeting of Student Scientific Expression. Saltillo, Coah. 2017
- Poster exhibition in XXIX National Congress of Medicine Research. Monterrey, N.L. 2017
- Poster exhibition in University Meeting of Science, Innovation and Art. Arteaga, Coah. 2016

“La muerte no es solo el final de la vida, sino una manifestación inevitable del riesgo inherente en el vivir.”

Gawande, A. (2014). *Being Mortal: Medicine and What Matters in the End.*